Università degli Studi di Salerno

Dottorato di Ricerca in Fisica IX Ciclo

Facoltà di Scienze Matematiche Fisiche e Naturali

Dipartimento di Fisica

Tesi di dottorato in

Detailed Study of Local and Regional Seismicity Recorded by the Underground UNDERSEIS Array at Gran Sasso (Central Italy)

Tutors:
 Prof. Roberto Scarpa

 Dott. Mario La Rocca

PhD Coordinator:
 Prof. Giuseppe Grella

PhD Student:
Luisa Anna Formisano

Anno Accademico 2009-2010

Ai miei genitori
e a tutte le persone che mi sono care

Contents

Introduction

In this work I analyzed seismic data recorded by two arrays installed in the area of Mt. Gran Sasso (Central Italy), one located at 1.4 km depth, and the other at surface. At the beginning of modern seismology seismic arrays were set up mostly to achieve an improvement of the signal to noise ratio (SNR) by waveform stacking. Later, when the first array methods of analysis were available, seismic arrays were used for monitoring chemical and nuclear explosions. During the last two decades a large number of seismic arrays were deployed in many different environments and for various purposes. This was possible due to the availability of high quality instruments (seismometers and data loggers) and computing facilities. Thus seismic arrays proven very useful in many fields of seismology, such as the monitoring of local and regional seismicity, active volcanoes, artificial seismic sources (explosions), and so on. Many techniques have been developed and applied to any kind of seismic signals, leading to detailed analysis of seismic noise, earthquakes, volcanic and non-volcanic tremor. Source location of emergent signals, study of site effects, investigation of local velocity models, and identification of low energy secondary phases hidden in the seismograms are only some common applications of array seismology.

The great limit of experimental seismology is the shallowness of any instruments. In fact, even the deepest borehole station reach a depth which is less than a thousandth of the Earth radius. Recording seismic signals in the deep interior of the Earth, where surface effects and background noise could be negligible, would give a renewed opportunity to the investigation of deepest structure of the planet. In this thesis I studied seismic data recorded by an array located 1.4 km deep. This is still a very shallow depth, if compared

with the crust thickness, surface effects are still present and local noise is far from being negligible. However, the analysis of these data, and the comparison with data recorded by a surface array in the same area, constitutes an unprecedented opportunity. UNDERSEIS array is operating since 2003 inside the underground Laboratorio Nazionale del Gran Sasso (INFN), beneath Mt.Gran Sasso at 1.4 km depth. It significantly contributes to the detection of microearthquakes in the Gran Sasso area, and was useful in the monitoring of the local seismicity during the seismic crisis started on 6 April 2009. In 2007 another seismic array was installed for six months upon Mt.Gran Sasso, in a site named Fontari. Both arrays are composed by three component, short period stations.

The principle of seismic arrays is to obtain a spatial sampling of a coherent seismic wavefield. This requires that the array must be composed of instruments deployed in a geologically homogeneous area at distances such that the seismic signals to be studied maintain significant similarity among the array stations. If the recorded waveforms have similar shape, except for the time delay among the stations and local noise, then the array methods of analysis can be applied to investigate the properties of coherent signals. For its underground location and geologically homogeneous rock, the laboratory where UNDERSEIS array is located is a very good site to record earthquakes in conditions of low seismic noise.

The performances of UNDERSEIS array will be illustrated in this thesis through the description of results obtained by the analysis of local and regional earthquakes. Fontari array was installed to compare the seismic signals recorded at surface with those recorded at depth. In six months of acquisition hundreds of earthquakes were recorded. I analyzed all data recorded by UNDERSEIS array from 2004 to 2009 and all data recorded by Fontari array for 6 months in 2007. Numerous comparisons have been done on signals recorded by the two arrays and between the results of array and polarization analysis.

The coherence of the seismic signals among the array stations was computed on all available data to measure the waveform similarity and to detect potentially interesting events different from regular tectonic earthquakes. This analysis could be a useful tool in a continuous monitoring of seismic signals,

being sensitive to any variations of background coherent noise not related with earthquakes.

In this work I used three techniques of array analysis, BF (Beam Forming), HR (High Resolution), ZLCC (Zero Lag Cross Correlation). These array methods, together with detailed analysis of polarization, allow to study the wavefield through the values of slowness and backazimuth. Horizontal-to-vertical spectral ratios technique has been also applied to earthquake signals to identify the fundamental frequency of the investigated site. The seismic sequence triggered by the earthquake of April 6, 2009 $M_w6.3$ was well recorded by the array UNDERSEIS, 23 km from the epicenter of the main shock. Seismic signals recorded in the period April-May 2009 will be first described through their coherence and then analyzed with array and polarization techniques to identify anomalous and/or peculiar characteristics of the local seismicity during this period. Finally a statistical analysis has been applied to the parameters estimated by array and polarization techniques. The comparison of the results obtained at surface and at depth shows some significant and interesting differences.

Chapter 1

Description of arrays

A *seismic array* (or antenna) is a set of seismic instruments placed at discrete points of an area that is preferably chosen plane and geologically homogeneous. It is a powerful tool for several purposes: improvement of signal to noise ratio (SNR) with respect to individual recordings, study of site effects, search of velocity models of the Earth'crust, high-resolution tomographic images and many others [1]. Another useful application is in volcanic areas to study signals that do not show sharp onset. The aim is to obtain a spatial sampling of the seismic wavefield in time. In the area where a seismic array is installed, it produces high-quality data compared with local or regional seismic networks, as the incident wavefield maintains significant similarity throughout the different array stations. The recorded waveforms must be very similar, except for the time delay among the stations and local noise. Often large aperture arrays can be considered as local networks. Seismic arrays may be used in addition to the networks for local monitoring of hazardous areas.

Dense spatial samples of the seismic wavefield allow us to detect small amplitude signals compared with seismic noise, especially those with not well defined onset. One of the main advantages of using arrays is a detailed analysis of the recorded wavefield by estimating ray parameter and propagation backazimuth with the *array techniques*. The information obtained from array recordings can be used in many different ways to study fine-scale structure of the Earth's interior. Array recordings are also useful to analyze

the characteristics of seismic noise in an area.

In the design of an array, many factors must be considered: the array extension, the instrument spacing, the number of stations, the sensor features and the purposes of experiment. The array aperture depends on the characteristics of waves to analyze and on their frequency content. The inter-station spacing concerns the largest resolvable wave number, while the use of many stations generally improves the performances. The geometry of the array is important for a good "array response" and to reduce the spatial aliasing. Three component stations are necessary to determine accurately the wave types of the recorded signals. This condition is required to apply a polarization analysis and to distinguish among different phases. Generally, a good configuration is obtained by circular array with not uniform spacing of the stations in order to deal with different wavelength. But quite often the array installation is constrained by practical factors, as geological conditions or expensive deployment, that limit the extent and the achievement of an optimal configuration.

A homogeneous site response is important to have the recordings more similar among them. The array should be located in an area with little topographic variation, since they can amplify or attenuate seismic signals. The stacking of all signals, each one shifted in time of an appropriate amount to compensate for the propagation delay, will improve the SNR. All the seismic stations must have the same characteristics and must be synchronized among them. This last condition allows us to apply different array techniques to analyze the kinematics characteristics of the recorded seismic waves. Most array methods assume a plane wavefronts arriving at the array. This approximation is generally used, but if the hypocenter is close to the antenna, spherical wavefronts must be considered. The number of seismic stations and their configuration, together with the geological and environmental characteristics of the site, determine the resolution capability of an array.

This work analyzed data from two seismic arrays located in Central Italy, UNDERSEIS array and Fontari array. The first is permanently installed beneath Mt. Gran Sasso, while the second one was deployed temporarily in 2007. Their configuration, described below, was designed with the aim of
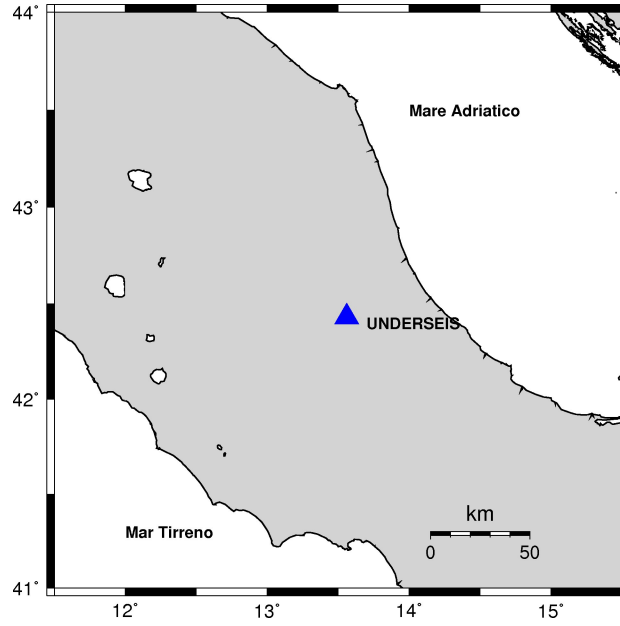
Figure 1.1: UNDERSEIS Array position in Central Italy (42.455°, 13.575°).

studying the features of seismic wavefield recorded at depth and at surface.

1.1 UNDERSEIS Array

UNDERSEIS (UNDERground SEISmic Array) (see fig.1.1) is the first seismic array installed in an underground setting in Italy. It is located in Central Italy, in the Gran Sasso underground Physics Laboratory (LNGS-INFN). The system of many tunnels, where particle physics experiments are realized, is situated about 960 m above sea level. A 1400 m cap of limestone lays above the laboratory. The peculiarity of being inside a mountain is rare to find in the world. UNDERSEIS project [2] was devised in the Nineties, beginning to work in May 2002 with 13 seismometers. In the following years more stations were added, as listed in tab.1.1, reaching the final configuration of 20 stations, shown in fig.1.2.

UNDERSEIS array (UND) consists of 20 short-period MARK L4C-3D, 3-component seismometers characterized by 1 Hz proper frequency. Since 2007 a seismometer was replaced by a broad-band (U33). The aperture of the array is about 500 m, while the average sensor spacing is about 90 m.

Period	Stations number
September 2003	13
January 2004	13
March 2005	16
October 2005	18
September 2006	19
July 2007	20

Table 1.1: List of working stations and relative activation periods.

The configuration of UND is constrained by the underground tunnel geometry and its shape is roughly triangular.

Seismic signals are acquired with a dynamic range of 24 bits and the sampling rate is 100 samples per second. Every station includes a 24 bit A/D converter connected to a central data server by Ethernet link. Temporal synchronization is obtained by a Master Oscillator.

The Mark L4C-3D is a short period seismometer which yields a voltage proportional to the ground velocity. The Mark L4C-3D frequency response function is calculated using its characteristics[1]:

- natural frequency $1Hz$;

- sensitivity $G = 170V/m/s$;

- damping constant $h = 0.707$;

- two zeros at zero;

- poles: $p_{1,2} = -4.44 \pm 4.44i$.

The frequency response function, whose amplitude and phase are shown in fig.1.3, with blue lines, is:

$$T(j\omega) = G \frac{(j\omega)^2}{(j\omega - p_1)(j\omega - p_2)}. \tag{1.1}$$

UNDERSEIS array is located on a main seismogenetic fault of Apennines
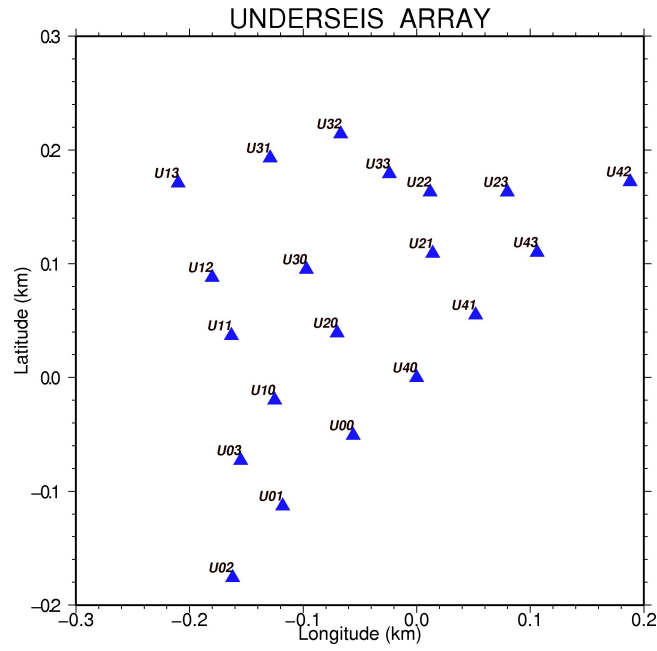
---

[1]Visit www.IRIS.com .

Figure 1.2: UNDERSEIS Array configuration. All seismic stations are three components and only one is a broadband (U33).
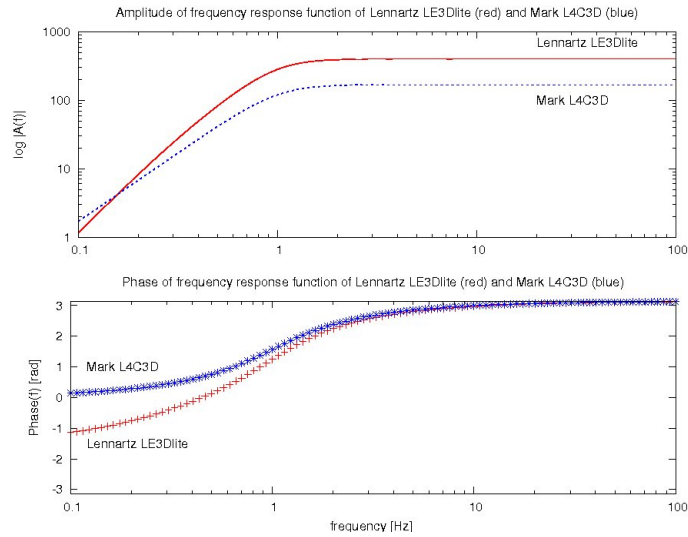

Figure 1.3: Amplitude and phase of the frequency response function Mark L4C-3D (blue, UND) and Lennartz LE3D lite (red, FON).

chain, which produces slow earthquakes continuously monitored through two wide-band geodetic laser interferometers (*Amoruso et al., 2002*)[3]. For its underground location, UND array results to be an ideal site to record earthquakes in conditions of low signal to noise ratio. The recording conditions should be less affected by noise, since the array is away from the free surface. In spite of its position, we will find periods of increased noise level. It meaningfully contributes to the discovery of *microearthquakes* (local magnitude $Ml < 2.5$) in Gran Sasso area. It is particularly important in the monitoring of the local seismic activity in Abruzzo after the recent seismic crisis, improving the completeness of seismic catalogue for the central Apennines. The performances of UNDERSEIS array (preliminarily examined in *Saccorotti et al., 2006*)[4] will be illustrated in this thesis. Instrumental improvements after the first years of operation and detailed analysis show that UNDERSEIS antenna has high capability in detecting and measuring small seismic signals.

1.2   Fontari Array

In June 2007 a temporary array was installed by INGV - Osservatorio Vesuviano at Fontari (Campo Imperatore, Italy). Fontari array (FON) acquired data for about six months, in the period from June 2007 to November 2007. It was composed by six seismometers, Lennartz LE3D lite, with 3 components and natural frequency of 1 Hz. The aperture of array was about 600 m (fig.1.4). Seismic signals were acquired with a dynamic range of 20 bits and the sampling rate was 125 samples per second. Lennartz LE3D lite frequency response function is calculated using its characteristics:

- natural frequency $1Hz$;

- sensitivity $G_1 = 400V/m/s$;

- damping constant $h = 0.707$;

- three zeros at zero;
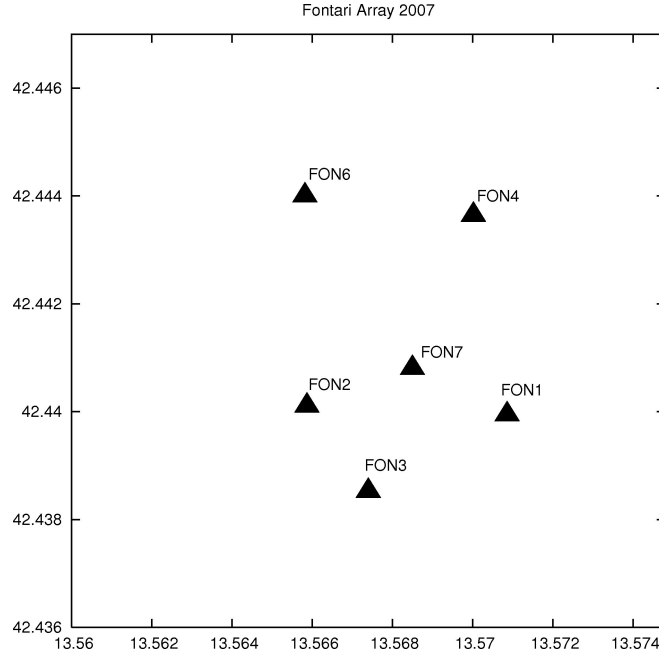
- poles: $p_{1,2} = -4.21 \pm 4.66i$; $p_3 = -2.105$.

Figure 1.4: Fontari Array configuration (42.441°, 13.567°).

The frequency response function, whose amplitude and phase are drawn in fig.1.3, with red lines, is:

$$T\left(j\omega\right) = G_1 \frac{(j\omega)^3}{(j\omega - p_1)(j\omega - p_2)(j\omega - p_3)}. \tag{1.2}$$

FON array was installed to compare the seismic signals recorded at surface with those recorded at UND array. In six months of acquisition, about one thousand earthquakes were recorded. The horizontal distance between FON and UND arrays is about 1.5 km, while the elevation differs by about 1 km (fig.1.5).

1.3 Geological setting of the Gran Sasso area

Gran Sasso massif is the highest mountain of the Apennines chain with 2912 meters asl. of 'Corno Grande' peak. The Apennines chain was generated by the contemporaneous opening of the Tyrrhenian Sea, the eastward migration of a compressive front and the retreat of the lithospheric plate dipping below
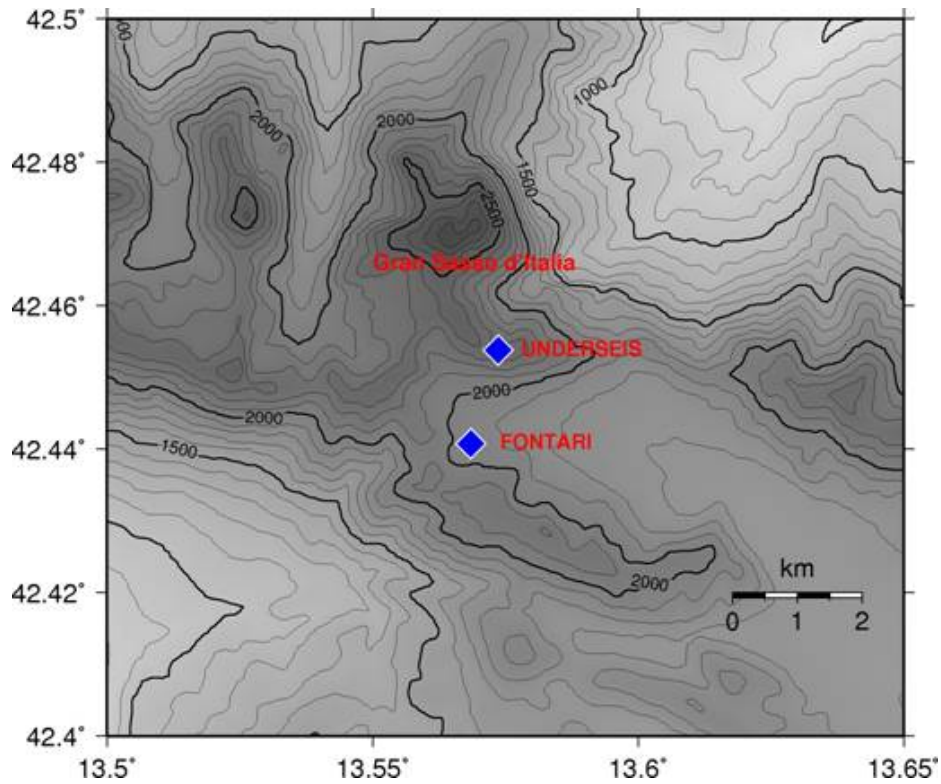
Figure 1.5: Fontari and UNDERSEIS arrays. Topographic image of the Gran Sasso area.

the Italian peninsula.

Since Miocene, it was affected by compressive tectonics, represented by NW-SE striking thrusts, whose evidences are in the formation of an impressive topographic ridge dominating the landscape of central Apennines. The subsequent extensional tectonics was conditioned by the geometry of the older thrust systems, resulting in the development of three main normal fault systems in the Gran Sasso region: the Assergi, Campo Imperatore and Mt.Cappucciata-Mt.San Vito (*Galli and Galadini, 2002*)[5]. Since the late Pliocene, NW-SE striking normal faults were responsible for the formation of large intermountain basins and for the recent filling of intramontane plains by alluvial deposit. This fault system, located 35 km south of the 2009 L'Aquila earthquake, emerged by paleoseismological analysis [5]. Paleoseismic data confirmed the presence of active seismic fault along the Gran Sasso massif with slip of 15 meters in the last 18000 years. Continuous

ground deformation measurements with an underground laser strainmeter [41] (installed in the same tunnel where UNDERSEIS array is located) show the presence of aseismic and coseismic dislocation processes. Subsequently the periods of thrust and compression generated a system of fractures and subsidence as Val Maone, Venacquaro Valley, Campo Pericoli, Campo Imperatore. Moreover, a Moho doubling under the central Apennines reflects the geometry of the mantle wedge between the subducting Adriatic lithosphere and the Apennines chain.

From a geomorphological point of view, the Gran Sasso massif is composed of sedimentary dolomite, limestone (Southern block), generally compact, and marl (North block). There are many infiltration processes, typical of karst areas. In the Apennines, fluids may activate faults responsible for large earthquakes [6, 7].

Active extension and earthquakes are mainly concentrated along the axial belt of the chain, close to the main topographic ridge. The main event was the historic earthquake of Avezzano in 1915 with a magnitude $M_s = 6.9$. Historical seismicity indicates that the region was affected by destructive earthquakes. Among the strongest occurred in a radius of about 50 km from the array are the 1349 ($M_{eq} = 6.3$, Abruzzi Apennines), 1461 ($M_{eq} = 6.3$, L'Aquila), 1703 ($M_{eq} = 6.7$, L'Aquila), 1762 ($M_{eq} = 5.6$, L'Aquila).

Located in the core of Gran Sasso massif, in the tunnel about 1400 m asl, there is the National Laboratory of Gran Sasso (LNGS), owned by the National Institute of Nuclear Physics (INFN), where UNDERSEIS array is installed. LNGS is the largest underground scientific laboratory in the world.

Actually, the area around the Gran Sasso is affected by a considerable seismic activity, associated mainly to distensive NE-SW tectonics, result of stress state of upper crust along the chain. Many micro-earthquake with local magnitude $Ml = 1$ occurs every day within a radius of about 20 Km from LNGS-INFN. The events concentrate in the upper 15 km of the crust. Among the main purposes of installing the UNDERSEIS array there is the monitoring of local seismicity, in a region of high seismic risk.

1.4 Array response patterns

The response of an N-station array is computed by the *Beam Pattern* function (*Capon*, 1969)[8]:

$$B(S) = \frac{1}{N^2} \left| \sum_{j=1}^{N} \exp(i\omega \overrightarrow{S} \cdot \overrightarrow{r_j}) \right|^2 \tag{1.3}$$

where r_j is the position of the jth station. This function (often called *array transfer function* or *array radiation pattern*) describes the shape of the broad-band wavenumber spectrum for a vertically-incident plane wave. It is useful to check the effect of spatial aliasing, which may yield biased estimation of **S** (or **k**), and to understand the influence of the array geometry on its resolution. A sharp peak at the center of k-space is an ideal response: sharper is the peak at the center, better is the determination of the slowness. An ideal response is obtained with a circular array with many stations. The presence of other peaks around the central maximum represents the spatial aliasing.

Beam pattern spectrum at Fontari array is shown in fig.1.6 for 1 and 3 Hz. The array analysis results are quite independent by the propagation direction at 1 Hz. At high frequency, effects of spatial aliasing are present. UNDERSEIS array is elongated in NE-SW direction. At 1 Hz (fig.1.7), its response shows a large peak around the center, indicating a slightly anisotropic response with NW-SE trend. At 3 Hz, the peak of the correlation function is much sharper than at low frequency. Aliasing peaks are negligible. The consequence of spatial aliasing will be treat in chapter 3. Even though at high frequency seismic signals should be resolved more accurately than at low frequency, the coherence of seismic wavefield usually decreases as the frequency increases. This must be considered in the interpretation of array analysis results.

1.5 Data Pre-Elaboration

I analyzed all data recorded by UND array from 2004 to 2009 and all data recorded by FON array for 6 months in 2007. Preliminary analysis was made
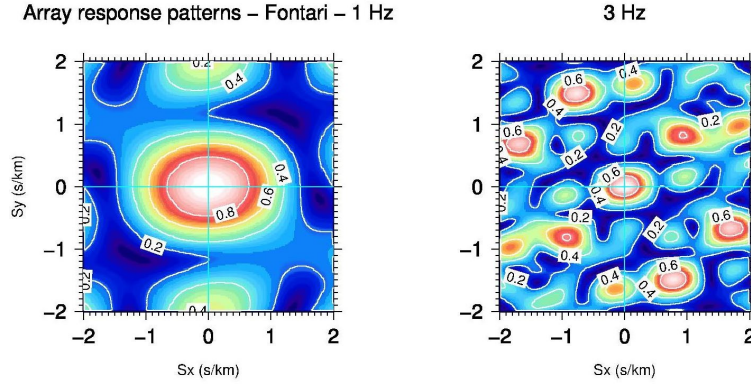
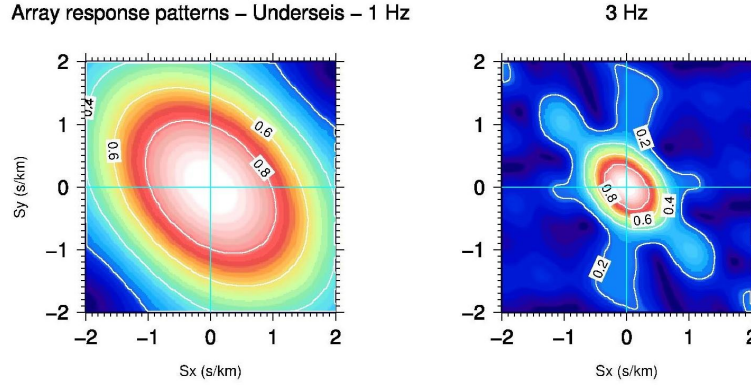Figure 1.6: Fontari array response pattern at two different frequency (left 1 Hz, right 3 Hz).

Figure 1.7: UNDERSEIS array response pattern at two different frequency (left 1 Hz, right 3 Hz).

on FON data. The first step was to look hour by hour all data of FON, to create a catalog of events. Then, from the catalog the events were selected on the basis of their amplitude and of a good signal to noise ratio. The next step was the selection of temporal windows containing the chosen events and then the same was made on UND data. Temporal windows were preferably chosen with the same length to have a better comparison. Recorded data were converted in sac format (Seismic Analysis Code, www.llnl.gov/sac) in order to be plotted and elaborated easily. Then, data were organized in short files which are more handly.

After this procedure, about 60 earthquakes (see fig.1.8 which afterwards
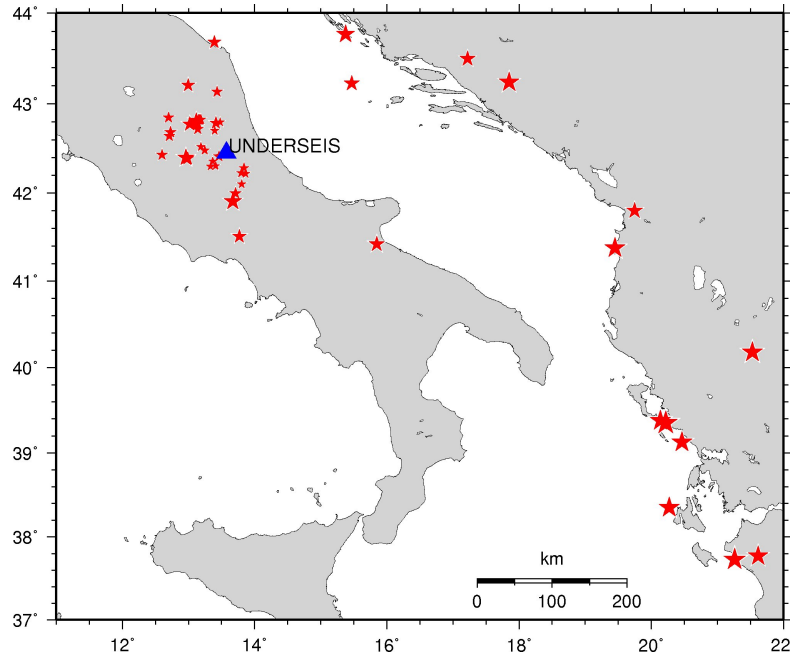
Figure 1.8: Selection of strongest events chosen for analysis. The stars indicate their epicenters.

name our data set) were selected. Several analysis such as some array techniques (BF, HR, ZLCC), polarization analysis, site response study, coherence calculus and statistical analysis were applied to evidence the differences or analogies between underground stations and surface ones. The same was done on other earthquakes recorded at UNDERSEIS array in previous years and after 2007. At the end of this chapter there is the table of the 60 selected earthquakes (tab.1.2). Their location was taken by the ISIDE catalog[2]. The backazimuth variations between the two arrays are negligible.

Backazimuth distribution of selected earthquake onset is shown in fig.1.9. The histogram shows some preferred directions. The most of selected earthquakes is located in Central Italy, around Gran Sasso massif, while the most of regional events come from East, South-East and North-East with respect to UNDERSEIS array. This graph will be important for the next statistical analysis.

Afterward, two examples of earthquake are shown. For each one seismo-

---

[2]see http://iside.rm.ingv.it/iside/standar
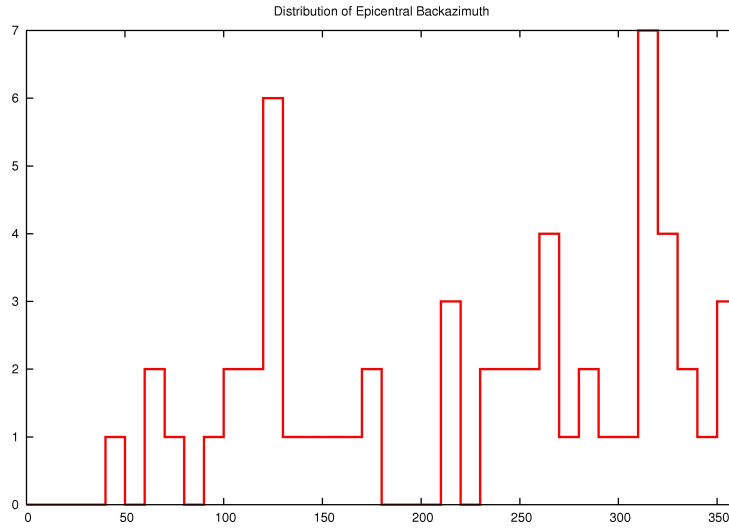
Figure 1.9: Backazimuth distribution of selected earthquake onset. Some seismic events have common backazimuth values.

grams and their spectra are shown for one station of each array. The first earthquake occurred on September 26 2007, at 08:14 am (see fig.1.10). It is a local earthquake with Ml = 1.8 located at 42.356°, 13.367° (near the city of L'Aquila).

It has a duration of about 30 seconds and FON seismograms immediately show more complex wavefield than those of UND. As expected for its position and as we will see from the array analysis, the contribution of surface waves at UNDERSEIS array is practically negligible. FON spectra show peaks at higher frequency of UND. They are larger and have higher amplitude compared to the second. We see that the amplitude of the seismic signal is smaller underground than at surface (see fig.1.10 and fig.1.11). It is clear from both graphs: the first, in which on left seismograms of earthquake are shown and the second in which only the noise after the same event is shown (but the situation is the same for any temporal windows of noise). This is what we aspect for the relative position of the two arrays. The environment of the two arrays are different as it will be explained in more detail later. Since FON array is installed on free surface its recordings are more noisy. For it the characteristics of free surface as weather effect or human activity are more evident.
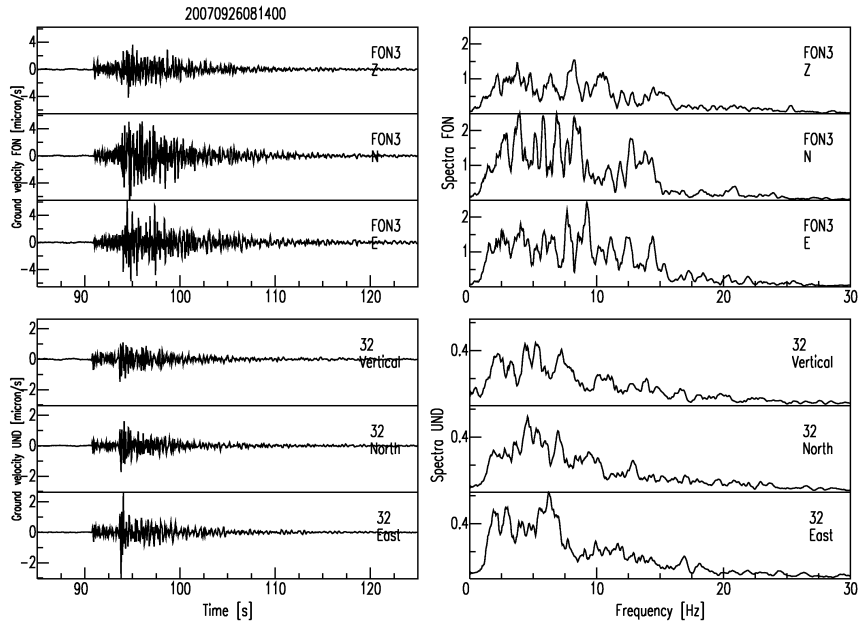
Figure 1.10: 200709260814 earthquake. Seismograms and spectra at FON (FON3, top) and UND stations (U32, bottom).
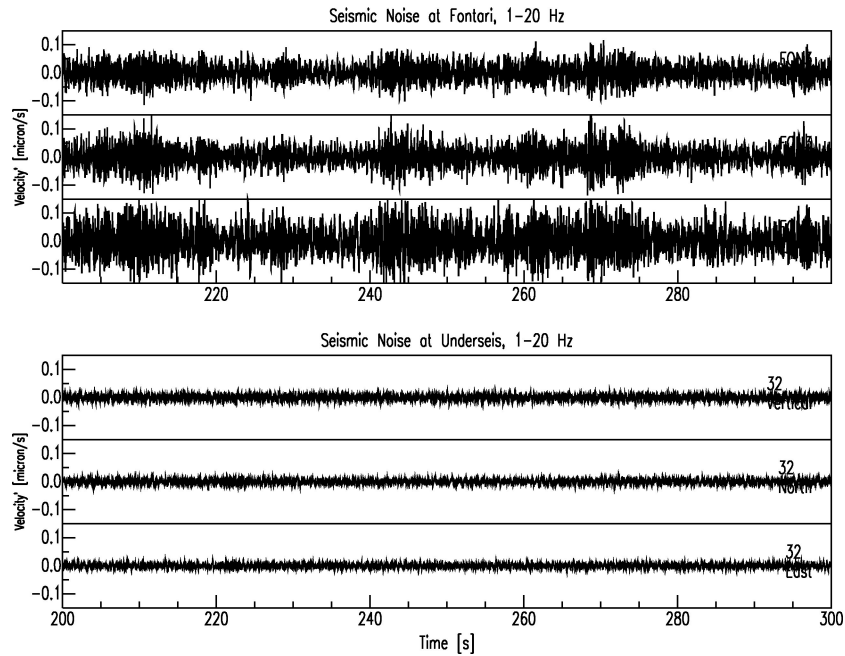
Figure 1.11: 200709260814 noise after the earthquake (FON3 and U32).
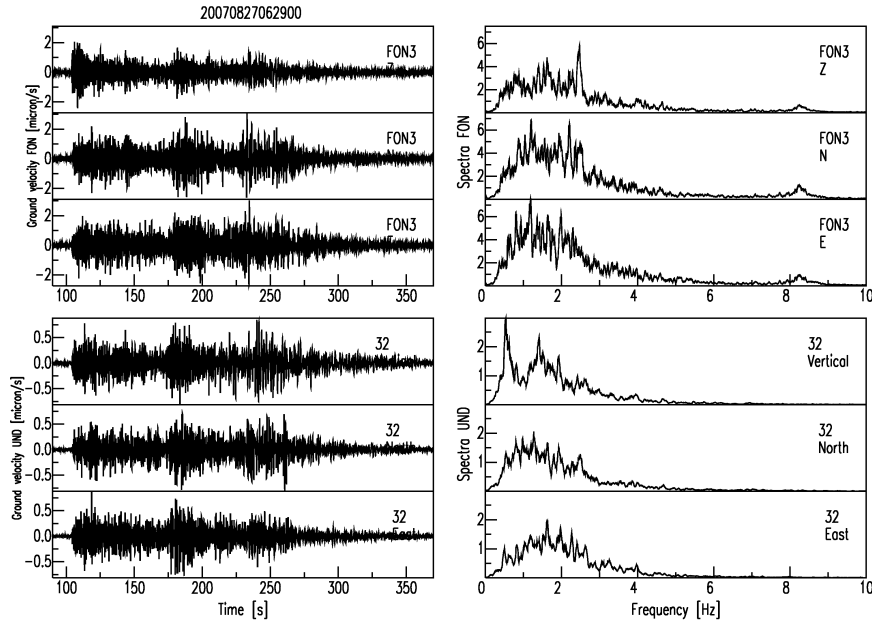
Figure 1.12: 200708270629 earthquake. Seismograms and spectra at FON and UND stations (FON3 and U32).

The second event occurred on August 27 2007, at 06:29 am (see fig.1.12). It is a regional earthquake with Ml = 4.7 located at 38.35°, 20.27° (Greece). It has a duration of about five minutes and also in this case FON spectrum shows peaks at higher frequency compared with UND and greater amplitude compared with the second. The spectrum does not exceed five Hz because it is a regional earthquake.

These earthquakes will be studied in detail in the next chapters. Numerous comparisons will be done on signals recorded by the two arrays. In fig.1.13 and fig.1.14, the onset of 200709280659 earthquake is shown for both arrays. As we can see, the recordings are more similar among all stations of UNDERSEIS array respect to Fontari where noise can be different for each stations. Obviously, seismic waves arrive first to underground array. Moreover we find a different duration of the same earthquake at the two arrays. The duration depends on magnitude, on source-receiver distance and seismic noise. In our case, also amplitude is an important factor. As the location and environment between two arrays is different, we see longer

earthquakes at depth and the differences are in the range 5-40 sec. Later it will be also shown that UND array is a good antenna to record telesismic waves.
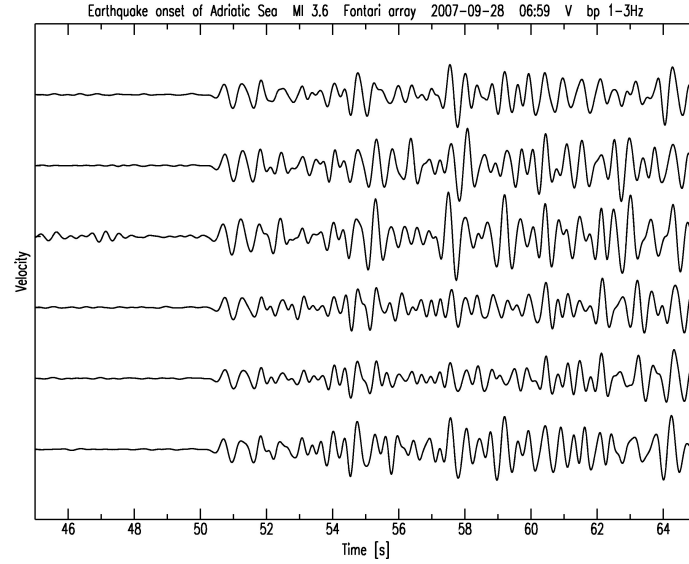
Figure 1.13: 200709280659 earthquake onset at all stations of Fontari array, Vertical components.
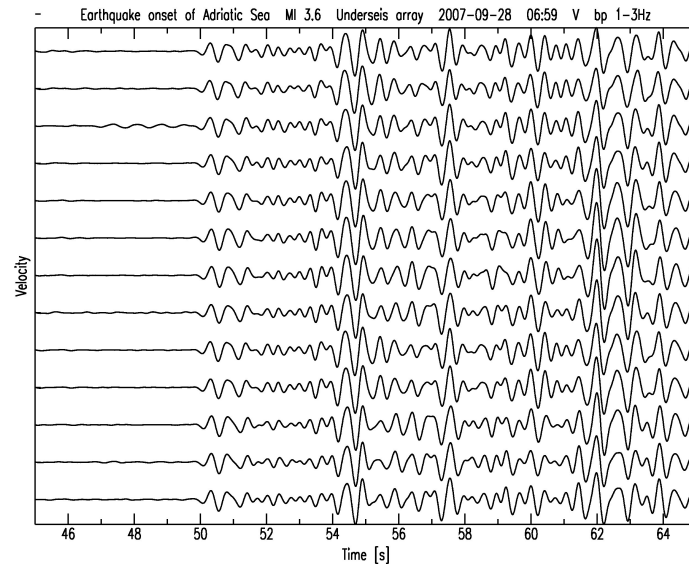
Figure 1.14: 200709280659 earthquake onset at all stations of UNDERSEIS array, Vertical components.

1.6 Local Magnitude

We need a magnitude formula to estimate the size of local earthquakes and to have an idea of their seismic energy. Gran Sasso area is rich of local earthquakes but many of them are not listed in the catalogs as they are very small. These earthquakes are often called *microearthquakes.*

In the 1930, Wadati and Richter were the first to think up a scale for the earthquake size based on measurements of seismic phase amplitudes, as the amplitude is related to the seismic energy. They introduced the concept of earthquake magnitude as a measure of the relative size between earthquakes. Different magnitude scales exist and they are based on two assumptions. The first is that between two different earthquakes, the "larger" event will on average produce larger amplitude arrivals, if the two events are recorded in the same source-receiver geometry condition. The second is that the effects of geometric spreading and attenuation are known in a statistical sense. The general form of all magnitude scales is given by

$$M = \log \frac{A}{T} + f(\Delta, h) + C_s + C_r \tag{1.4}$$

(*Lay and Wallace, 1995*)[55] where A is the ground displacement of the phase on which the amplitude scale is based, T is the period of the signal, f is a correction for epicentral distance correction (Δ) and focal depth (h), C_s is a correction for the site effect and C_r is a source region correction. Eq.(1.4) is appropriately modified for the different magnitude scales. Four magnitude scales are in use today: Ml (local magnitude), Mb (body-wave magnitude), Ms (surface-wave magnitude), Mw (moment magnitude). The last one uses the relationship between seismic energy ,that is proportional to seismic moment, and magnitude. It is more reliable because the total size of an earthquake is best represented by seismic moment. As the seismic wave amplitudes of earthquakes vary enormously, the logarithm scale is used. In fact a unit increase in magnitude corresponds to a 10-fold increase in amplitude of ground displacement.

For small size earthquakes, the local magnitude (Ml) is used. For the law of local magnitude, two factors are important: the local small earthquakes generate negligible surface waves and they are significantly affected by local
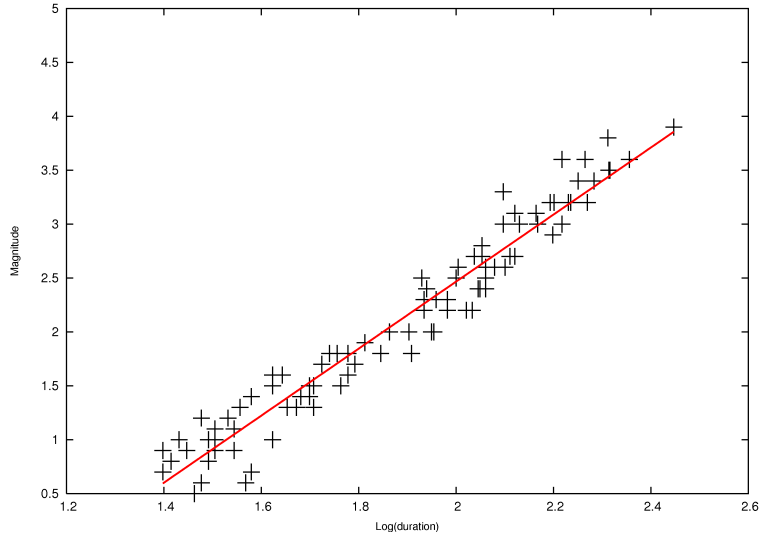
Figure 1.15: Linear fit of Magnitude versus duration.

conditions (site effects, radiation pattern, attenuation). Therefore, the most stable and easily measurable parameter for the formula is the duration of the event instead of its amplitude. The used formula is

$$M_L = A \log x + B \qquad (1.5)$$

where x is the duration of an event and A,B are two experimental parameters. The form is similar to the original Ml . I used magnitude values of Italian seismic Network for about 100 earthquakes of different size. For each of these, I calculated temporal length by *rms* of signals and then I took the best fit of these data to compute A and B values (see fig.1.15).

$A = 3.146$

$B = -3.817$

In this way knowing only the earthquake duration, it is possible to estimate the earthquake magnitude. The graphic of this equation is shown in figure fig.1.16.

For example, a local small earthquake, not listed in the catalog, is shown in fig.1.17. To estimate the magnitude of this event, its duration is calculated. It is about 19 seconds and so its magnitude by eq.(1.5) is 0.2.
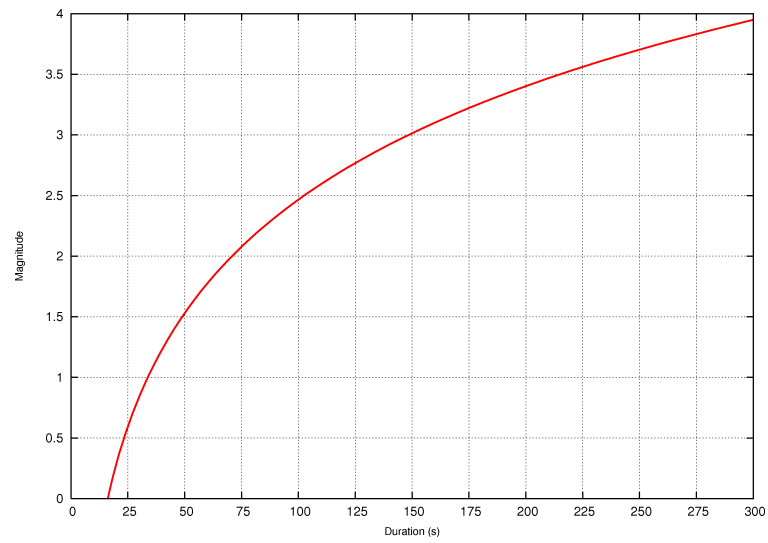
Figure 1.16: Magnitude versus duration for Gran Sasso area.
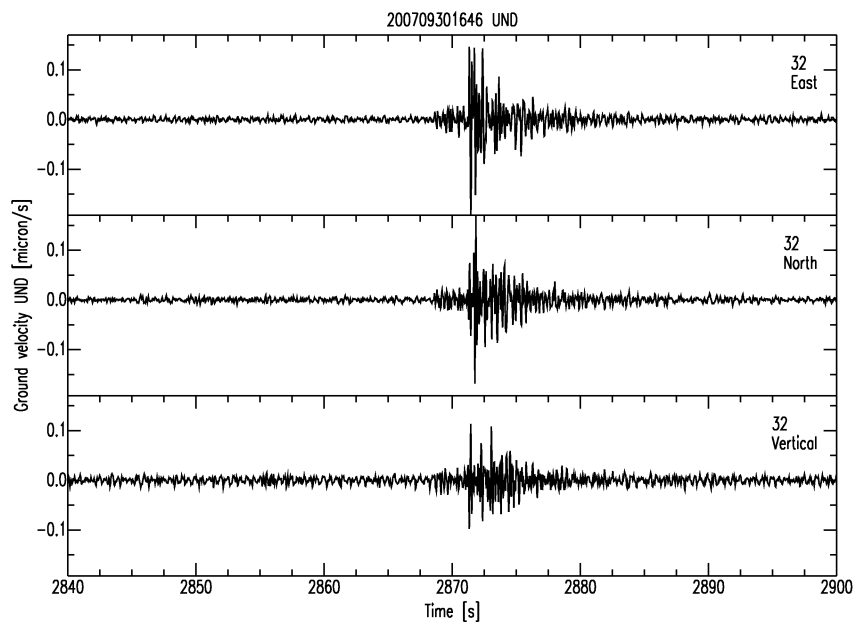
Figure 1.17: 200709300164 earthquake. Seismograms of an UND station (U32).

Earthquake	Lat	Lon	Depth (Km)	M	Distance (Km)	Backazimuth
200706190349	42.48	13.25	9.6	2.2	26.2	279
200706280153	42.52	13.19	10.3	2.1	32	286
200706291809	39.35	20.22	25	5.4	656.9	119
200706292221	39.38	20.14	10	4.8	649.3	119
200707101158	41.42	15.85	1.8	3.6	220.8	120
200707171823	40.18	21.53	10	4.7	711.5	108
200707181053	43.77	15.38	20	4.2	208.8	44
200707202205	42.85	12.7	5	2.5	83.7	303
200707221725	41.91	13.67	15.7	4	60.2	171
200707270458	42.82	13.16	7.8	2.6	53.7	322
200707280040	43.68	13.39	8.2	3.1	138.5	354
200707312250	42.31	13.42	9.7	1.7	18.6	219
200707312250	42.31	13.41	9.3	1.7	19	219
200708061709	42.41	13.46	10.2	2.5	8.7	249
200708062300	42.42	13.47	10.7	1.4	8.1	254
200708070031	42.42	13.47	10	1.3	7.3	255
200708120151	42.78	13.02	7.3	3.4	58	310
200708121121	39.13	20.47	2.8	4.7	688.4	120
200708121924	42.78	13.04	9.5	2.3	57	312
200708121931	42.78	13.04	9.4	2.2	56.8	311
200708160028	42.81	13.12	8.2	3.5	54.9	318
200708160424	42.82	13.13	9.1	1.8	54.7	320
200708161135	42.31	13.41	9.7	1.9	19.4	219
200708162045	41.51	13.77	6.9	3.2	104.9	170
200708230930	43.14	13.43	3	2.6	78	352
200708232337	42.82	13.17	7.9	2.5	52.9	323
200708250354	43.5	17.22	40	3.5	320.4	67
200708270629	38.35	20.27	10	4.7	727.8	126
200708280906	37.77	21.62	73	4.5	859.7	124

Table 1.2: Table of 60 selected earthquakes recorded by both arrays. Distance and backazimuth are computed with respect to UND array.

Earthquake	Lat	Lon	Depth (Km)	M	Distance (Km)	Backazimuth
200708290400	42.83	13.19	6.1	2.3	52.5	324
200708300420	41.8	19.75	2	3.7	515.6	95
200708301441	42.68	12.73	10.9	2.7	73.2	292
200709011432	42.3	13.33	10.3	1.8	24.1	230
200709031848	42.29	13.84	9.2	2.3	28.8	126
200709050508	41.38	19.45	10	4.8	501.6	101
200709141718	42.72	13.14	1.3	2.5	46.1	312
200709142214	42.77	13.14	7.2	2.2	50.4	316
200709162135	42.36	13.37	9.5	1.7	18.1	241
200709171926	42.1	13.81	22.1	2	42.9	151
200709250028	42.22	13.87	10.5	2	35.3	134
200709260814	42.36	13.37	9.8	1.8	18.4	239
200709271415	42.43	12.6	8.1	2.6	79	269
200709280659	43.23	15.47	20.7	3.6	178.5	60
200710070635	43.21	13	46.8	3.1	96.9	331
200710110356	42.77	13.13	8.6	2.5	51.3	316
200710181541	43.24	17.85	20	4.5	361	74
200710182325	42.8	13.48	11	2.1	40.2	350
200710210354	42.4	12.96	8	3.9	49.2	265
200710250738	42.39	12.99	9.1	2.9	47.5	263
200710250914	42.39	12.99	7.7	2.9	46.9	263
200710270530	37.73	21.26	20	5.1	838.5	126
200710271339	42.23	13.8	21.6	2.2	30.8	140
200711051552	42.79	13.42	9.2	2.8	40.3	342
200711090055	42.7	13.4	9.4	2.1	31.9	335
200711110906	42.64	12.71	10	2.5	73.2	288
200711161235	42	13.71	17.8	2.7	51	165

Table 1.3: Table of 60 selected earthquakes recorded by both arrays. Distance and backazimuth are computed with respect to UND array.

Chapter 2

Coherence

The first analysis applied to all data recorded by UNDERSEIS array was the computation of the coherence of the seismic wavefield among the array stations. It consist in estimating the coefficient of coherence among time recorded series to measure quantitatively their similarity. This procedure allows us to discover all coherent phases of an event that can not be only an earthquake, but also any other natural phenomenon which is present at all stations of the array. This technique isn't valid for seismic networks, where the wavefield is very different among various stations and would lead to low values of coherence. The site choice where deploy seismic stations of an array is very important to improve the coherence. The homogeneous geology and planar topography are necessary to avoid variation of seismic wavefield over short distances. It is important to take into account that coherence for P and S waves decrease as frequency increases and as distance among stations increases.

Coherence could be very useful in a process control, as continuous monitoring by seismic array (as the task of UNDERSEIS array), leading to discovery of coherent signals. Coherence was calculated on all data recorded by UNDERSEIS array since 2003. In these years, some *anomalies* of coherence value emerged, as will be explained later.

2.1 Definition of coherence

The coherence between two signals (*Foster and Guinzy, 1967; Hinich and Clay, 1968*)[12, 13] was introduced by Wiener in 1930. Two time series $x(t)$ and $y(t)$ of the same length are considered. Their power spectra $f_{xx}(\omega)$ and $f_{yy}(\omega)$ and their cross spectrum $f_{xy}(\omega)$ are calculated. The *coefficient of coherence* is defined as

$$\gamma_{xy}(\omega) = \frac{|f_{xy}(\omega)|}{\sqrt{f_{xx}(\omega)f_{yy}(\omega)}} \tag{2.1}$$

if $f_{xx}(\omega)f_{yy}(\omega) > 0$, otherwise it vanishes. The eq.(2.1) is also called *cross-correlation spectrum*. By its definition it is clear that $0 < \gamma_{xy}(\omega) < 1$. The coherence is similar to cross-correlation but is calculated in the frequency domain where many applications, are favored. Theoretically, the formula (2.1) will always give one, independent of frequency and this would be not aN useful outcome. This is avoided by applying a smoothing over a frequency band in eq.(2.1). As in the spectrum, the use of a limit data window produces estimates of parameter which do not allow a correct application of the theoretical formula. For example, in the observational case, it is impossible to have an infinite integration interval and so it is impossibile to eliminate completely the windowing effect. Moreover shorter is temporal window, stronger is the smoothing effect. As an array is composed of more than two stations, the eq.(2.1) must be generalized for all couples of stations and obviously for the three components of each seismograms. It becomes

$$\gamma(\omega) = \sum_{i \neq j} \frac{|c_{ij}(\omega)|}{\sqrt{c_{ii}(\omega)c_{jj}(\omega)}} \tag{2.2}$$

where i,j are indexes for different stations, taking values from 1 to N (N is total number of signals). $c_{ij}(\omega)$ is cross-spectrum matrix with smoothing defined by

$$c_{ij}(\omega) = \sum_{k=-N}^{N} a_k F_i^*(\omega + k\Delta\omega)F_j(\omega + k\Delta\omega) \tag{2.3}$$

where $F_i(\omega)$ is Fourier transform of i-signal and a_k are smoothing coefficient

taking value in the range 0-1. Often it is more useful to report coherence in function of time, to compare immediately it with seismograms of the event to which it relates. This is possible taking mean coherence in a selected frequency band for each windows of analyzed data and next taking a mean of three components. In general, when coherence is plotted versus time, a steep peak indicates an earthquake. High values are obtained especially for local earthquakes. Coherence calculus is done by a PC through an appropriate program in C language.

2.2 Applications of coherence

At UNDERSEIS array, coherence analysis shows a value of background noise of about 0.35 until 2007 and 0.4 in the next years after improvement of the amplification of stations's recorder while at Fontari array it is about 0.35. In the graphs of coherence versus time, this is important because a variation of background noise indicates the presence at that time of a coherent event at all stations of the array. For many calculi it is necessary to resample FON signals to have the same sampling rate of UND. For the most of subsequent graphs only one sliding window of the same length (same number of samples) for two arrays is used. In this way the value of coherence will be independent by the choice of sliding window. The displayed value of coherence is a mean for the three ground components.

As noise is coherent at low frequency, we expect for it a close curve of the coherence with a maximum around low frequencies. For example again for 20070926 day, in fig.2.1 and fig.2.2 noise coherence of two arrays is shown. The coherence is relative to temporal window of top seismogram. From observations of numerous windows containing only noise, we could see that at UNDERSEIS array the noise is coherent at higher frequencies than Fontari, arriving until 4 Hz. This is evident even if only two stations for each array are used for calculus (see fig.2.3 and fig.2.4). Different tests are made between couple of stations of the same array. In these cases coherence show similar values at depth and different values among the couple of superficial stations. Fontari array is installed on free surface and its recordings are quite different among them. Some stations are more noisy than others and so among

the stations, noise can be more or less coherent. At UNDERSEIS array the amplitude and the characteristics of noise are very similar among all stations. Although the noise is spatially uncorrelated, there are some periods of time that even in the absence of earthquakes, probably for particular meteorological conditions, coherent seismic signals may propagate across the array. We noticed this phenomenon in some cases at UNDERSEIS array.

Another test (fig.2.5) is to use some stations taken from two arrays to form a unique array of 12 stations (six from FON and six from UND). The frequencies at which the noise is coherent are almost the same of precedent case of FON array (see black line in fig.2.5). Then the presence of FON recordings bias the result.

Analyzing the window in which 200709260814 earthquake is included, the curve of coherence is more large compared to the noise and it remains large until 30 Hz as this event is local respect to the arrays (fig.2.6 and fig.2.7). The trend of two lines is unlike. Unlike Fontari, at UNDERSEIS array it remains high for almost all frequency. In the recording of an earthquake, at depth seismograms are more similar in a large band of frequency. In the case of the unique array, as previously, the presence of FON stations bias the trend of coherence (see green line in fig.2.5). Then recordings between two arrays are quite different, as coherence assumes a mean value lower than two other values. As noted by *Vernon* [14] the measured seismic wavefield can be distorted substantially over short distances, scale lengths of 500 meters, also for sites that appear to be very similar. In my studies, principal differences between two recordings of the same wavefield concern the coda and the amplitude of an earthquake. Other site effects will be treated in chapter 5. From these and subsequent observations, we can see that the same wavefield is much coherent at UNDERSEIS array than at Fontari and this result is particularly evident for the earthquake onset (fig.2.8). In this last sliding window, only ten seconds from direct P were analyzed. In general the maximum coherence value for a same earthquake is obtained at UNDERSEIS array.

The situation is the same for another local earthquake 200710110356, located at 42.477°, 13.126° (Monti Sibillini, near Norcia) with Ml =2.5 (black and red color respectively for FON and UND in fig.2.9). Also in this case,
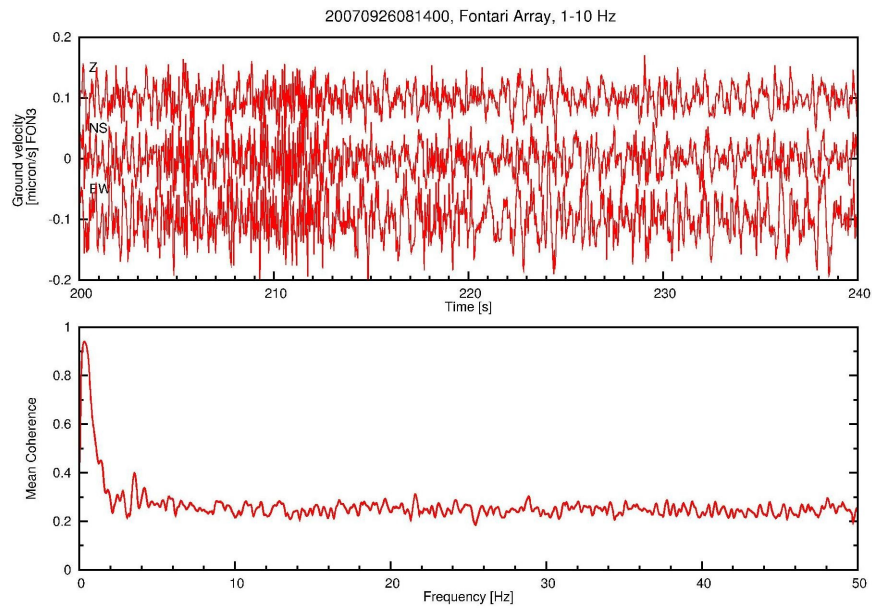
Figure 2.1: 20070926 noise. Seismograms and coherence calculated between all stations of FON.
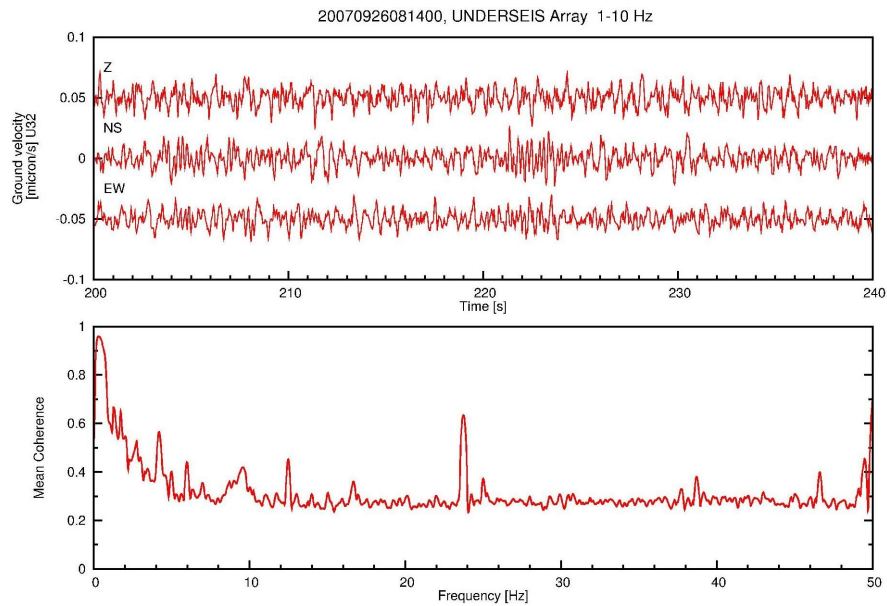
Figure 2.2: 20070926 noise. Seismograms and coherence calculated between all stations of UND.
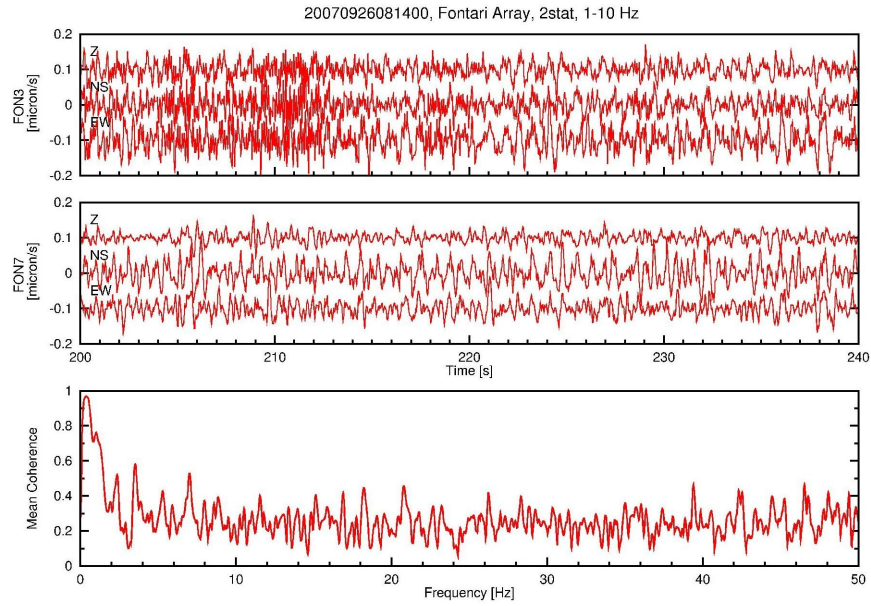
Figure 2.3: 20070926 noise. Seismograms and coherence calculated among two stations of FON.
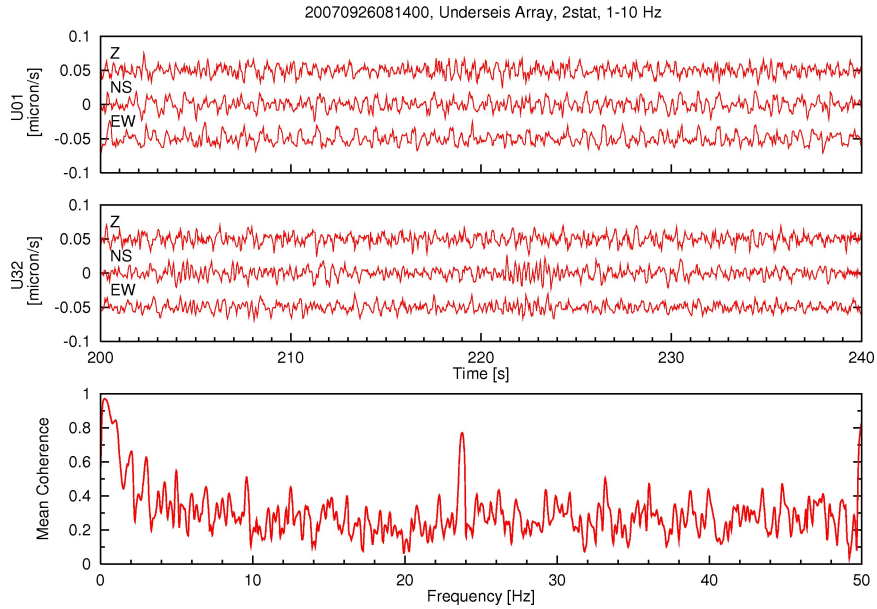
Figure 2.4: 20070926 noise. Seismograms and coherence calculated among two stations of UND.
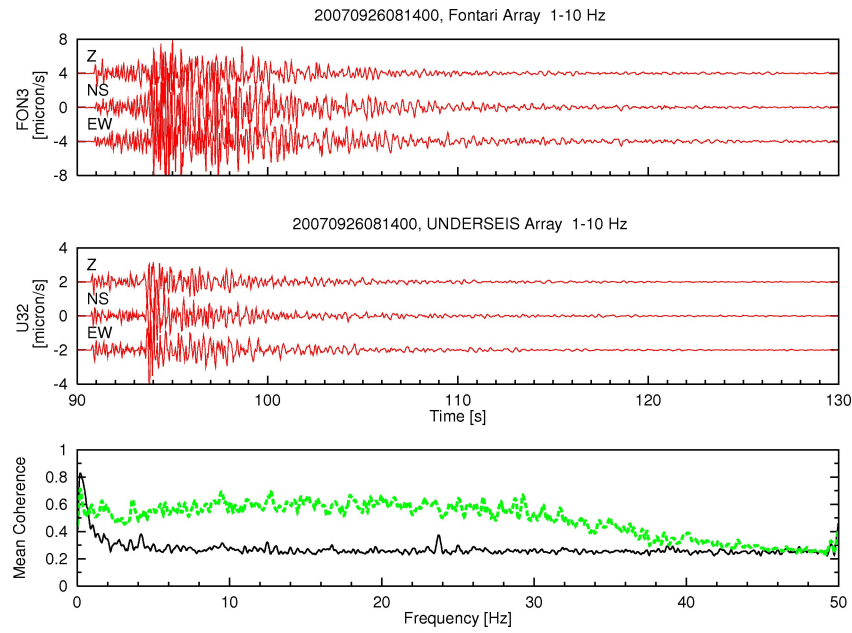
Figure 2.5: 20070926 noise(with black line) and earthquake (with green line). Seismograms and coherence calculated between stations of FON and UND.
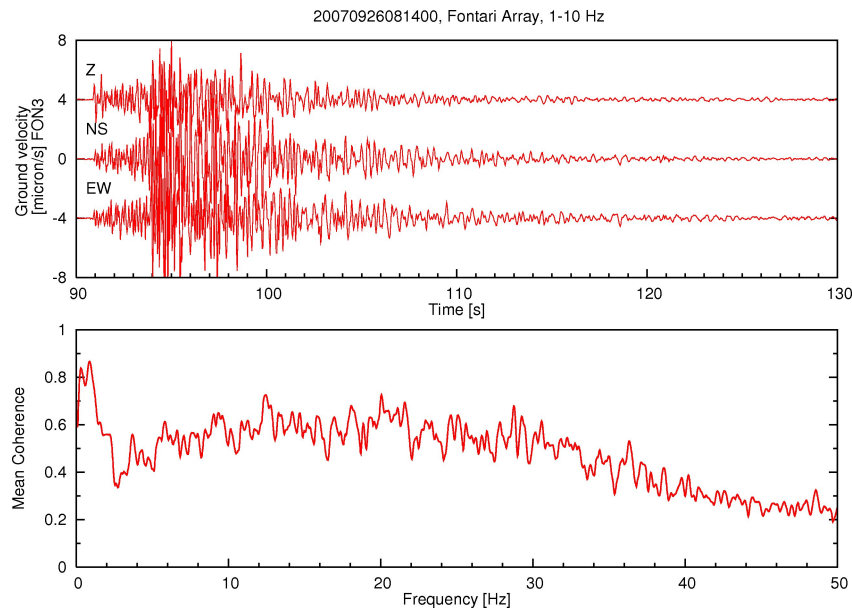
Figure 2.6: 200709260814 earthquake. Seismograms and coherence calculated between stations of FON.
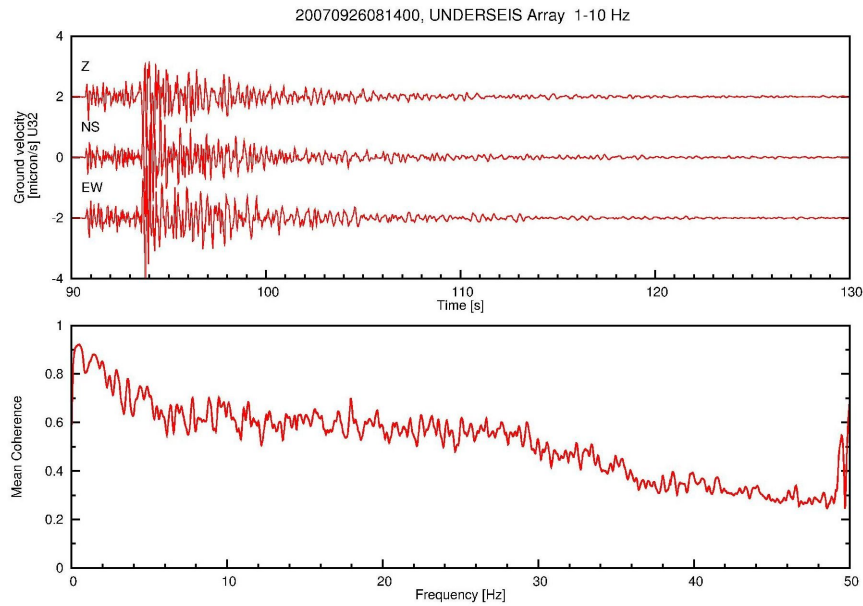
Figure 2.7: 200709260814 earthquake. Seismograms and coherence calculated between stations of UND.
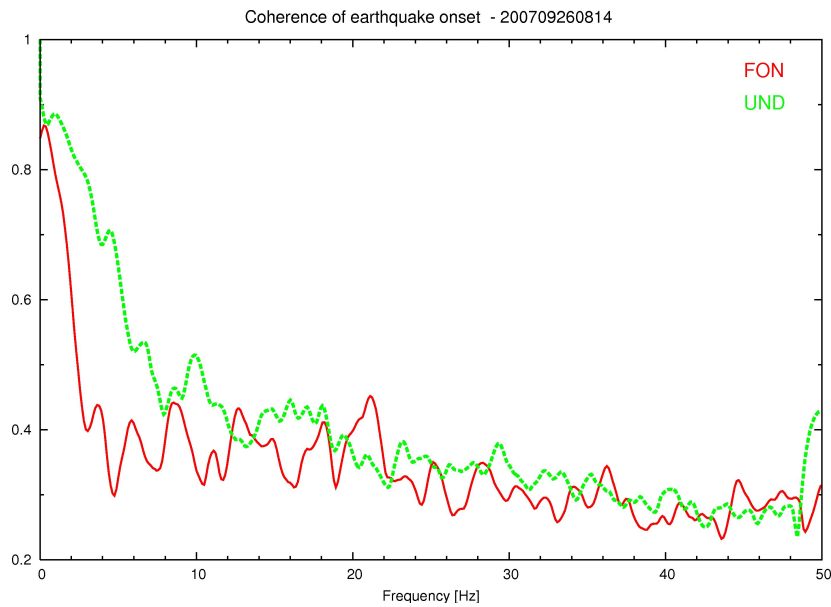
Figure 2.8: 200709260814 earthquake. Seismograms and coherence of FON(red) and UND(green) earthquake onset.

UNDERSEIS coherence is higher than Fontari in a large band of frequency. The presence of Fontari stations reduces coherence value calculated using stations between two arrays (see green line in fig.2.9).

If the same procedure is applied to a regional earthquake, for example 200708270629, which has already been considered before, we see that the curve of the coherence for both arrays (black and red color respectively for FON and UND in fig.2.10) is closer than local one. The waves composing the earthquake are more coherent at UND than at FON in a large band of frequency. Then, as seen for local earthquakes, we understand that UND recordings are more similar among them than those of FON particularly for the beginning of the earthquake and showing less background noise. UNDERSEIS array records more coherent seismic wavefield than Fontari. Often an event recorded by FON is partially covered by the noise and so the seismic waves don't result much coherent among stations.
Finally to see the trend of noise coherence in different days and in different hours, for example day and night, some test were made at UNDERSEIS array. This analysis was done to detect a gradual and apparently random increase of coherence, as were fluctuations (for an example see fig.2.11). For most cases, the seismic noise is coherent for low frequency (< 2 Hz). Only for some case it is coherent for frequency grater than 2 Hz. I think that this anomalous behavior could be caused by human activity of underground laboratories, because this increase does not generally exceed 0.5, does not have peaks and is concentrated for many cases in a limited period of time, preferably during the day. Another hypothesis is strong periodic influence of atmosphere conditions. These fluctuations should not be confused with sporadic events that have gradual but higher coherence value, as the event of 20040113, which will be illustrated later.

2.2.1 Coherence of 2007

In the graphics of the daily coherence versus time, evaluated in the range of frequency 1-8 Hz, UND curve is smoother than that of FON. The reason is in the site where FON is located, more exposed to noise conditions. Because of weather and other already mentioned conditions, coherence value fluctu-
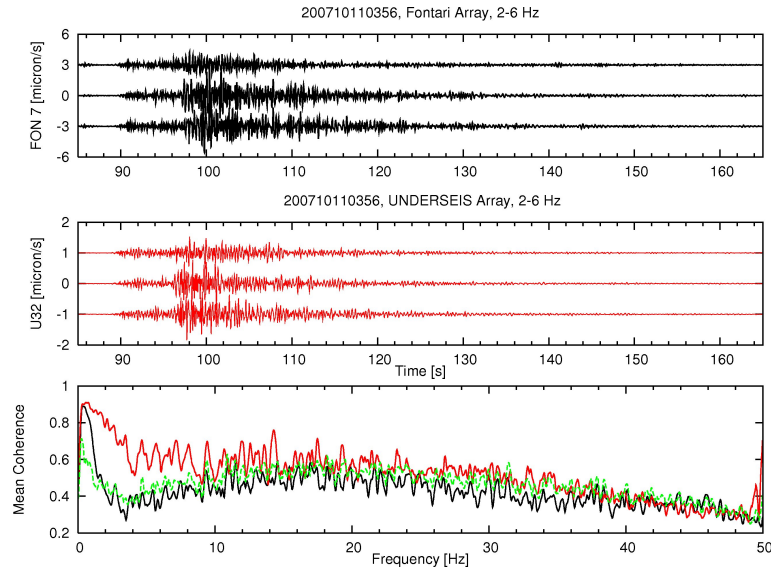
Figure 2.9: 200710110356 local earthquake. Seismograms of FON (black line), UND (red line) and coherence calculated among stations of FON (black), UND (red) and among stations of two arrays (green).
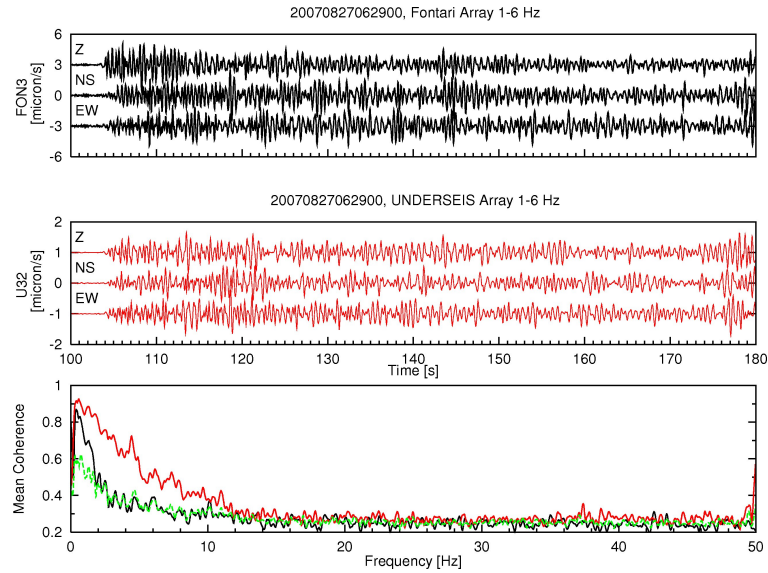
Figure 2.10: 200708270629 regional earthquake. Seismograms of FON (black line), UND (red line) and coherence calculated among stations of FON (black), UND (red) and among stations of two arrays (green).
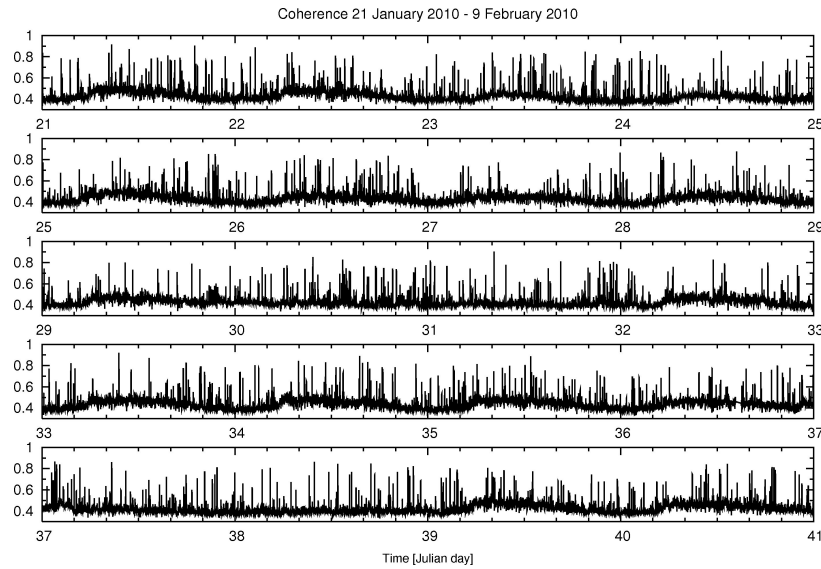
Figure 2.11: From 21 January 2010 to 9 February 2010. Coherence versus time at UNDERSEIS array. A background effect, as a fluctuation, can be seen especially during the day.

ates over time. Gaps on the chart indicate that in those hours or days, for some problems, the arrays don't acquired. For some comparisons between the coherence calculated at two arrays, we show an example in fig.2.12 and in fig.2.13. Many earthquakes (corresponding to peaks) are more clear in UND graph. For example 321 Julian day (17 November 2007) many earthquakes are more evident at UNDERSEIS array than Fontari. Common ones have much higher coherence at UNDERSEIS array and so it is more able to record small earthquakes. In this sense, the use of underground stations is an advantage respect to superficial ones. Obviously underground or borehole sensors aren't easily to install and rarely are possible to realize. Moreover, Fontari array has only six seismometers, few compared with those of UNDERSEIS. The use of several stations improves the quality of the stacking among the recordings, a fundamental characteristic of multichannel data. Also coherent coefficient is biased by number of stations. This explain lower coherence values at Fontari array. Often, as noted previously, there are gradual increases in the coherence background value of UNDERSEIS array. This moderate increments are rare at FON recordering. Coherence analysis

of June-November 2007 period shows no particular phenomenon.
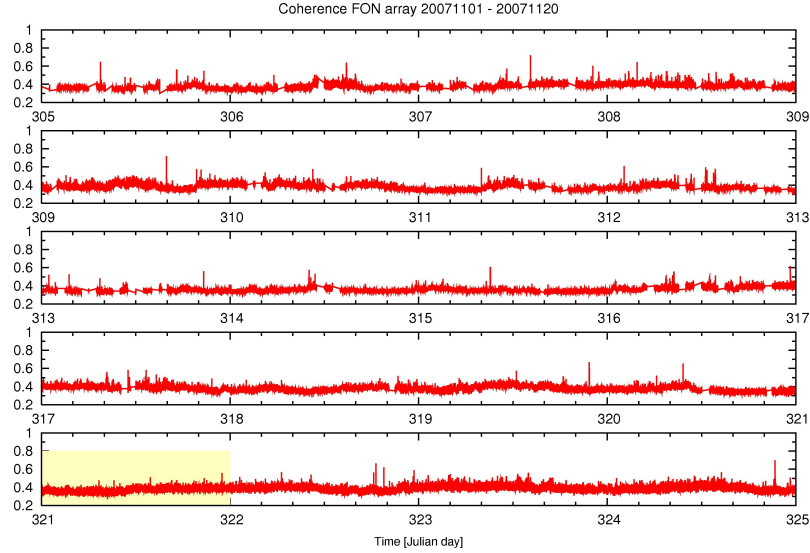
Figure 2.12: Coherence at FON from 20071101 to 20071120. Yellow box-car shows 321 Julian day (17 November 2007) during which many earthquakes are more evident at UNDERSEIS array than Fontari.
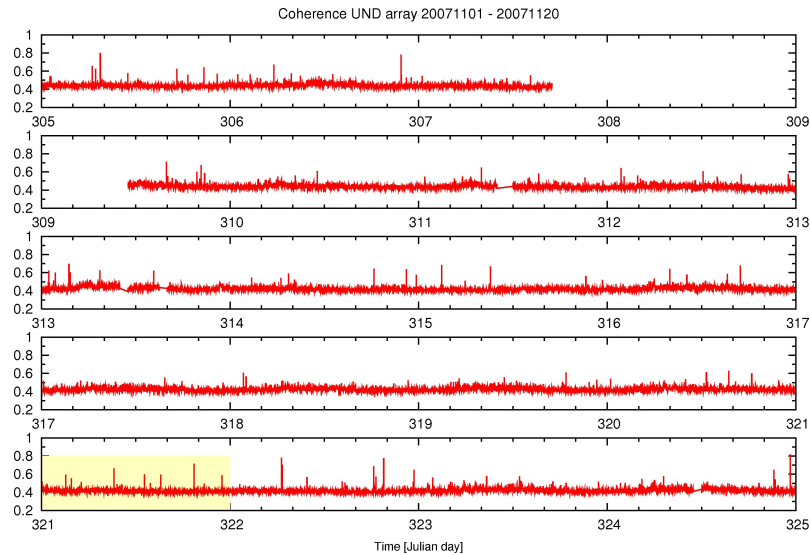
Figure 2.13: Coherence at UND from 20071101 to 20071120. Yellow box-car shows 321 Julian day (17 November 2007) during which many earthquakes are more evident at UNDERSEIS array than Fontari.

2.3 Anomalies

Some *anomalies*, variations of coherence background noise not relatable to earthquakes, were discovered in the graphs of coherence versus time. The coherent events were found at all stations of the UNDERSEIS array.

2.3.1 2004 January 13-14

I report the event of 13 and 14 January 2004 as an example. Variations of coherence background value are marked to detection of natural phenomena. In January 2004 an anomaly in the graph of coherence versus time is evident in the frequency band 1-8 Hz (fig.2.14). It is a gradual increase of coherence value with the shape of bell. It is more clear in the frequency band 1-4 Hz (fig.2.14 and fig.2.15) and it remains high for some hours. Its duration and the absence in the seismograms relative to those hours of well defined P phases, are the most characteristics of this event. All the studies, performed in the past, showed many similarities with non volcanic deep tremor. In those years the signal to noise ratio at UNDERSEIS array was particularly bad and so few information could be obtained by numerous applied analysis. Finally, we couldn't affirm this event is classifiable as non volcanic deep tremor. From this event, attention is remaind high to discover other similar phenomenon. Next some anomalies of coherence are reported, confirming the importance of continuous recording in a seismogenic area as that of Gran Sasso.

2.3.2 2008 March 21-22 and 2009 September 21

The figure 2.16 shows a gradual increase of coherence value on 2009 March 21-22 (81-82 Julian days). Its duration is about twenty hours. Its maximum is in a minimum of the curve which approximate coherence trend. From coherence analysis at UNDERSEIS array, higher values of coherence are obtained during the day, especially in the morning. Discovered event is mainly contained in the part of day in which human activity in underground laboratory are weak. Its seismograms evidence immediately artificial noise with anomalous peaks for almost all hours. These peaks are present at about all
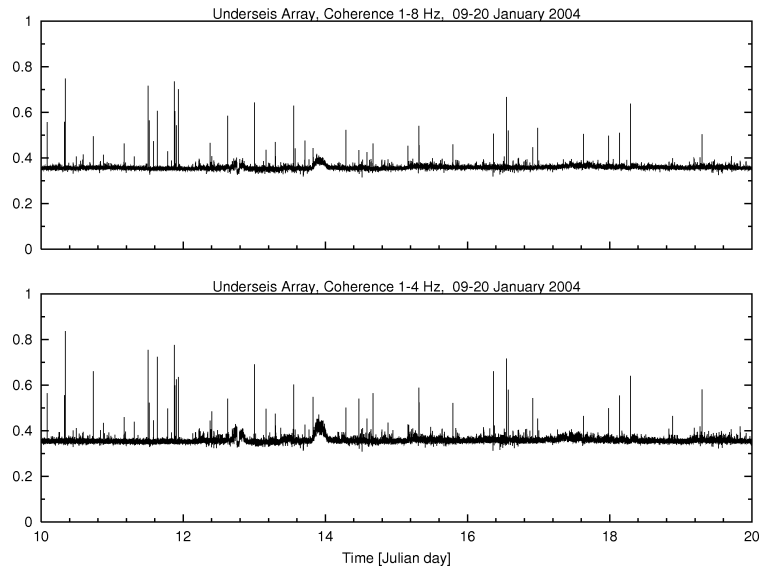
Figure 2.14: 2004 January 13-14. Coherence analysis in the frequency band of 1-8 Hz (top) and in the frequency band of 1-4 Hz (bottom). A gradual increase of coherence value with the shape of bell is observable.
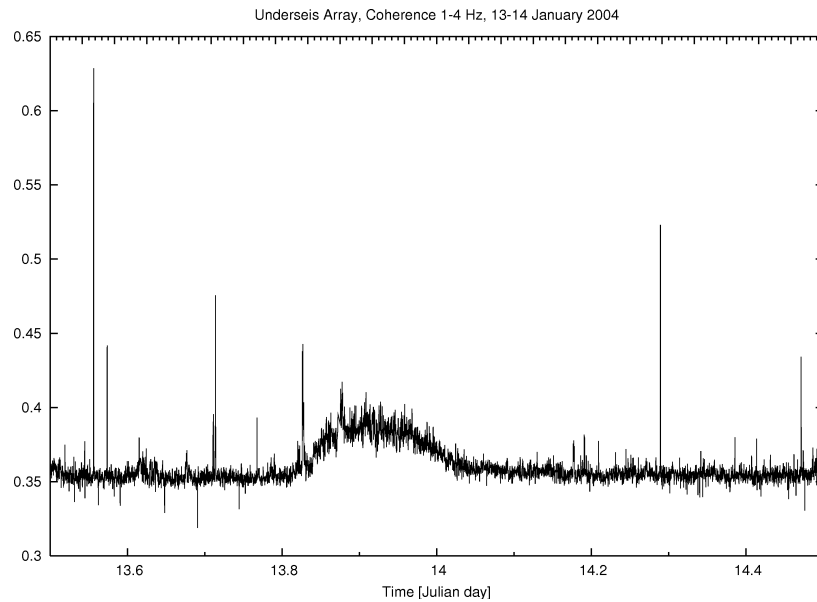
Figure 2.15: 2004 January 13-14. In the frequency band of 1-4 Hz, the gradual increase of coherence value is more evident.

stations of UNDERSEIS array. Coherence was calculated on many temporal windows of 300 seconds, selected in the hours where the phenomenon occurred (for an example see fig.2.17). Especially for 22 pm of 21 March 2008 coherence value remains high on a large band of frequency. Spectra of those hours (for an example see fig.2.18) show energy at low frequency. Established the presence of several artificial peaks in the recordings, the coherence was forced to increase.

Another singular phenomenon occurs on 2009 September 21 (264 Julian day), indicated by the large peak of coherence in fig.2.19. In order to classify this event many analysis were made. Also in this case, it is classifiable as an artificial event. As it is present at all stations of UNDERSEIS array, coherence mean value increases. No P or S waves are clearly identifiable in seismogram of those hours and it doesn't have typical trend of an earthquake. Its spectra (fig.2.20) show energy on a large band of frequency. In first analysis these two events manifest similar coherence characteristics to 2004 January event. While for this last, the seismograms showed many S waves clearly identifiable with array and polarization analysis, for these two events the recordings are principally composed by artificial noise. Coherence analysis is a good instrument to detect natural or not events. For our purposes it was indispensable for an overview of all recordings at UNDERSEIS array.
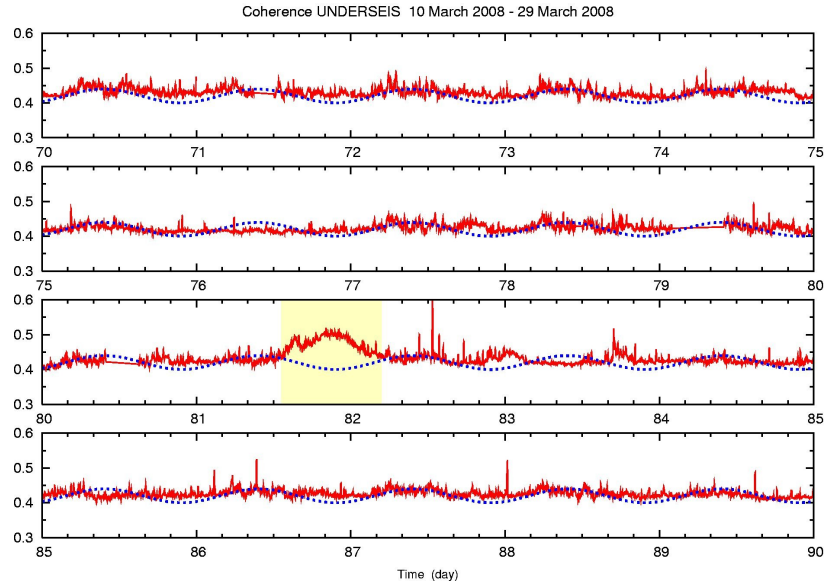
Figure 2.16: 2008 March 21-22. Yellow box-car shows 81-82 Julian days during which a gradual increase of coherence value is evident at UNDERSEIS array.
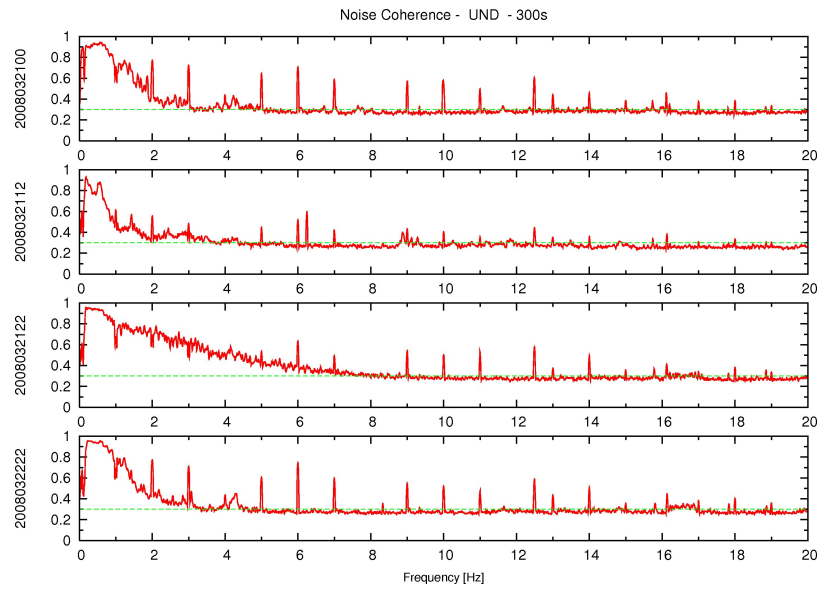
Figure 2.17: 20080321 coherence at UND, calculated on many temporal windows of 300 seconds, selected in the hours where the phenomenon occurred.
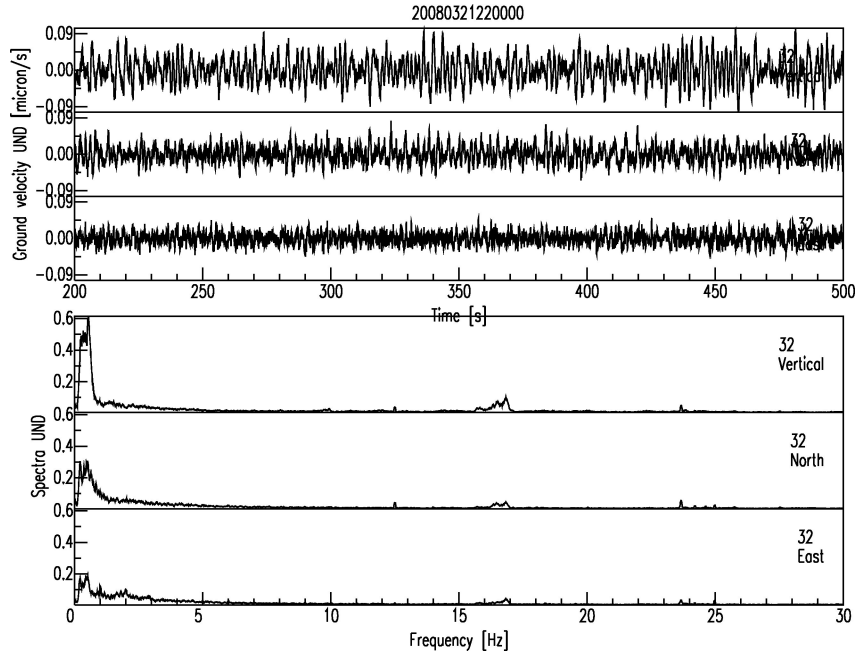
Figure 2.18: 20080321 UND Spectra. Spectra of those hours show energy at low frequency.
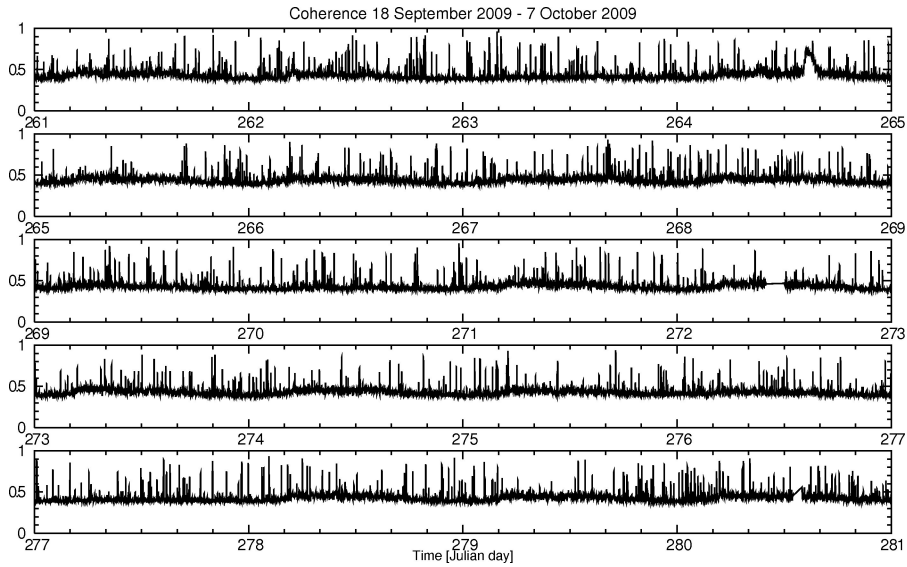
Figure 2.19: September 2009. In the 264 Julian day, 21 September 2009, a large peak of coherence is visible.
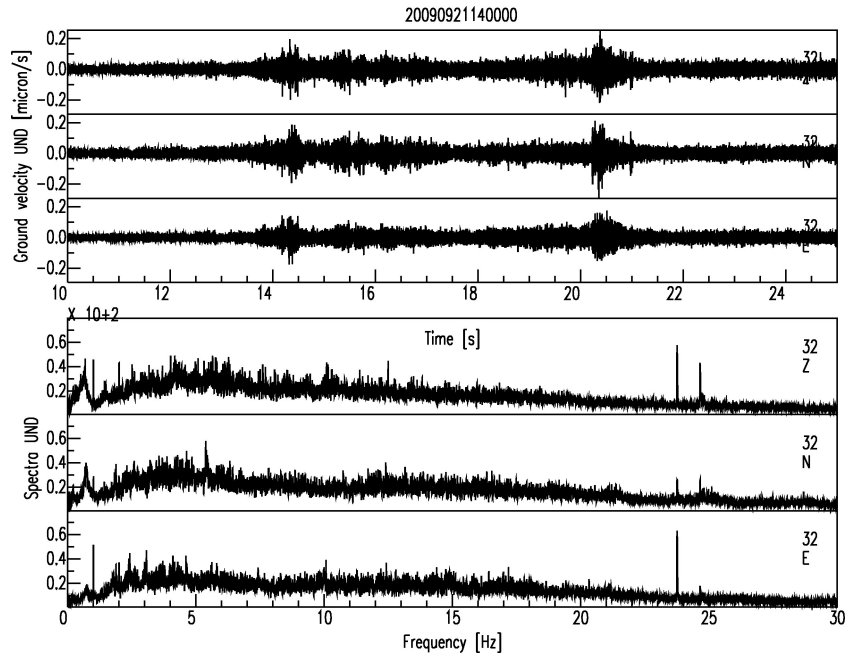
Figure 2.20: 20090921 UND Spectra. Spectra of those hours show energy in a large band of frequency.

2.4 Coherence analysis of coda waves

Coda waves are a superposition of reflected, refracted and scattered waves with properties depending on frequency, on scatterers in the crust and many others factors. Coda waves have similar features for different earthquakes, especially local, recorded at the same site. The coda of an earthquake is composed mostly of secondary waves, i.e those arriving after direct body and surface waves. The coda of a local earthquake is composed mostly of S radiation scattered by inhomogeneity in the crust with almost random backazimuths and an apparent velocity that decreases with increasing lapse time along the coda. Main observed properties of coda waves are: duration proportional to local magnitude, regular envelope well approximate by a decreasing exponential, independence by distance between source-receiver location and by site effects. Theoretical models that explain the origin of the coda are numerous. The first was the single-scattering theory of *Aki* [52]. He showed a simple model of coda waves as a superposition of secondary

waves backscattered from randomly distributed heterogeneities and with hypothesis of spatial uniformity (scatterers placed in random but uniform way). The single-scattering model is widely used to estimate the quality factor of an area. Obviously, to account for the measured decay of coda, a nonuniform media should be considered.

Geological heterogeneity (or the so-called scatterers) in propagation media can be detected from a correct interpretation of the coda waves parameters. Seismic wave attenuation is caused by two major factors: scattering at heterogeneities in the earth and intrinsic absorption by inelasticity of the earth. Intrinsic absorption reduces both the direct wave amplitude and the coda wave amplitude with propagation distance, while scattering reduces the direct wave amplitude but enlarges the coda wave amplitude. The overall quality factor Q_t, representing the total attenuation, can be given by $1/Q_t = 1/Q_s + 1/Q_i$, where Q_s and Q_i are the quality factors due to scattering losses and intrinsic absorption respectively. Here we don't derive the values of quality factors and don't use techniques to detect the position of scatterers. We will note some common characteristics of coda waves recorded by two antennas using analysis of array. The first concerns the coherence of coda waves.

The mean coherence, averaged among the three components in a broad frequency range, has been computed at the two arrays. As we could see in this chapter, for earthquakes the results show much higher values at depth than at surface. This particularity is evident also for coda waves. For each event of data set, the coda beginning was estimated as two times the Ts (shear-wave travel time) and the duration of earthquake was estimated too. For an example of coda waves we show their coherence of 200709260814 earthquake. It is higher for UND (green line in fig.2.21) for almost all frequency. The same result can be illustrated with 3D graphs, fig.2.22 and fig.2.23, where coherence versus time and versus frequency is drawn. The seismograms, which it is referred are those of fig.2.6 and fig.2.7 (top plots). The coherence values are reported with colors indicated in the scale on right. Yellow color indicates that coherence is high for longer time at UNDERSEIS array. The smaller duration of earthquake at FON is also evident by coherence value, which after 10 sec became again that characteristic of noise,
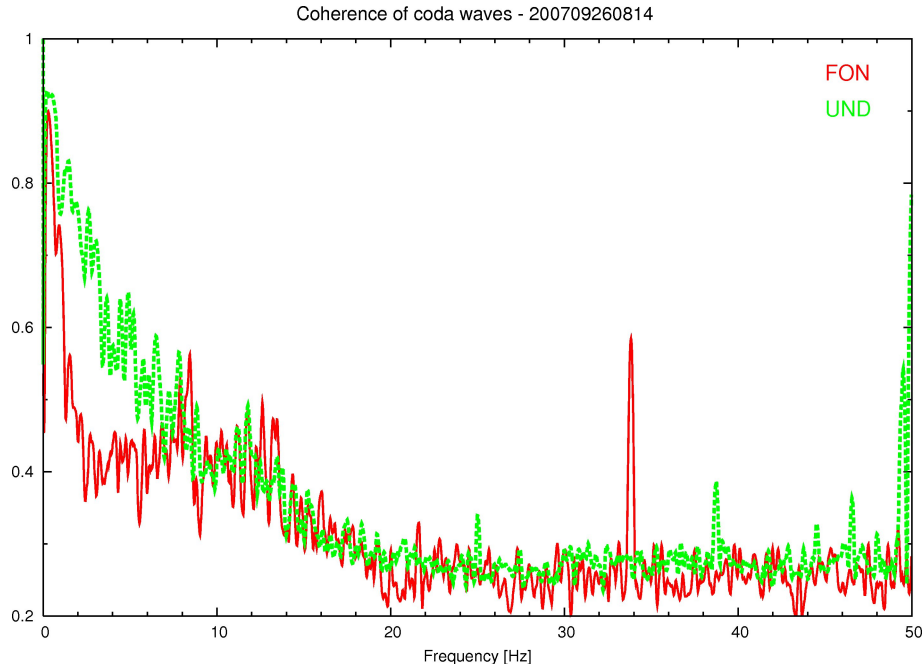
Figure 2.21: 200709260814 earthquake. Seismograms and coherence of FON(red) and UND(green) earthquake coda.

while at UND is high for almost 30 sec.

This result can be generalized for all selected events. Both body and coda waves have at UNDERSEIS coherence higher than Fontari. In the next chapter, the composition and other properties of coda waves at two arrays will be analyzed.

2.5 A note on coherence calculation

Numerous proofs show the dependence of coherence calculation on several factors. The number of samples (window length) and smoothing coefficient are among the most important. The effects of tapering on coherence estima-tion should be also considered. Some observations are reported by *Saunders et al.(1982)* [18] , especially on cross spectrum calculations. Here I analyzed the effects of window length in the time domain and those of smoothing in frequency domain.

First I tested the dependence on window length. I selected both coherent
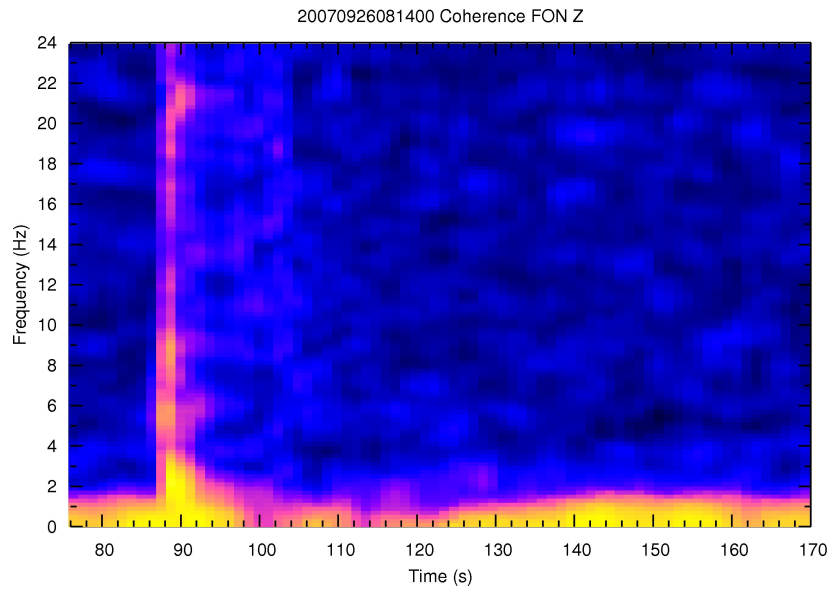
Figure 2.22: 200709260814 earthquake. Coherence 3D at Fontari array. Yellow color indicate high values of coherence.
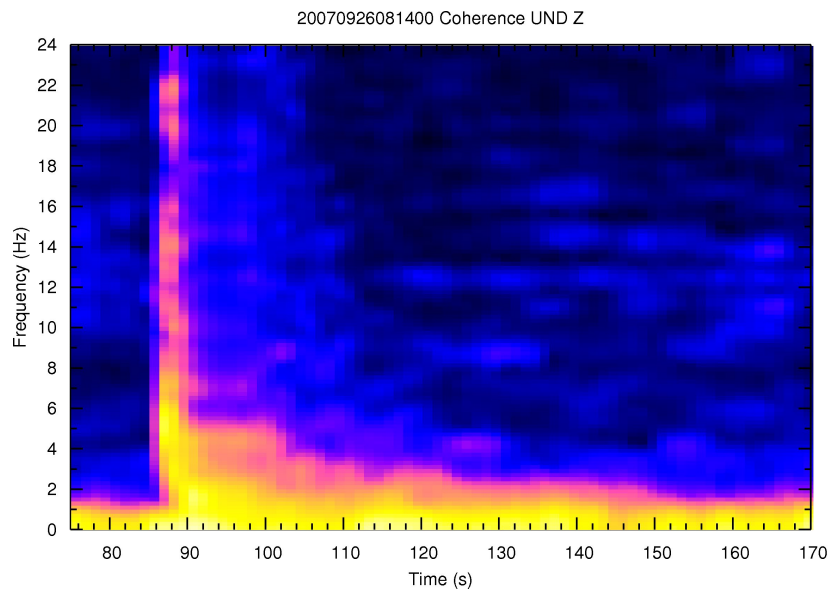
Figure 2.23: 200709260814 earthquake. Coherence 3D at UNDERSEIS array. Yellow color indicate high values of coherence.

seismic signals, as deep tremor, and earthquakes. I used the data recorded in Cascadia in spring-summer of 2004 at SEQ array [25](see fig.2.24). I used 5 minutes of tremor, calculating the mean of coherence on all selected temporal windows. The fig.2.26 shows the coherences obtained by varying smoothing coefficient and taking constant the number of samples. The same procedure was applied on 5 minutes of UND recordings (fig.2.25) which contain many earthquakes recorded after the mainshock of L'Aquila earthquake (see fig.2.27). The results on the same seismic signals, taking constant the smoothing coefficient and varying the number of samples, are shown in fig.2.28 and fig.2.29, respectively for SEQ and UND array. Coherence values between the two arrays (SEQ and UND) are different because the latter refers to earthquakes. Both for SEQ than UND array, higher is the smoothing coefficient lower is the coherence. This is true for any temporal windows and it is more evident at low frequency for deep tremor signals. For low smoothing coefficient (as 2 in fig.2.28 and fig.2.29) coherence results are independent from the number of samples. With the same smoothing, longer windows (number of sample 4096) are more coherent (in fig.2.28 and fig.2.29 the curve is higher). From this observation we can see that the coherence calculation is independent of the window when the recordings are similar among them. It depends mostly on the smoothing that is applied to the spectra.
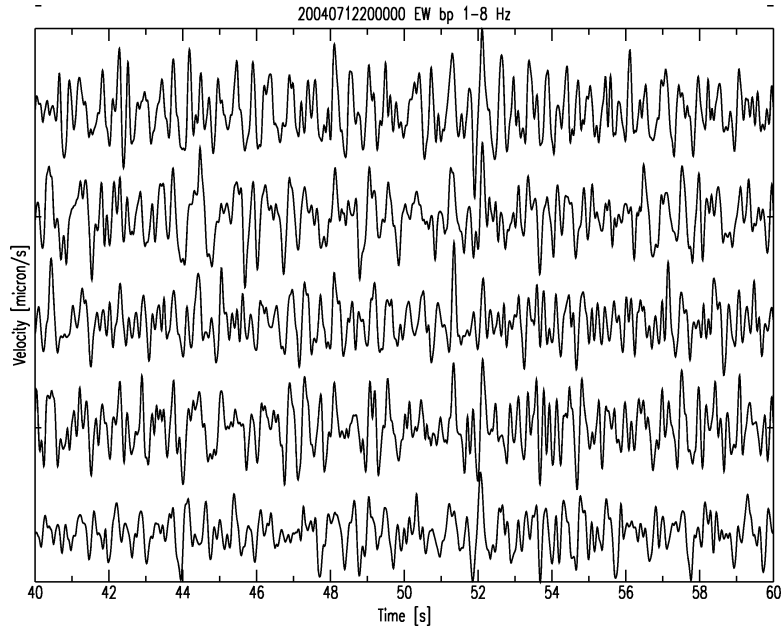
Figure 2.24: Deep Tremor recorded in Cascadia. Five stations of SEQ array, EW component. The tracks are very similar among them.
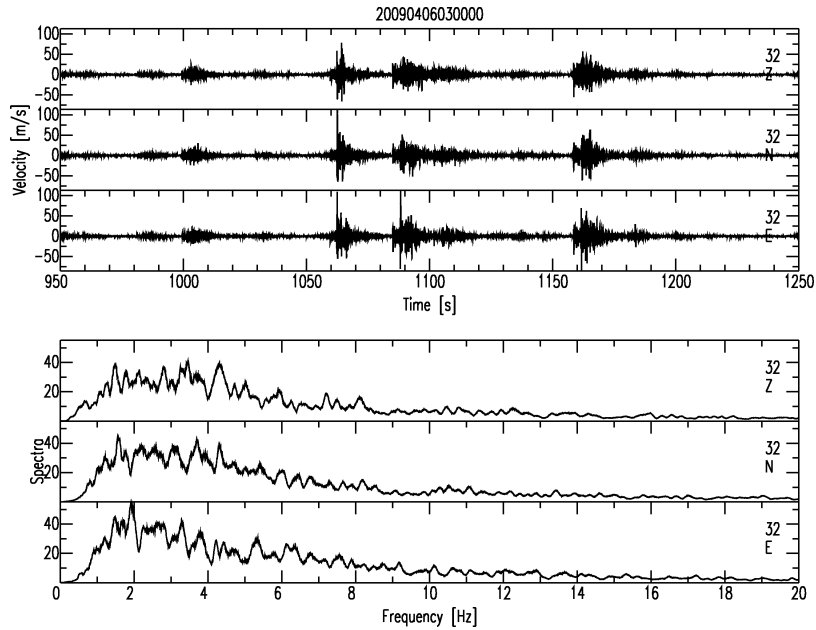
Figure 2.25: 20090406, after the mainshock of L'Aquila earthquake. Seismograms and relative spectra at one station (U32) of UNDERSEIS array. The window contains many overlapped earthquakes.
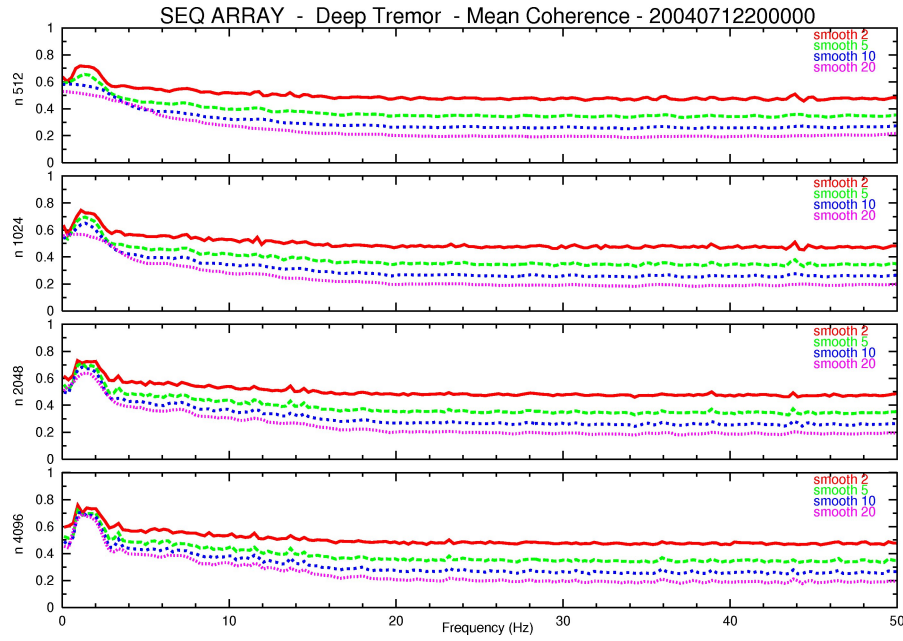
Figure 2.26: Coherence of Deep Tremor fixing the number of samples.
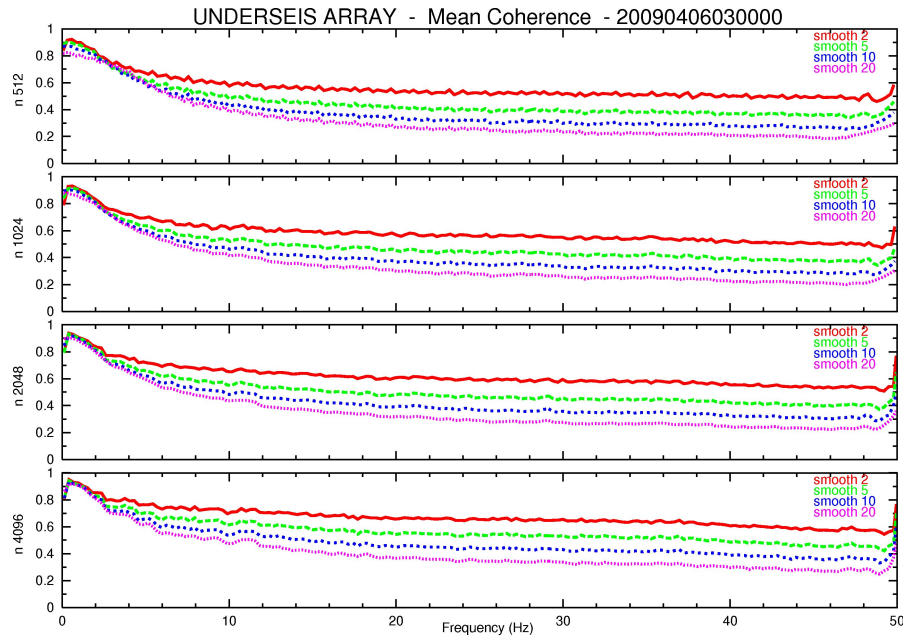
Figure 2.27: Coherence at UNDERSEIS array fixing the number of samples.
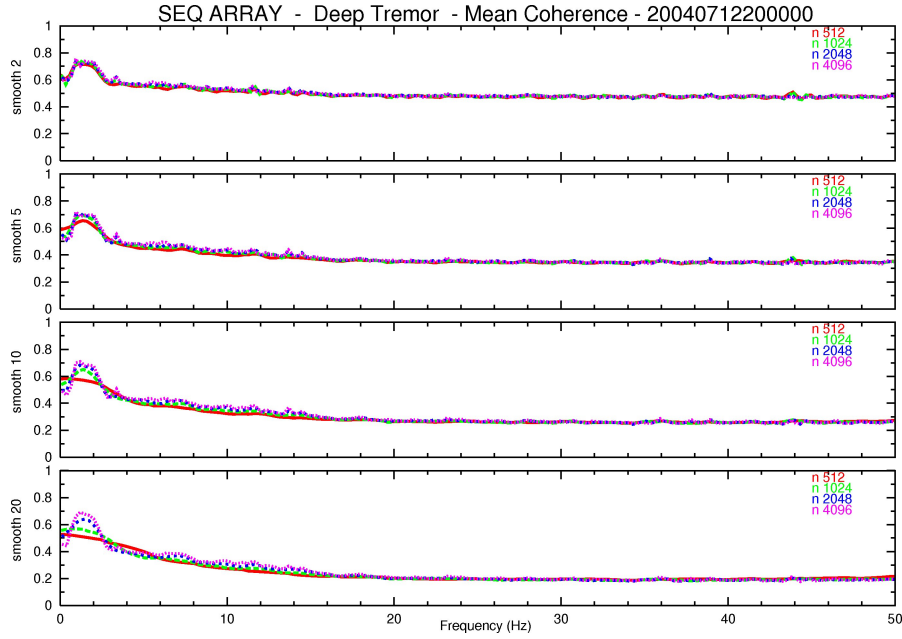
Figure 2.28: Coherence of Deep Tremor fixing smoothing coefficient.
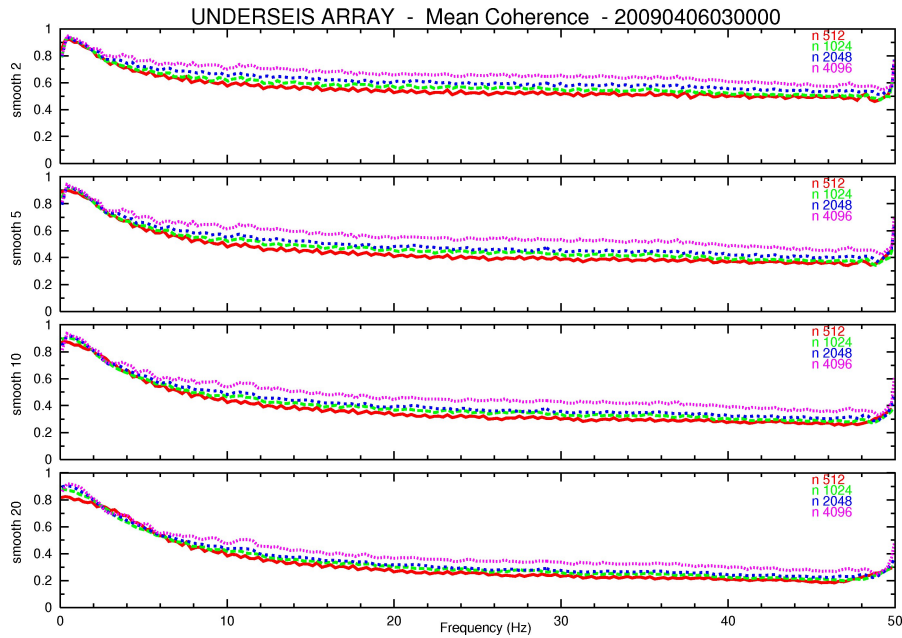
Figure 2.29: Coherence at UNDERSEIS array fixing smoothing coefficient.

Chapter 3

Methods of array

Seismic arrays can be used for many purposes, therefore several different mathematical formalisms have been developed, named "array analysis techniques". Most array methods measure the velocity vector of an incident wave front on free surface, *slowness*, and the *backazimuth*. In the plane-wave approximation, slowness is defined as the inverse of the apparent velocity of the wave front across the array, while backazimuth is defined as the angle of the wave front arriving at the array, measured between north and the direction to the epicenter clockwise. Slowness is related to v_{eff} (the medium velocity beneath the array) by the equation $S = sin(i)/v_{eff}$, where i is the incidence angle. These two parameters are principally used to distinguish between different seismic phases of an event and to analyze the complete wavefield combined with the polarization parameters. Moreover, they are used to improve the signal to noise ratio (SNR), compared to single seismic station by stacking with respect to the varying slowness of different phases.

In my work I used three techniques of array analysis, BF (*Beam Forming*), HR (*High Resolution*), ZLCC (*Zero Lag Cross Correlation*). The first two methods work in the frequency domain, the last works in time domain.

3.1 Beam Forming and High Resolution Methods

Both BF and HR calculate, in a different way, the power spectrum that is defined as:

$$E_{12}\left(\omega\right) = \int\limits_{-\infty}^{+\infty} C_{12}\left(\tau\right)e^{-i\omega\tau}d\tau, \tag{3.1}$$

where the cross correlation $C_{12}\left(\tau\right)$ is:

$$C_{12}\left(\tau\right) = \int\limits_{-\infty}^{+\infty} f_1\left(t\right)f_2\left(t+\tau\right)dt \tag{3.2}$$

and where $f_1(t)$ and $f_2(t)$ are two temporal series, i.e. two different recordering. Obviously, this calculus for power spectrum is extended to all stations of the array. The Beam-Forming (*Rost and Thomas, 2002*) [1] separate coherent and incoherent parts of a signal. In its temporal formulation, it uses the different travel times of the plane-wave front to stations that constitute the array: travel time difference depends on the slowness of the wave. So the Beam-Forming method amplifies phases with the same slowness, while suppressing incoherent noise and phase with different slowness. The estimate of slowness and backazimuth can be done both in time and in frequency domain. Using Capon's method (*Capon et al., 1969*)[8], the power spectrum is calculated by:

$$f_{nn}\left(\vec{u},\omega\right) = W\bar{W}^T\bar{U}^T\left(\vec{k}\right)S\left(\omega\right)U\left(\vec{k}\right), \tag{3.3}$$

where $S(\omega)$ is the cross-spectral matrix, W is the array's vector of weight and $U(\vec{k})$ is the vector whose elements are $U_j\left(\vec{k}\right) = e^{i\vec{k}\cdot\vec{x}_j}$. This last vector means the effect of temporal delay of a plane wave that propagates with wave vector $\vec{k}$ between the j-th station and a reference point. In eq.(3.3) bar and T respectively indicate the complex conjugate and the transpose. In general, the estimate of $S(\omega)$ for stationary signals is made by averaging on different temporal windows. The analysis of a seismic signal requires a windowing of the seismograms. Often a smoothing of the signal spectra is also appropriate. So $S(\omega)$ is defined as

$$S_{jl} = \sum_{-M}^{M} a_m u(\vec{x}_j, \frac{w+2\pi m}{T})\bar{u}(\vec{x}_l, \frac{w+2\pi m}{T}) \tag{3.4}$$

where $2M + 1$ is frequency discrete number, a_m are normalized weights used in the frequency smoothing and $\overrightarrow{u}(\overrightarrow{x}, t)$ is the recorded signal defined by the generalized Fourier Transform :

$$\overrightarrow{u}(\overrightarrow{x}, t) = \int\limits_{-\infty}^{+\infty} \int\limits_{-\infty}^{+\infty} \overrightarrow{u}(\overrightarrow{k}, \omega) \exp(-i(\overrightarrow{k} \cdot \overrightarrow{x} - \omega t)) d\overrightarrow{k} \, d\omega. \qquad (3.5)$$

Different spatial weight, i.e. different W vectors, are applied in the two methods BF and HR. The BF method uses a weight $W_j = \frac{1}{N}$. The estimate of the power spectrum is

$$P^{BF}(\overrightarrow{k}, \omega) = \frac{1}{N^2} \overline{U}^T(\overrightarrow{k}) S(\omega) U(\overrightarrow{k}). \qquad (3.6)$$

The HR method, proposed by Capon (*Capon, 1969*) [8]uses different and more complex weights respect to BF method. The W_j weights must satisfy two conditions: 1. a pure plane wave, with $\overrightarrow{k}_0$ wavevector should pass undisturbed through the filter. 2.the variance of the noise (signals with wavevectors $\overrightarrow{k} \neq \overrightarrow{k}_0$) should be minimized. The weights, which satisfy these conditions, are different for each frequency and wavenumber. Capon demonstrated that these weights are equivalent to valuate power spectrum by

$$P^{HR}(\overrightarrow{k}, \omega) = [\overline{U}^T(\overrightarrow{k}) S^{-1}(\omega) U(\overrightarrow{k})]^{-1}. \qquad (3.7)$$

HR considers the inverse of the cross spectral matrix $S(\omega)$. Another difference among the two methods is the weight they give to the eigenvectors of $S(\omega)$. For BF the weight is linearly proportional to associated eigenvalue, for HR it is inversely proportional to the associated eigenvalue. This means for BF, greater eigenvalue are associated to seismic signal while smaller ones to noise. For HR the situation is reversed and it uses statistical property of noise to improve resolution.

Both belong to the category of '*Frequency-Wavenumber Spectrum Analysis*, allowing to calculate the full vector of slowness, i.e. backazimuth and horizontal slowness.

3.1.1   Examples of BF and HR analysis

Numerous earthquakes were elaborated with BF and HR methods. Many of them were recorded both by FON and UND arrays and they were chosen to compare the results. Preliminarily, different frequency bands were adopted for the calculus, to choose later the best one for each event. For each band, the most appropriate parameters, as length (number of samples) and shift of sliding window, the smoothing and the grid (number of values of slowness to analyze) were chosen. Then, spectral analysis Beam Forming and High Resolution was done on the three components (Z, NS, EW). The most stations were not included in the calculus. To show the results of two techniques for an earthquake, the temporal windows have the same length for both arrays.

In fig.3.1 and fig.3.2 BF and HR vertical component analysis are shown for 200709260814 earthquake, respectively for FON and UND arrays. Red crosses and blue dots graphically indicate the outcomes, respectively for BF and HR, and they are plotted according to an established threshold of coherence. Threshold value is different between the two arrays because to have appreciable results for FON it must be very low. In fact coherence values at FON remains high only for about ten seconds of earthquake's beginning, while for UND it is high for almost the entire duration of the event. So, backazimuth and slowness values of FON are principally those of first phases, P waves, that generally produce higher coherence. These values are in good agreement with those of UND. Instead, all phases of the earthquake recorded at UND are clearly visible in fig.3.2. With a coherence threshold of 0.6 we see the arrival of P wave, then the S and many others. For the few values of slowness and backazimuth of FON, the agreement between BF and HR methods is almost perfect. For UND it is almost perfect for the main phases and very good for the others, especially for backazimuth. In particular, BF shows more stable backazimuth values, consistent with that of the first phases. The agreement is roughly the same for two other components, N-S and E-W, but the best agreement between the two methods is for V component. In fig.3.3, fig.3.4, fig.3.5 and fig.3.6 are shown the results for the two methods, respectively BF and HR, and for the two arrays, respectively

FON and UND. The colors indicate the results for each component of motion. For FON array, the values of slowness and backazimuth for the three components, with a threshold of coherence greater than 0.4, are very few. The vertical component has the highest coherence, so most of the outcomes refer to it. For UND array, instead, all curves of coherence for the three components have the same length and the number of outcomes for slowness and backazimuth is about the same for each of them. For HR (fig.3.6) the values are very scattered respect to BF, whose values (fig.3.5) are alike for the three components except for the coda. All these observations are confirmed in fig.3.7 where BF analysis for FON and UND vertical component are drawn and in fig.3.8 where the same is shown for HR. The same considerations can be done for the 200708270629 earthquake. The outcomes for BF and HR analysis, in fig.3.9 to fig.3.16, are shown for both arrays. In this case, using the same coherence threshold of the previous local event, 0.4, there are still less values of slowness and backazimuth for FON array. The coherence of FON, in fact, remains high much longer than the previous case but smaller than UND array. The slowness of beginning's earthquake for FON is lower than UND and the agreement between BF and HR for the beginning is better at FON. The backazimuth of FON is quite different than UND and it is shown principally for those phases that have higher values of slowness. The seismic wavefield of this regional earthquake appears more complex with respect to the local event and the results of two techniques are many more.

In both earthquakes and in others not showed here, the duration is always greater at UNDERSEIS array. Also the coherence of its wavefield is higher respect to Fontari array. This means that coda at UNDERSEIS array is longer although the presence of surface waves is negligible (lower values of slowness). In each of these graphs there is a good agreement between the two methods, because mostly values of BF and HR overlap. These array methods, together with detailed analysis of polarization, allow to understand and to study the wavefield through the values of slowness and backazimuth.
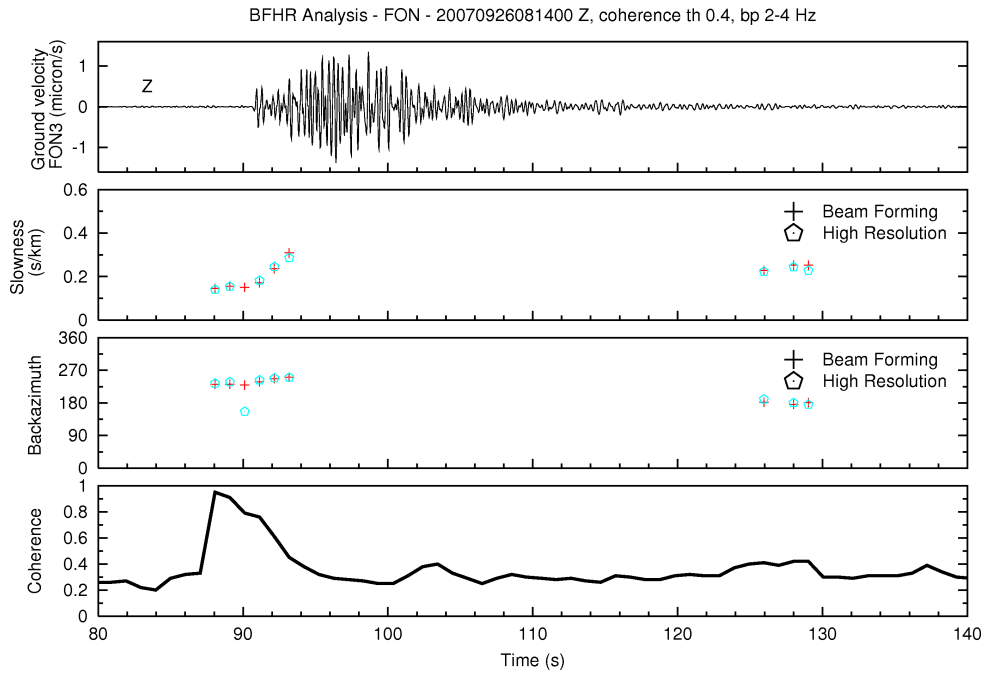
Figure 3.1: 200709260814. BF and HR analysis for FON.
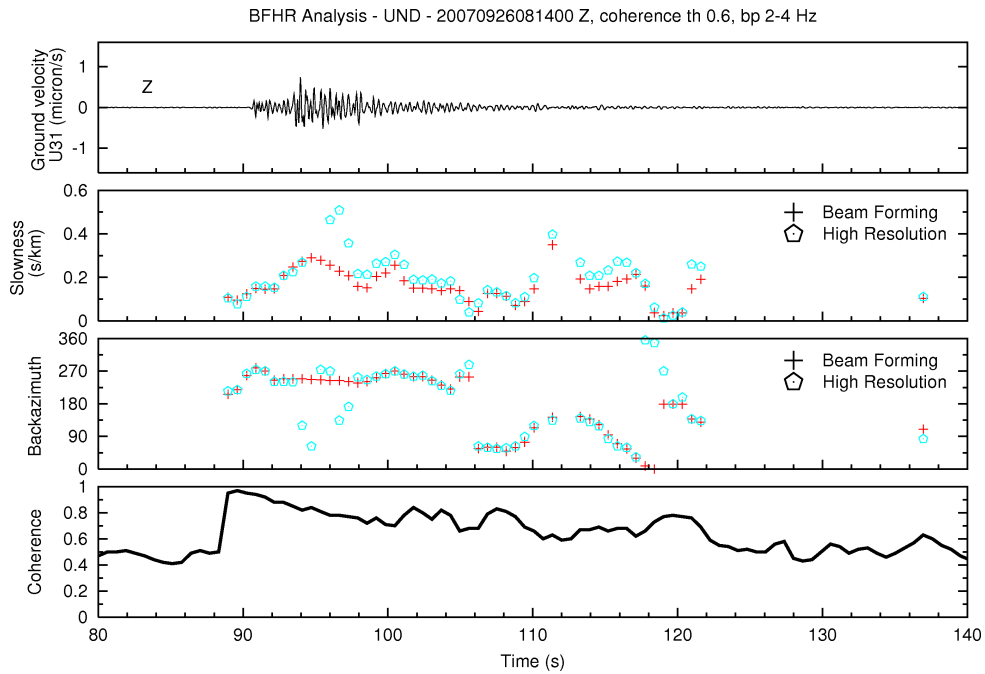
Figure 3.2: 200709260814. BF and HR analysis for UND.
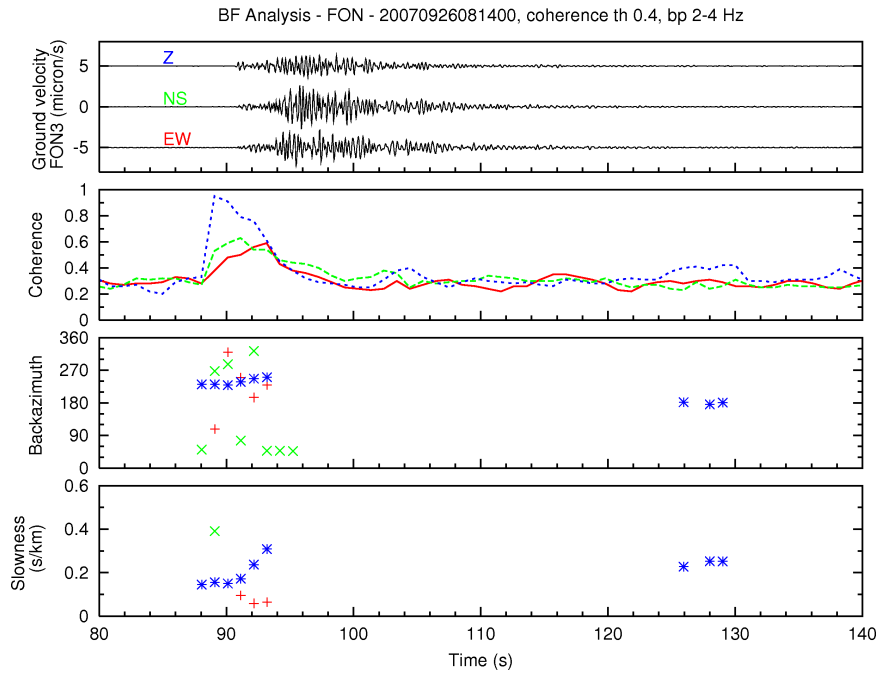
Figure 3.3: 200709260814. BF analysis for FON.
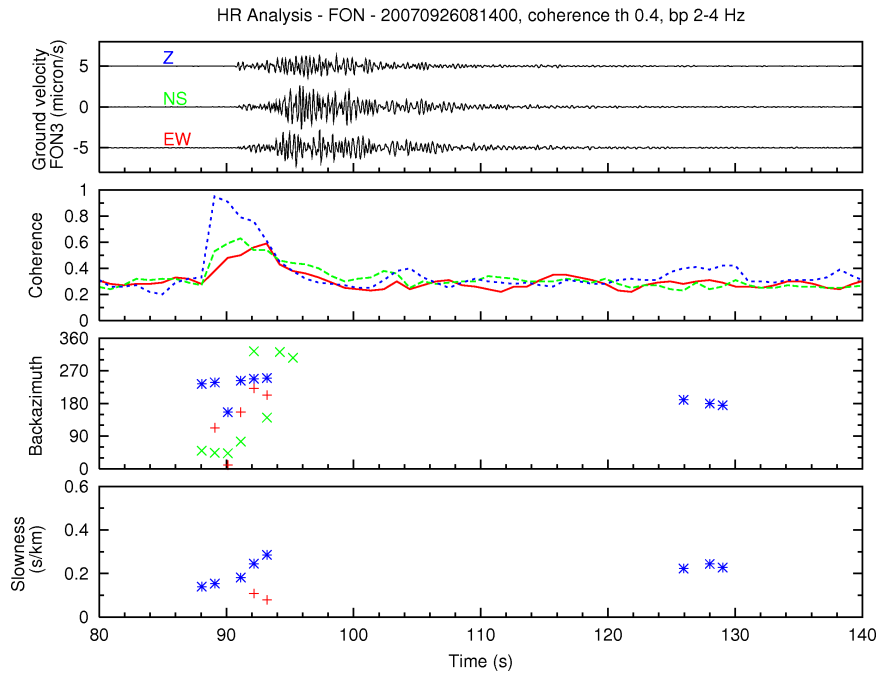
Figure 3.4: 200709260814. HR analysis for FON.
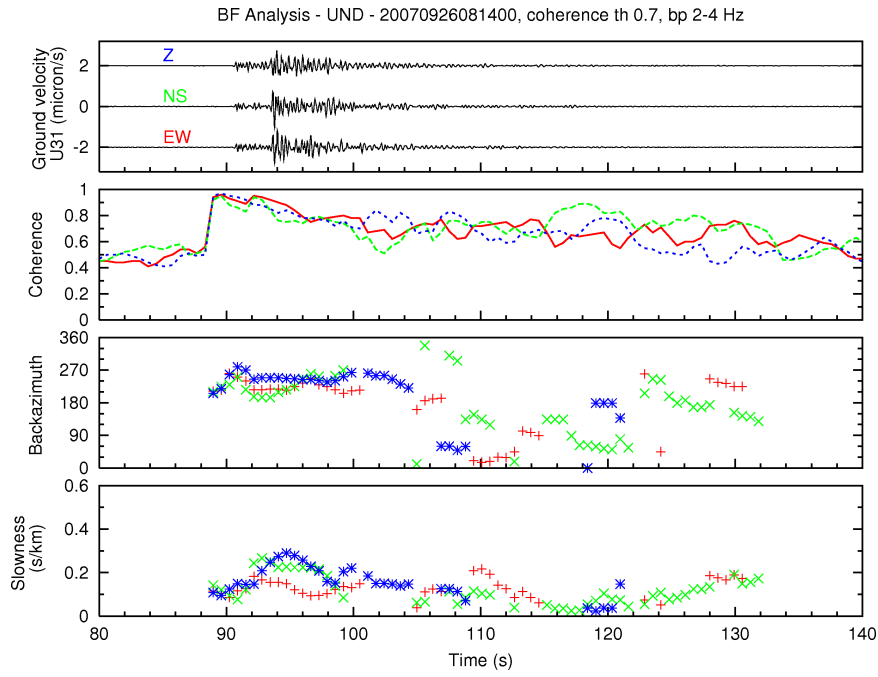
Figure 3.5: 200709260814. BF analysis for UND.
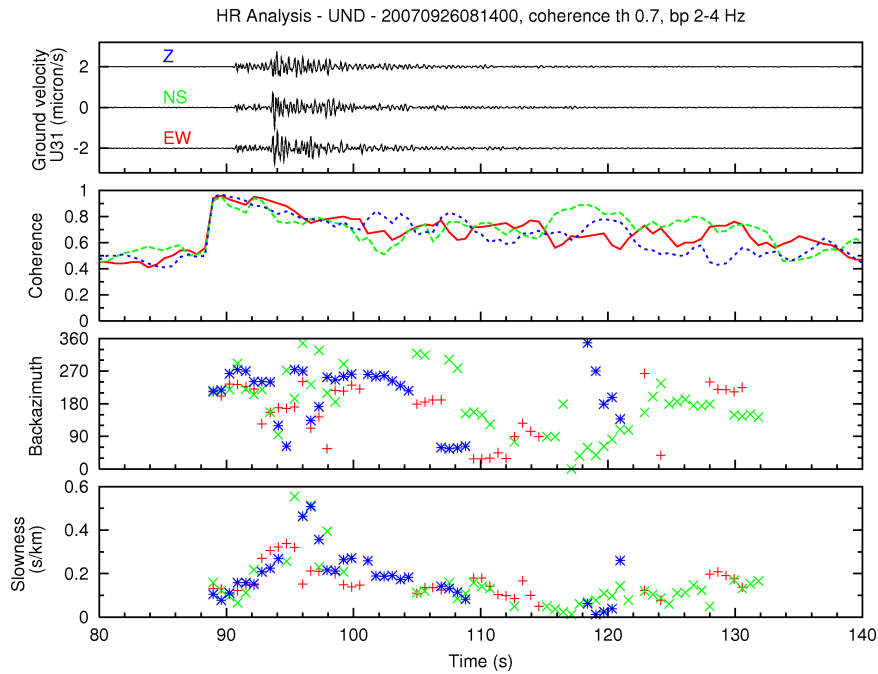
Figure 3.6: 200709260814. HR analysis for UND.
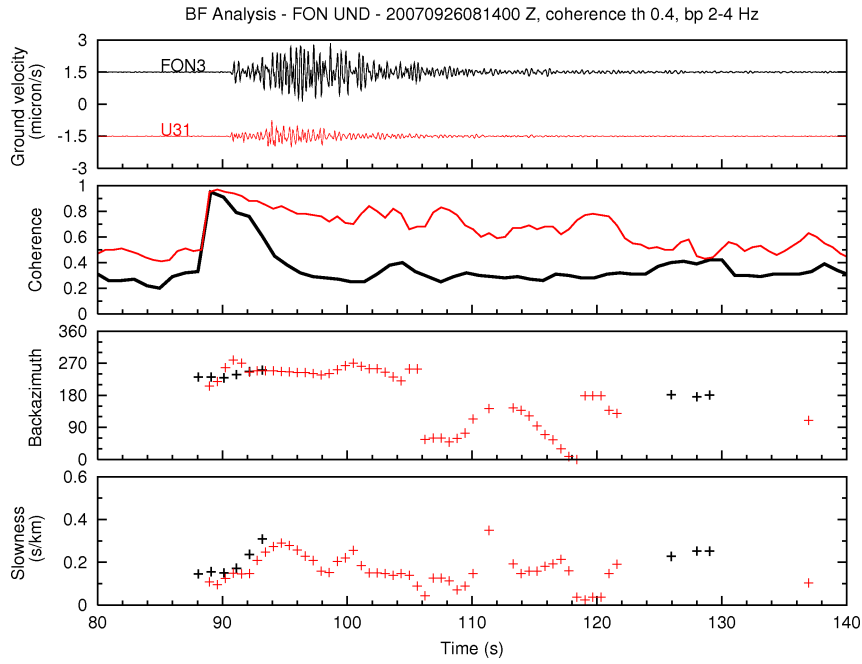
Figure 3.7: 200709260814. BF analysis for FON and UND, vertical component.
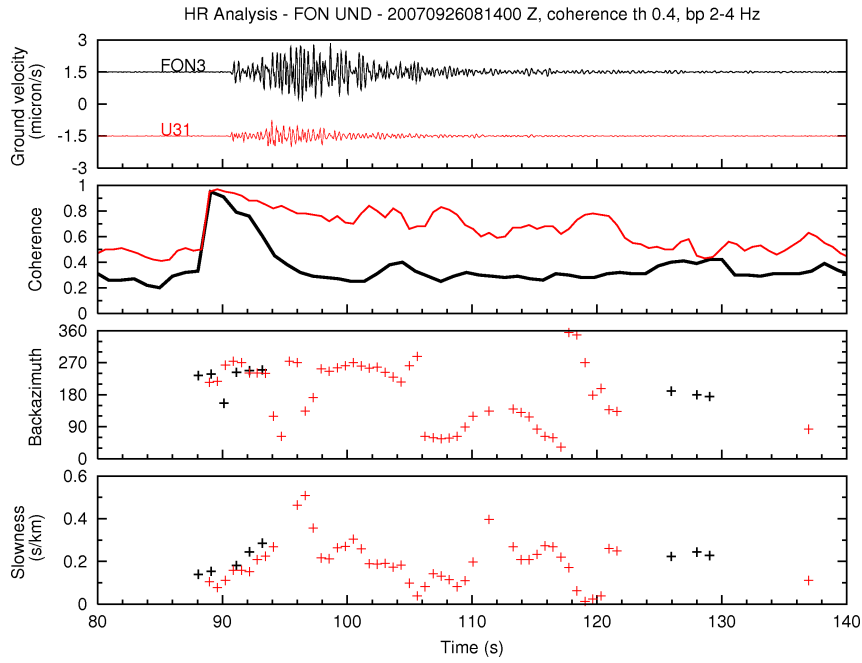
Figure 3.8: 200709260814. HR analysis for FON and UND, vertical component.
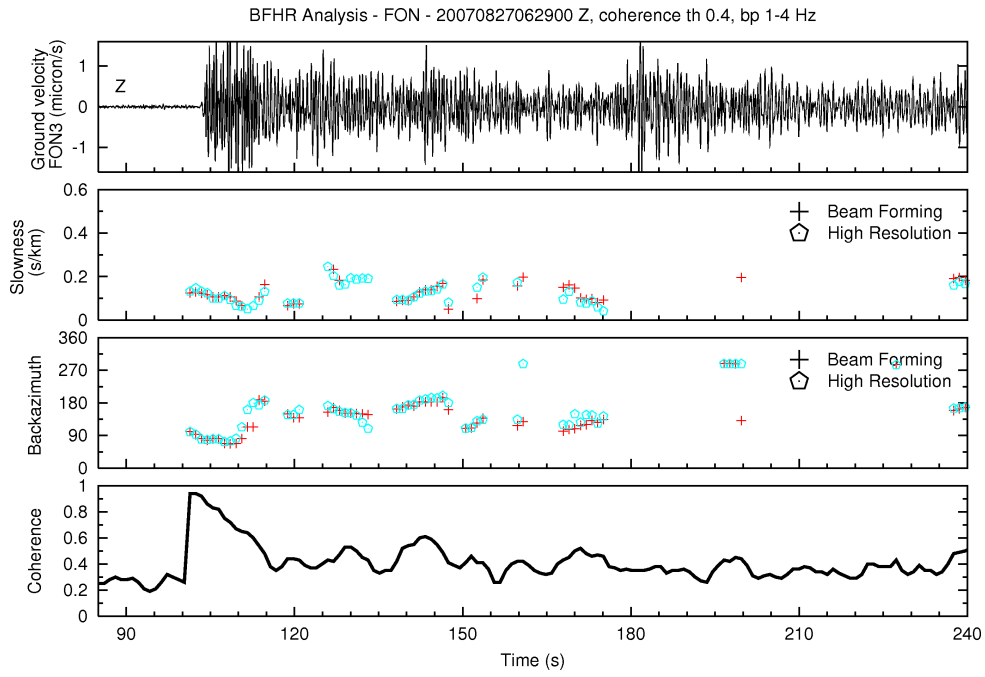
Figure 3.9: 200708270629. BF and HR analysis for FON.
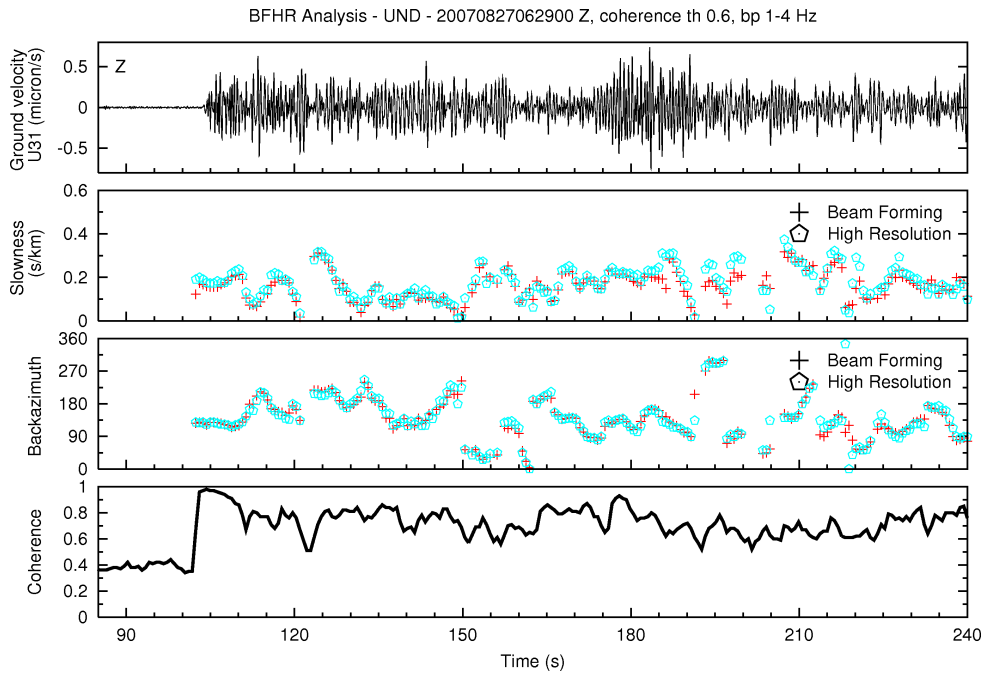
Figure 3.10: 200708270629. BF and HR analysis for UND.
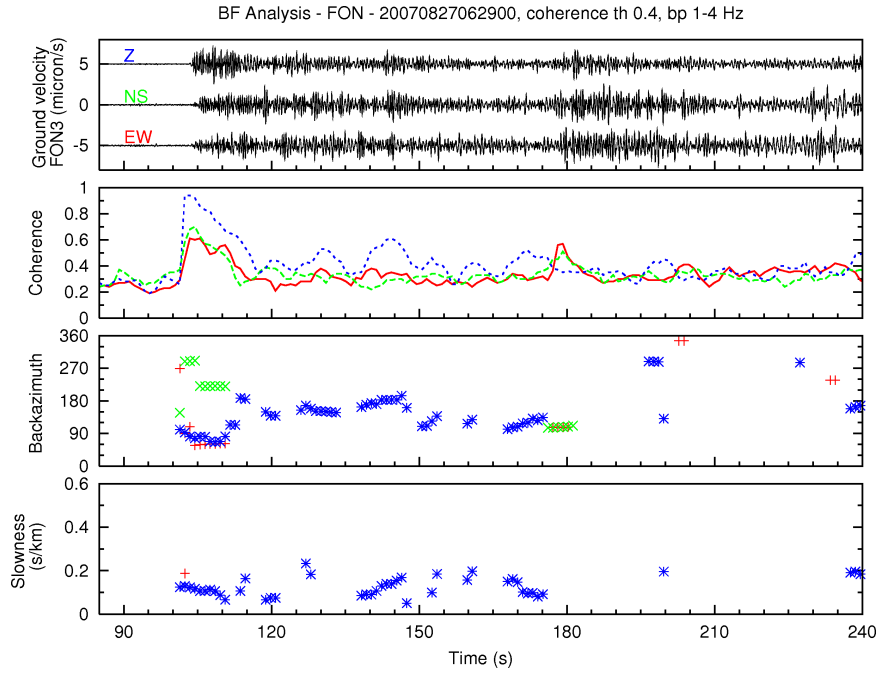
Figure 3.11: 200708270629. BF analysis for FON.
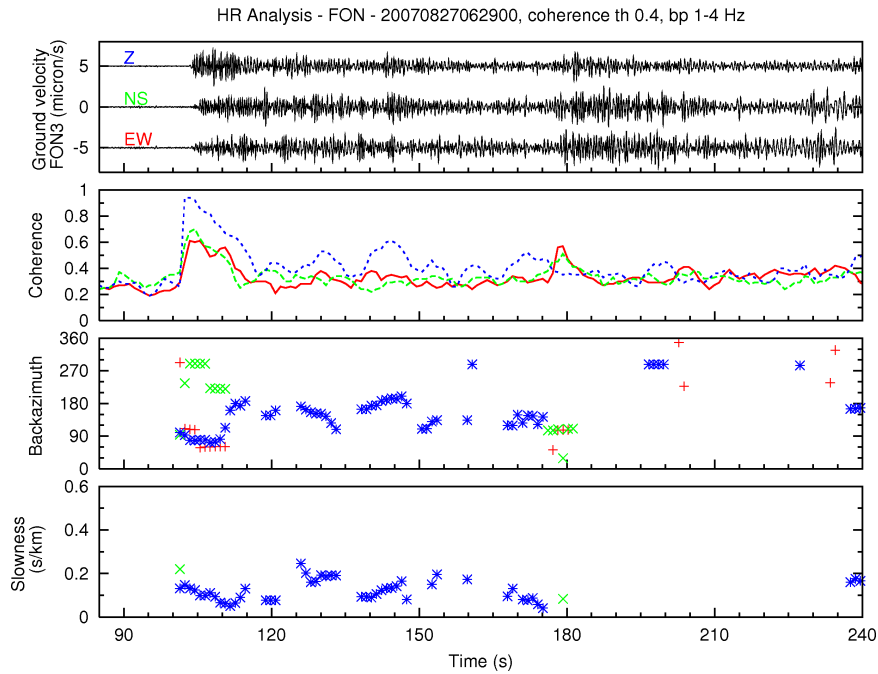
Figure 3.12: 200708270629. HR analysis for FON.
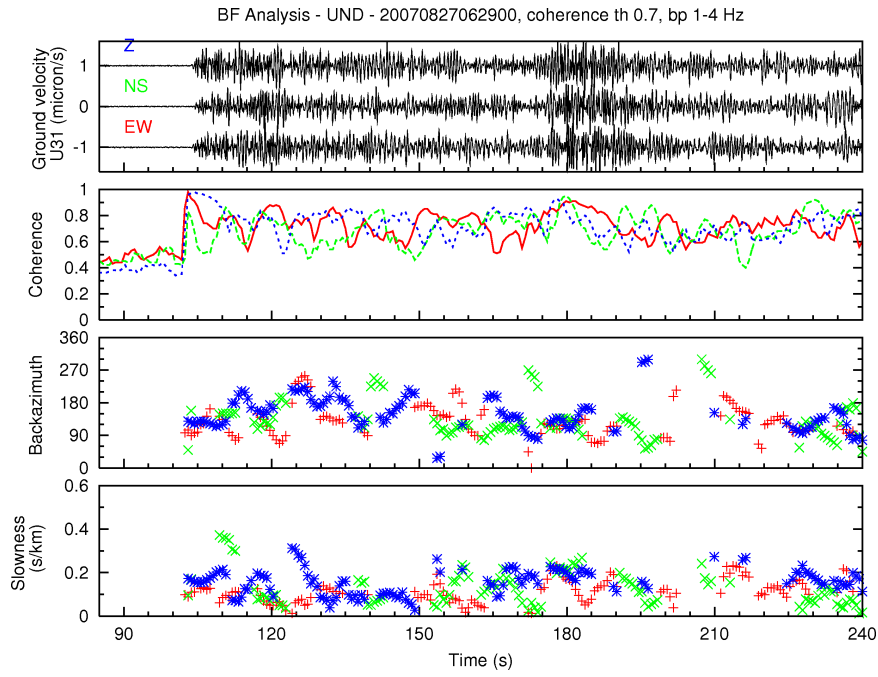
Figure 3.13: 200708270629. BF analysis for UND.
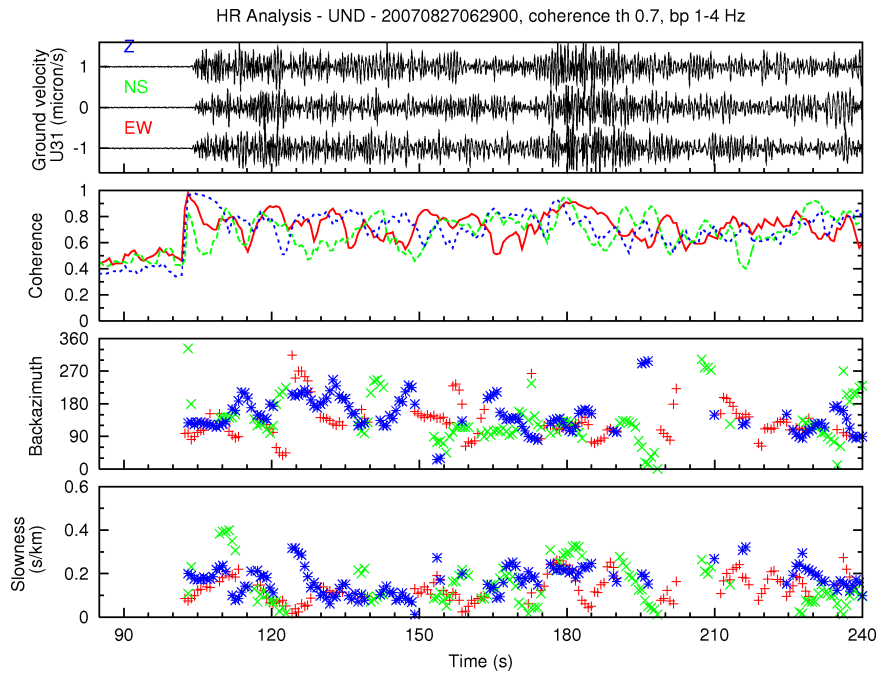
Figure 3.14: 200708270629. HR analysis for UND.
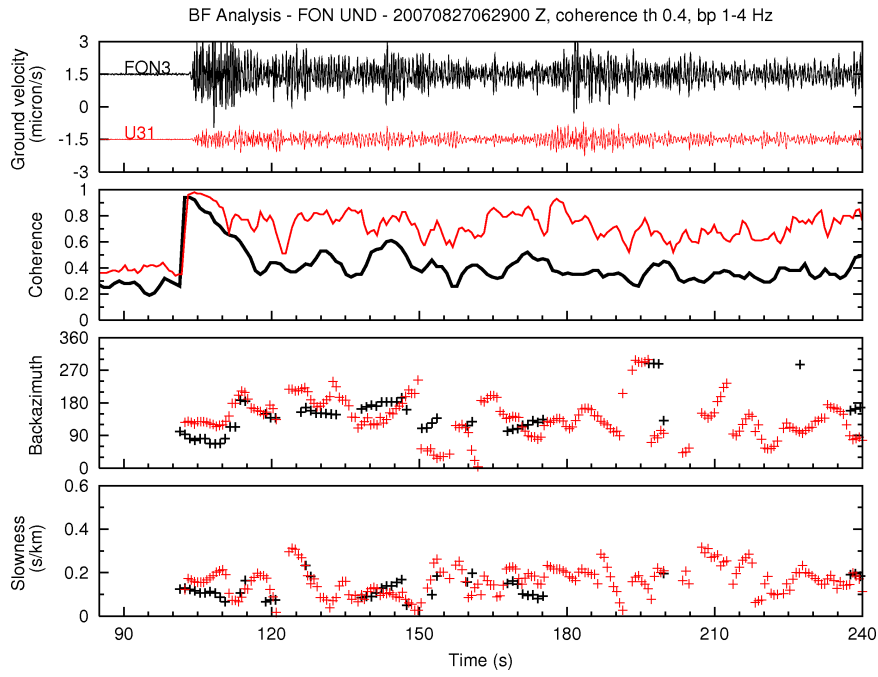
Figure 3.15: 200708270629. BF analysis for FON and UND.
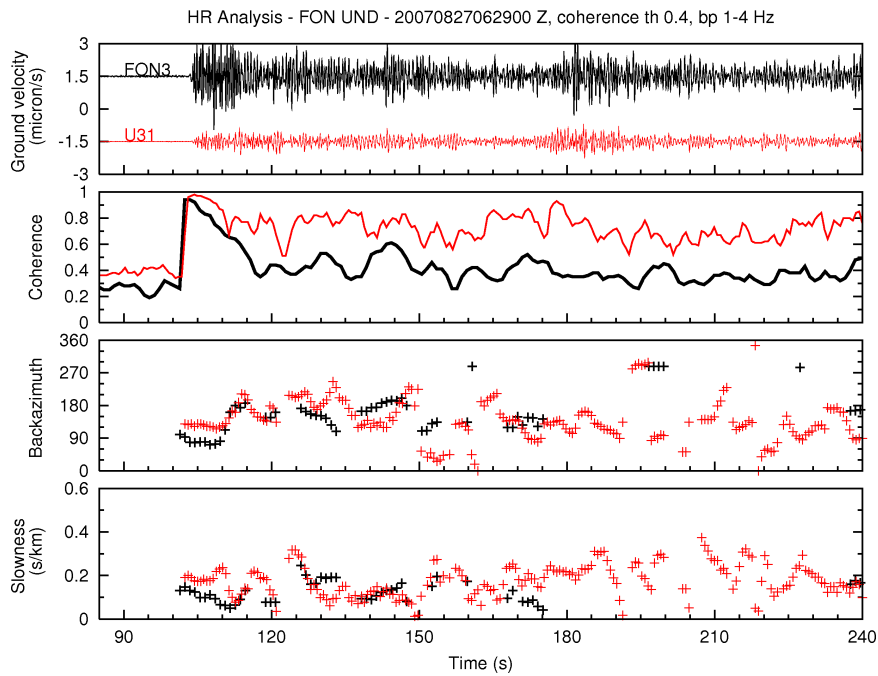
Figure 3.16: 200708270629. HR analysis for FON and UND.

3.2 Zero Lag Cross Correlation Method

Zero Lag Cross Correlation (ZLCC) is based on calculus of averaged cross-correlation between temporal series to estimate slowness and backazimuth of a wave traveling through the array. The *cross-correlation coefficient* [20] between two signals A^i and A^j is defined as

$$c_{ij} = \frac{\sum\limits_{k=1}^{M} A_k^i \cdot A_k^j}{\sqrt{\sum\limits_{k=1}^{M} (A_k^i)^2 \cdot (A_k^j)^2}} \tag{3.8}$$

where A is the seismogram amplitude, k is the time sample and M is the number of time samples. In plane wave approximation, the method searches the maximum value of cross-correlation on a square grid of slowness values (S_x, S_y). First of all, an appropriate reference point, which may also coincide with an array station, is chosen. Given a point of the grid, which corresponds to a particular value of slowness (S_x, S_y), for each couple of stations t_{ij} are calculated. t_{ij} are travel time difference between the stations i and j. Using t_{ij}, the seismograms are shifted and so we try to align the seismograms in order to reset the delay the wave arrives at different stations (thus *zero lag*). Then the c_{ij} coefficient is calculated for each couple of stations, and then averaged. This procedure is repeated for all grid points, obtaining a set of mean value of ZLCC coefficient. The maximum is selected and it corresponds to the couple of (S_x, S_y) values of the grid which in turn corresponds to the estimated slowness vector. So, the cross-correlation is linked to value of slowness on the grid and the goal is to find the couple (S_x, S_y) that has the highest correlation. Obviously, the module of slowness is given by

$$S = \sqrt{S_x^2 + S_y^2}. \tag{3.9}$$

The backazimuth is evaluated by the formula

$$\varphi = \arctan \frac{S_x \cdot}{S_y} \tag{3.10}$$

This calculation is done for any sliding window of the signal to be analyzed.

The parameters of this analysis, such as the slowness grid, window length, frequency band to filter the signals, and so on, must be decided carefully after looking at the signal features.

3.2.1 Examples of ZLCC analysis

In fig.3.17, in fig.3.18 and in fig.3.19 the results for ZLCC of 200709260814 earthquake are shown. For this method in time domain correlation is the analogue of the coherence. It is drawn for the three components with their respective symbols indicated in figure. Behind it, rms of the seismic signal is shown in logarithmic scale (green, red and black lines). In other two plots, backazimuth and slowness values are the results of grid search for ZLCC methods. Also in this case the correlation threshold can't be the same for the two arrays. For FON it must be lower than UND. The correlation for the three components remains high at UNDERSEIS array longer than at Fontari. This indicates a very correlated wavefield at UNDERSEIS array for all duration of the earthquake. At depth, the most of backazimuth values are very close to those of initial phases while those relative to coda waves are more scattered. Slowness values are almost always much smaller at UNDERSEIS array. The high correlation results on FON array are very few and relative to the earthquake onset. The wavefield is not much correlated and the most of outcomes are relative to vertical component. All these considerations are confirmed in fig.3.19 where ZLCC results of vertical components are shown. With the same correlation threshold, ZLCC method yields similar values between the two arrays only for few seconds after P phase arrival. The seismic wavefield is much more correlated at depth.

In fig.3.20, in fig.3.21 and in fig.3.22 another application of ZLCC method is shown respectively for FON and UND for the 200708270629 regional earthquake. The figures contain the information illustrated for previous case. In fig.3.20 and in fig.3.21, correlation threshold is the same for both arrays showing lower values at FON. This indicates again that the seismic wavefield is much more correlated at UND. For an immediate comparison ZLCC results of vertical components are shown in fig.3.22. Here, slowness and backazimuth are similar for the earthquake onset, while along the coda the

slowness assumes higher values at FON (black crosses).

All these considerations are found for all analyzed earthquakes. At depth the correlation is much higher than at surface. Seismic wavefield composition is quite different between the two arrays. The main differences are found along the coda.
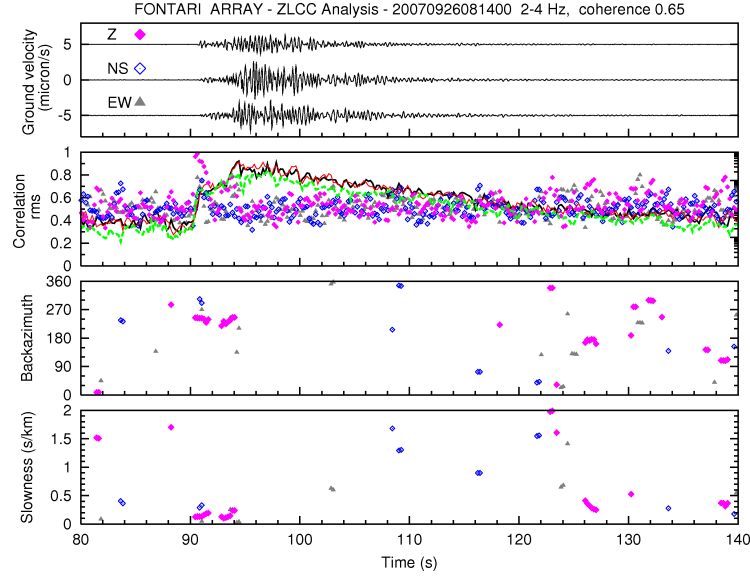
Figure 3.17: 200709260814. ZLCC analysis for FON. Correlation, rms, backazimuth and slowness results shown for the three components with their respective symbols indicated in top plot.

3.3 Comparison among the methods

All array techniques, described before, estimate two fundamental parameters of a seismic phase: slowness and backazimuth. The calculation is done in different ways but the results must be the same or quite similar when it refers to the same event. For each method an appropiate grid of S values (S_x, S_y) is used to search the highest coherence or the highest cross-correlation among all couples of stations. Once established the slowness value, backazimuth is obtained by (3.10), so the estimate of backazimuth is strictly correlated to that of slowness. Theoretical differences have been previously emphasized. In practice there may be a different resolution between the methods
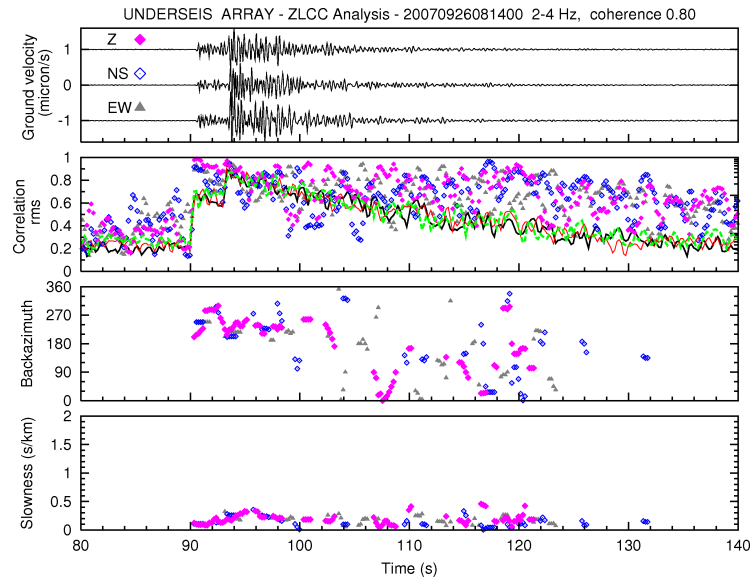
Figure 3.18: 200709260814. ZLCC analysis for UND. Correlation, rms, backazimuth and slowness results shown for the three components with their respective symbols indicated in top plot.
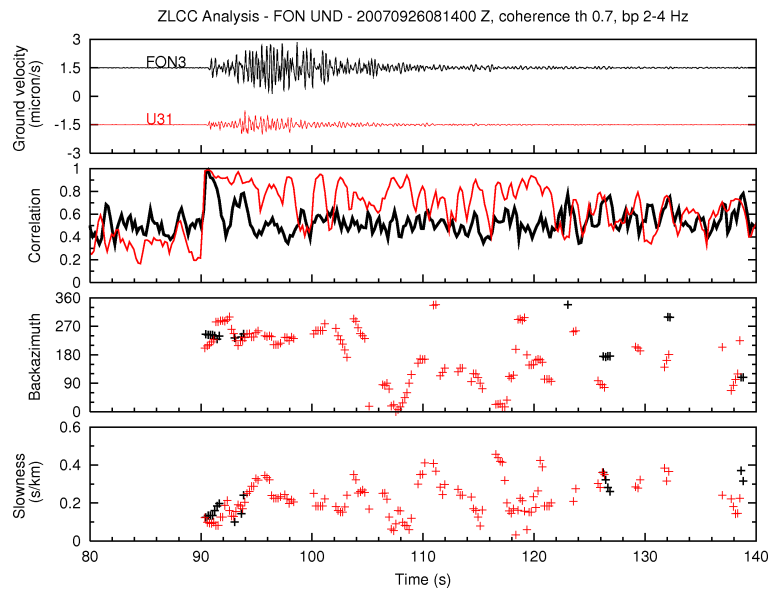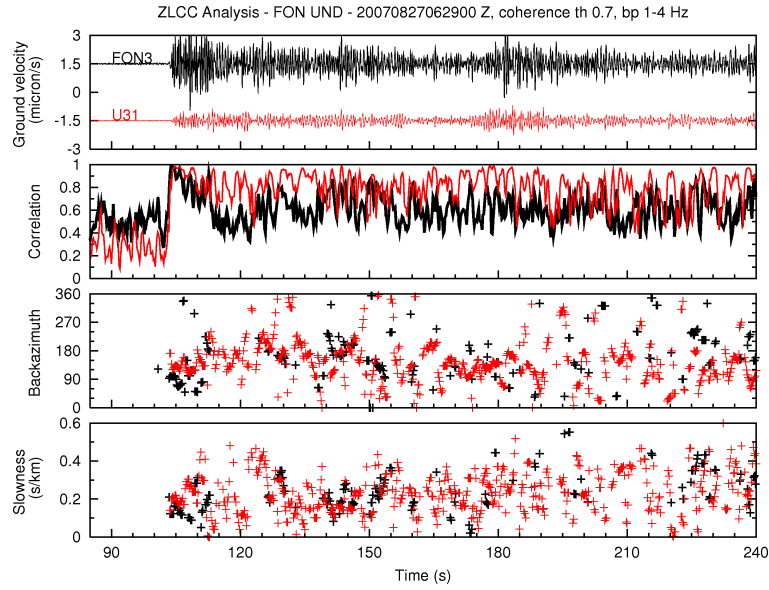

Figure 3.19: 200709260814. ZLCC analysis for FON and UND. Correlation, backazimuth and slowness results shown for the vertical component with respective color indicated in top plot.
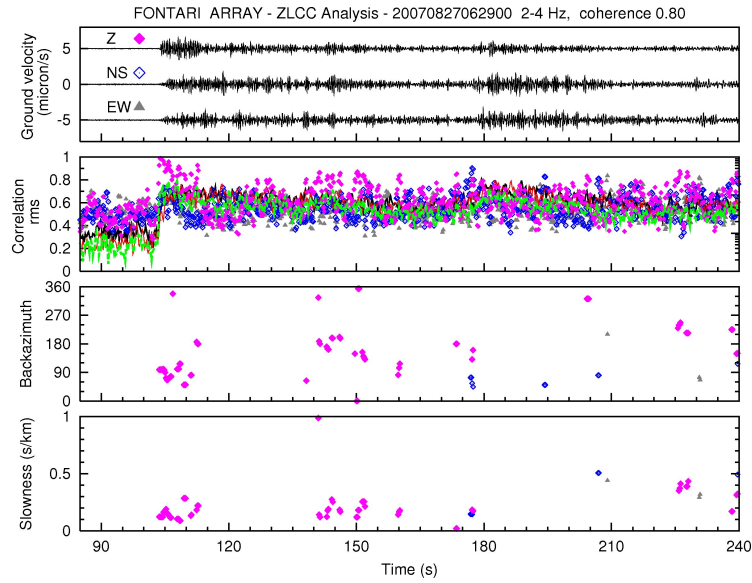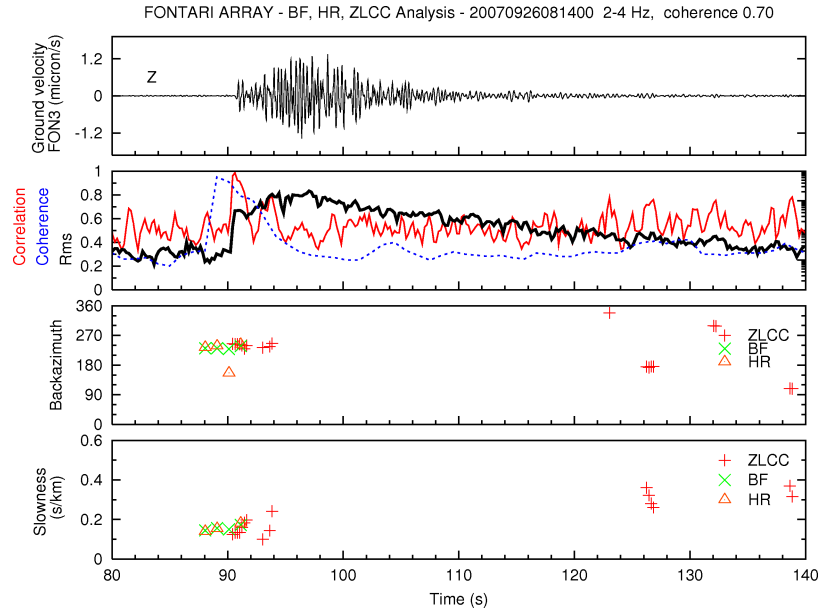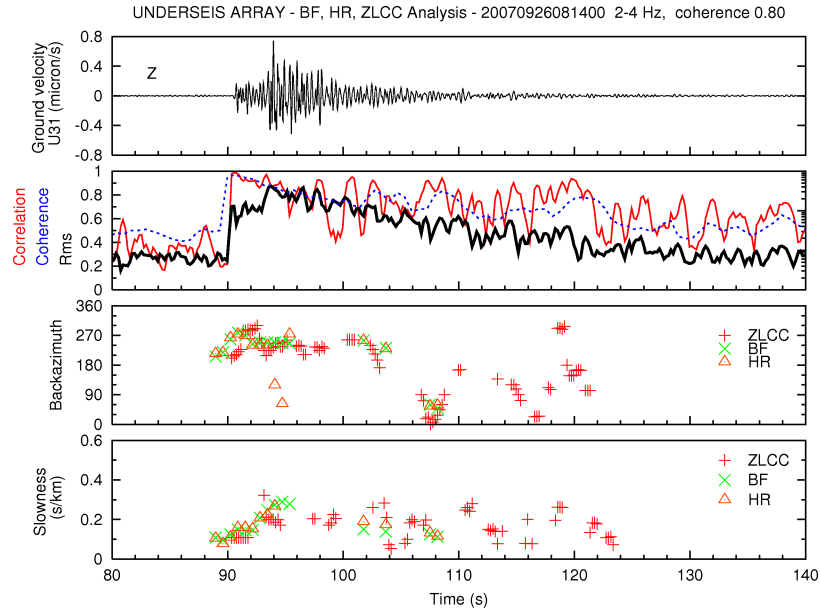
Figure 3.20: 200708270629. ZLCC analysis for FON. Correlation, rms, back-azimuth and slowness results shown for the three components with their respective symbols indicated in top plot.
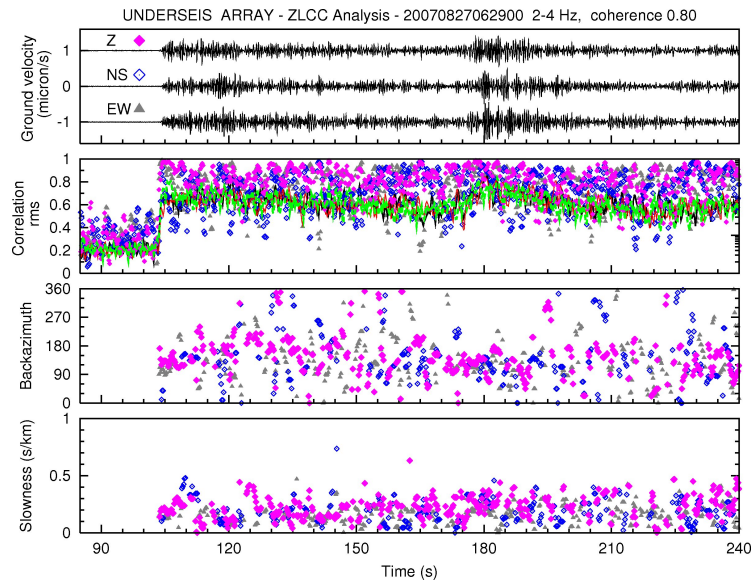
Figure 3.21: 200708270629. ZLCC analysis for UND. Correlation, rms, backazimuth and slowness results shown for the three components with their respective symbols indicated in top plot.

because the number of sliding windows is different and these last have different lengths. However in many graphics, the same scale is used to have a better comparison.

Several tests were made to make a quantitative comparison among the three array methods. For example I have used a set of 12 earthquakes with different epicentral distance, magnitude and depth. For each one, windows relative to the beginning of earthquake, in which coherence or correlation are high and the values of backazimuth are similar, are selected. Then, the corresponding values of slowness are selected. In table 3.2 and 3.3 are reported epicentral distance and backazimuth by catalogue for each earthquake, and slowness and backazimuth for every analysis. This is done in frequency band 2-4 Hz and the data are organized in three groups. For ZLCC methods, there are more values respect to the other two because I adopted a different resolution. Generally the slowness is very low and in same cases it is undeterminate. This happens for local earthquakes when their first phase arrives vertically respect to the array. The slowness is very similar among the three methods in windows where coherence or correlation are high with values in the range 0.05-0.3 s/km.

Another useful comparison between the three methods is done on backazimuth. From the obtained values, the mean value is taken for each group. The result in tab.3.1 are more similar for BF and for HR than ZLCC respect to those of the catalog and more similar to each other. The difference varies from few degrees, for most of the results, to almost 50° in some cases. Only for 200710070635 earthquake (regional, near Camerino MC, Italy), there isn't agreement between results, while for a 200710181541 earthquake (regional near Mostar, Bosnia-Erzegovina) it is almost perfect among the three methods but considerably different from the expected value.

All earthquakes have coherence or correlation much higher at UNDERSEIS array. The same seismic event recorded by the two arrays shows considerable differences. Its composition is very similar for the earthquake onset: backazimuth and slowness values calculated by three methods are in good agreement. Within the coda, the results are different: backazimuth is almost always scattered and slowness is higher in the surface recordings. All results of array analysis for three methods are shown for 200709260814 and

200708270629 earthquakes in fig.3.23, in fig.3.24, in fig.3.25 and in fig.3.26.

Earthquake	BF	HR	ZLCC	Expected value
200708230930	37	33	25	352
200708270629	127	128	155	126
200709050508	112	115	110	101
200709260814	227	232	207	239
200709280659	87	89	95	60
200710070635	42	101	150	331
200710110356	312	311	323	316
200710181541	102	105	106	74
200710250914	270	265	229	263
200710270530	110	116	124	126
200710271339	157	150	145	140
200711090055	64	78	24	335

Table 3.1: List of backazimuth values of the first P wave for three methods of arrays and from catalog.

3.3.1 Error evaluation

To associate an error to an estimated value, using three methods, the slowness is evaluated only for one window containing the beginning of each earthquake. This is performed in many frequency bands, with central frequency of 1Hz, 2Hz, 3Hz, 4.5Hz, 6Hz and 9Hz. A 2D graphic is used to show the values of slowness on the grid. For example, fig.3.27 shows slowness (S_x and S_y) of 200709260814 earthquake with Beam Forming method. The same is shown in fig.3.28 and fig.3.29 for HR and ZLCC. At 1 Hz BF method doesn't furnish a maximum value of slowness while HR is better than ZLCC. In fact at low frequency HR shows a narrow peak. BF exhibits wider curves around the maximum with respect to other methods. At high frequencies, all methods work better, as the peak is more narrow, but they are more unstable. Maxima of ZLCC are almost constant around the same value. All analysis shown fluctuations for frequency greater than 6 Hz. Only HR is more sta-

Figure 3.22: 200708270629. ZLCC analysis for FON and UND. Correlation, backazimuth and slowness results shown for the vertical component with respective color indicated in top plot.

Figure 3.23: 200709260814. BF, HR and ZLCC analysis for FON.

Figure 3.24: 200709260814. BF, HR and ZLCC analysis for UND.
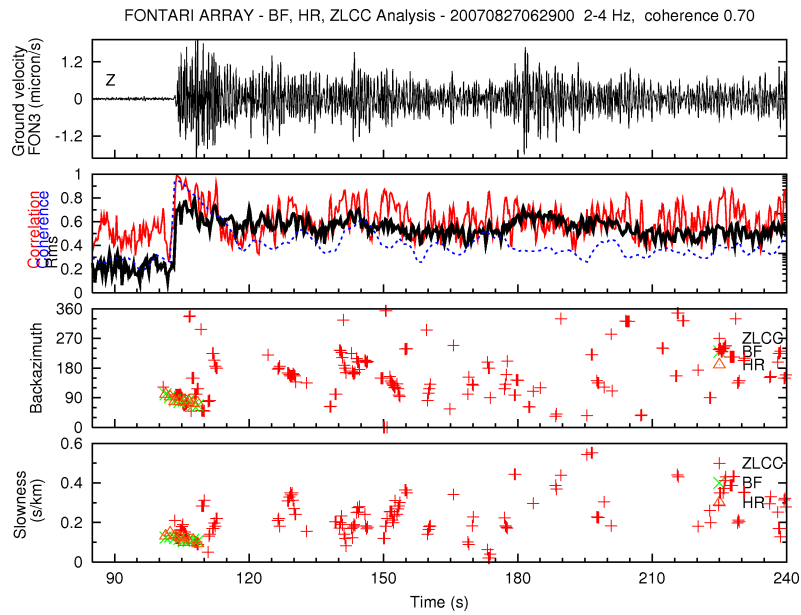
Figure 3.25: 200708270629. BF, HR and ZLCC analysis for FON.
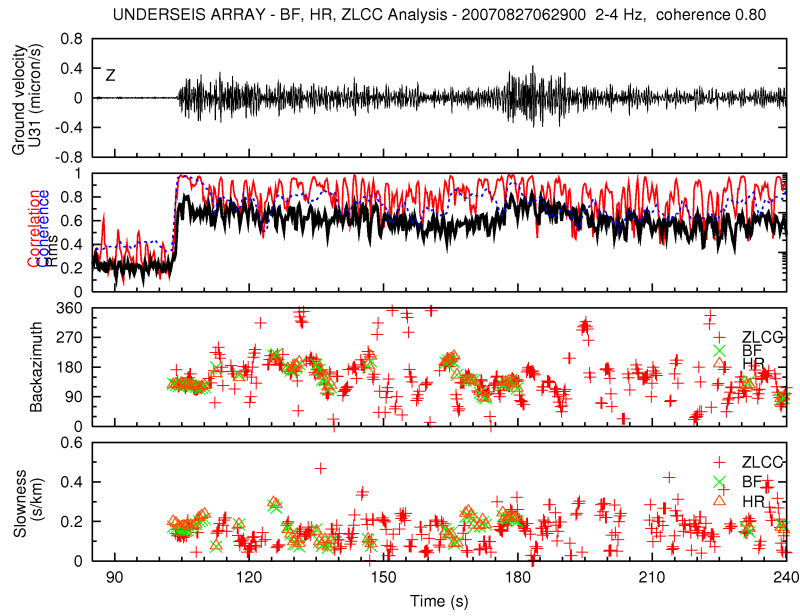
Figure 3.26: 200708270629. BF, HR and ZLCC analysis for UND.

ble, even though the maximum is obtained for few results. The results of BF and ZLCC are more similar at middle frequencies. Quantitatively, the peak width was calculated at half of its height. In some cases it can not be evaluated because the peak is not well defined. The error of slowness is proportional to peak width: more narrow the peak, smaller the error associated with slowness. Not reporting the tables of numerical values, the error of slowness was estimated about 0.05 s/km at central frequency of 5 Hz.
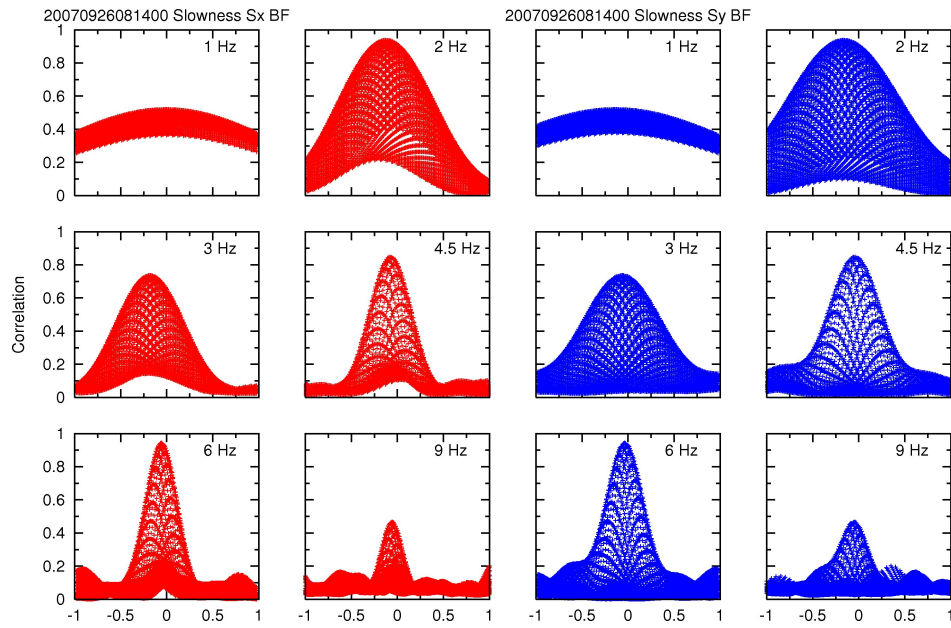
Figure 3.27: 200709260814. BF Slowness for UND.
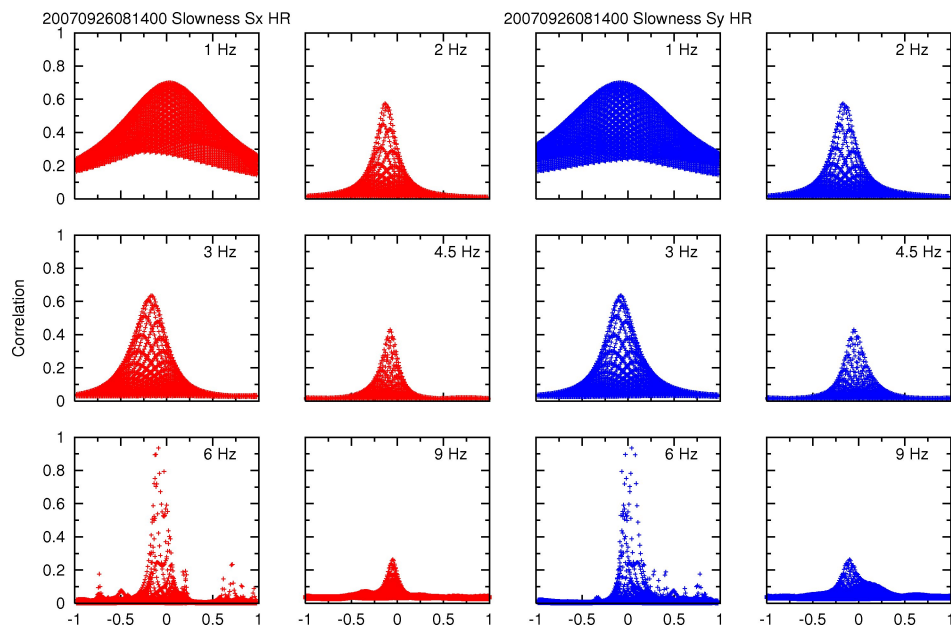
Figure 3.28: 200709260814. HR Slowness for UND.

Earthquake	Distance (km)	Backaz	Th. slown	BF slow	BF b	HR slow	HR b	Zlcc slow	Zlcc b
200708230930	78	352		0,098	29	0,093	23	0,076	23
				0,017	45	0,017	45	0,089	27
				0	45			0,089	27
								0,004	45
200708270629	727,8	16		0,173	129	0,2	127	0,189	138
				0,166	126	0,191	129	0,211	121
				0,159	122	0,176	123	0,207	123
				0,156	128	0,173	129	0,2	127
				0,156	128	0,173	129	0,22	133
				0,156	128	0,183	126	0,216	133
				0,166	126	0,176	123	0,202	132
200709050508	501,6	101		0,213	113	0,208	118	0,162	112
				0,218	116	0,197	111	0,197	114
				0,193	108	0,201	104	0,197	114
				0,199	100	0,223	99	0,197	114
								0,197	114
								0,197	114
								0,205	109
200709260814	18,4	239		0,109	206	0,105	215	0,123	201
				0,095	219	0,078	218	0,098	208
				0,124	258	0,111	263	0,094	212
				0,149	279	0,159	274	0,092	221
				0,146	270	0,159	270	0,099	228
200709280659	178,4	60		0,147	94	0,135	95	0,16	86
				0,183	89	0,183	89	0,152	92
				0,211	79	0,221	83	0,162	98
				0,151	75	0,161	81	0,173	92
				0,126	60	0,126	60	0,19	87
				0,116	71	0,109	63	0,216	81
								0,234	70
200710070635	96,9	331		0,066	21	0,062	78	0,059	23
				0,077	18	0,074	80	0,076	9
				0,012	89	0,088	146	0,092	13
								0,092	13
								0,092	13

Table 3.2: Epicentral distance, backazimuth by catalogue, and slowness and backazimuth for each analysis are reported for selected earthquake.

			0,113	310	0,095	309	0,057	315
200710110356	51,3	316	0,088	326	0,098	330	0,067	333
			0,071	300	0,082	296	0,1	323
			0,082	333	0,098	330	0,075	297
200710181541	361	74	0,149	99	0,175	102	0,177	106,4
			0,163	102	0,19	104	0,177	106,4
			0,149	99	0,187	101	0,177	106,4
			0,147	94	0,187	101	0,19	108,5
200710250914	46,9	263	0,055	243	0,044	236	0,085	225
			0,111	276	0,11	270	0,078	220
			0,224	292	0,22	289	0,067	243
			0,224	292	0,216	286	0,075	225
			0,224	299	0,208	298	0,067	243
			0,197	299	0,17	300	0,067	243
			0,136	296	0,12	293	0,114	255
			0,126	299	0,109	296	0,22	270
200710270530	838,5	126	0,147	114	0,197	119	0,128	129
			0,136	100	0,193	108	0,189	122
			0,127	106	0,186	113	0,229	122
			0,136	100	0,178	105	0,216	124
			0,139	105	0,181	109	0,216	124
							0,197	114
200710271339	30,8	140	0,262	152	0,295	150	0,192	141
			0,289	152	0,163	166	0,192	141
			0,306	156	0,153	241	0,194	153
			0,302	165	0,967	142	0,194	153
							0,224	153
200711090055	31,9	335	0,088	33	0,095	50	0,057	45
			0,082	26	0,098	60	0,082	14
							0,082	14
							0,082	14
							0,036	34

Table 3.3: Epicentral distance, backazimuth by catalogue, and slowness and backazimuth for each analysis are reported for selected earthquake.
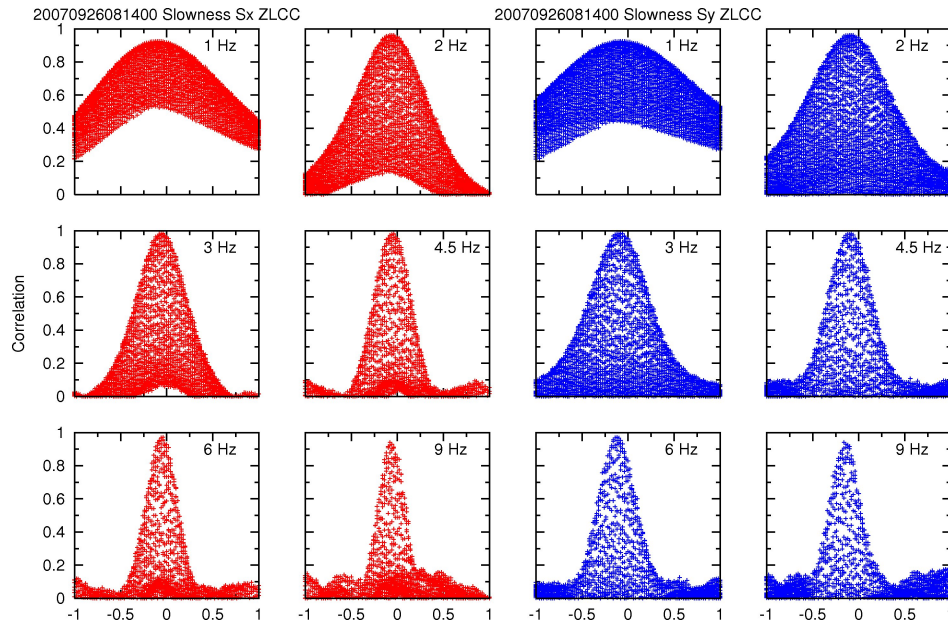
Figure 3.29: 200709260814. ZLCC Slowness for UND.

3.4   Analysis of a Landslide

Many seismic signals recorded by UNDERSEIS array were analyzed in great detail. Beside earthquakes, other natural phenomena can produce strong seismic waves. Among them, landslides are the most common in the Gran Sasso area. A large landslide occurred on 22 August 2006 at 6:28 am, and at the first analysis it doesn't have the shape of an earthquake. To study its wavefield several analysis were applied. It has a duration of about two minutes and is characterized by high amplitude.

The spectrum, shown in fig.3.30, has frequencies in the band below 10 Hz with peaks around 1 Hz. Its onset is not emergent so it was possible to establish the starting time with a good precision. All these considerations and the next analysis confirm that this event must be classified as a landslide. The sliding mass detached from the North-East of Corno Grande and was seen and photographed by people. *EIM* (Ente Italiano della Montagna) studied the landslide mass and estimated about 30 thousand cubic meters of sliding material. It came down from an altitude of 2700 meters and the runout was of 1200-1300 meters.
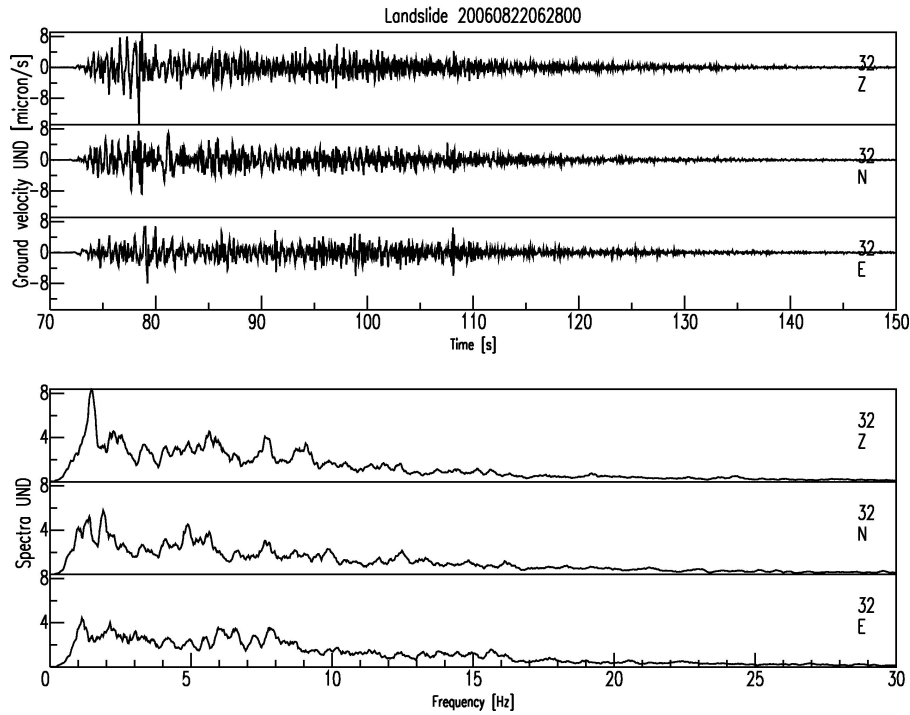
Figure 3.30: 200608220628. Landslide spectra. The event has frequencies in the band below 10 Hz with peaks around 1 Hz.

Generally, landslides produce a complex seismic signal, different from earthquake for the absence of impulsive seismic phases. Its envelope is irregular and its coda hasn't an exponential trend. The low frequency of spectrum, typical of landslides, indicate a slow release of seismic energy in time.

Landslides are part of the normal morphogenesis of the mountains and they can also be triggered by earthquakes, becoming one of the most damaging catastrophe in nature. High degree of rocks fracturing and a morphology with a very steep slope, typical of a mountain chain that is recently active, favor the landslide occurrence. The high degree of rock fracturing is evident at Gran Sasso. The numerous faults develop fractures and the rocks lose their mechanical properties and thus their resistance. The landslide can be caused also by temperature variation at high altitude, affecting groundwater and determining the formation and enlargement of pre-existing fractures. In fact the Gran Sasso massif is formed by karst rocks, very rich in water and
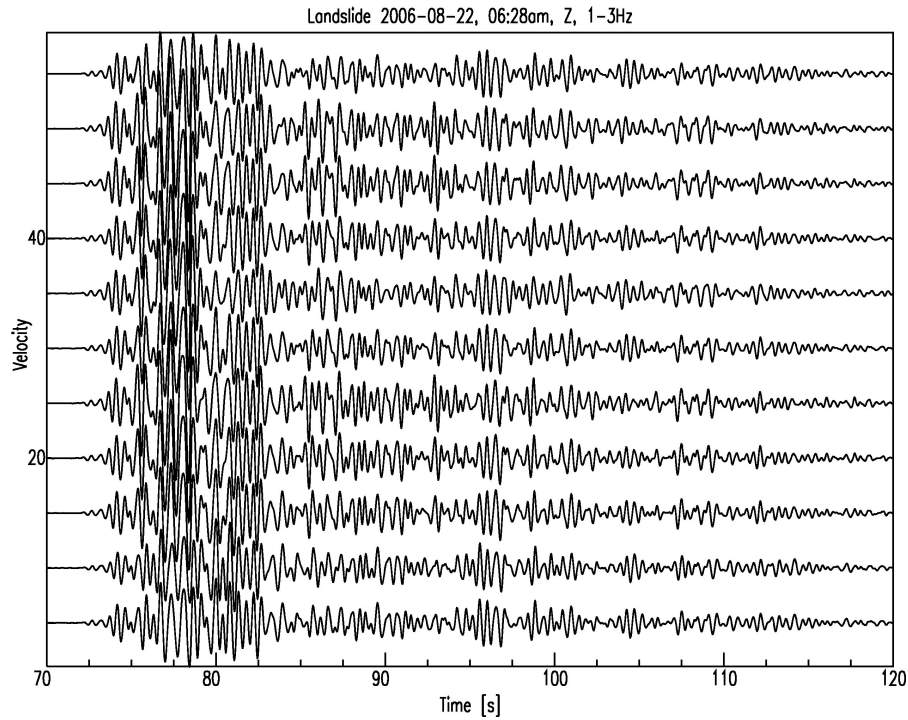
Figure 3.31: 200608220628. Seismograms of landslide (Vertical components) at the stations of UND.

groundwater. Moreover, the landslide can be caused by the long drought, followed by heavy rain.

On 22 August 2006, no significant earthquakes were recorded. The landslide wasn't caused by a seismic event. In fig.3.31 the seismograms of the vertical component for all stations of the array are shown. The event has very similar shape at all stations, justifying high values of coherence.

Applying array analysis, BF and HR in different frequency bands, (for an example see fig.3.32) it is clear for both techniques a backazimuth value quite constant in the range 0°-30° and slowness values between 0.3-0.4 s/km. The results are relative to vertical components, but the same is observed for the horizontal components. The trend of coherence and of rms are very similar. The coherence is high for almost all duration of the event. However these methods don't allowed a correct localization of the seismic source but they are only indicative of the source direction that in this case is North-East respect to the array. The values of the slowness, high also for the first

BFHR Analysis - UND - 20060822062800 Z, coherence th 0.6, bp 4-8 Hz
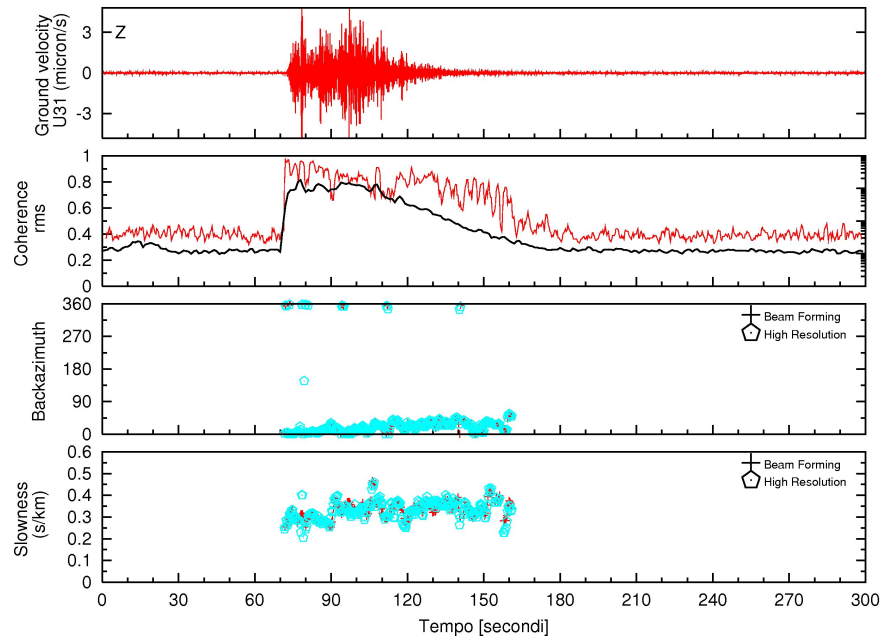
Figure 3.32: 200608220628. BF and HR analysis of landslide on Vertical components.

phases, indicate that the event is composed mainly of shear waves. Array analysis give many information on seismic wavefield but to classify a seismic signal, the observation of seismogram is very important.

Chapter 4

Polarization analysis

The observed seismic wavefield is complicated by many factors such as conversions and reflections of seismic waves, internal discontinuities of medium, presence of free surface and so on. To give a correct interpretation of every wiggle of the seismograms many combined studies must be carried out in this sense. Polarization analysis, together with the results of array techniques, permits to distinguish among various kinds of waves composing the seismogram. Both techniques were applied to many seismic events to determine their wave composition and to compare it between the two arrays. All results must be interpreted for each ground component.

In order to estimate polarization parameters, we used covariance matrix in time domain (*Montalbetti and Kanasevich, 1970* ; *Jurkevics, 1988*) [26, 27] defined by

$$S_{ij} = \frac{1}{N} \sum_{k-1}^{N} A_i^k A_j^k \qquad (4.1)$$

where A_i and A_j are two components of the same seismic station and i and j take three values corresponding to three ground components (respectively EW, NS and V). N is the number of samples in the time window. S is a symmetric matrix and has real eigenvalues which are ordered as $\lambda_1 > \lambda_2 > \lambda_3$ to which correspond eigenvectors v_1, v_2 and v_3. Maximum amplitude of particle velocity is in v_1 direction, proportional to λ_1. The particle motion

rectilinearity, RL, is computed by the formula

$$RL = 1 - \frac{\lambda_2 + \lambda_3}{2\lambda_1} \qquad (4.2)$$

where RL takes values between 0 (spherical motion) and 1 (rectilinear motion). So, it is possible to distinguish between Rayleigh waves (elliptical motion, RL = 0.5) and other waves (linear motion, RL $\cong$ 1). The **k** wave vector points to the direction of wave propagation (the same of slowness vector **S**). Its direction is obtained estimating incidence α angle, formed with z axis and given by the relation $\alpha = \arcsin(Sv_{eff})$. Generally v_{eff} isn't known and α can't be estimated. There is a method to calculate it, at least for direct P wave as discussed below. The direction of **k** projection on the horizontal plane is given by the azimuth φ obtained by the array analysis.

The polarization vector **p** is defined as that vector having the same direction of the eigenvector v_1, unitary modulus and positive direction of z components. The angle between **p** and z axis, named β, is called *polarization incidence angle*. When a P wave impacts on the surface with incidence α angle, it produces two reflected waves (*Aki e Richards, 1980*)[52], a P wave forming α angle with normal to the surface and a SV wave forming an angle smaller than α. In general the observed incidence angle is never equal to the true incidence α angle. For a P wave, we can accept β angle close to α angle, for low α angle ($< 20°$). When a P wave with this incidence angle is considered, **k** and **p** vectors must be very similar. Hence in these cases, it is possible to estimate direct P wave velocity in the shallowest layer. A high signal to noise ratio is required so that seismic noise does not affect the result.

Other angles in fig.4.1, γ (between **k** and **p**) and ψ (between the projection of **p** on the E-N plane and north) can be computed by **k** and **p** (*La Rocca et al., 2001*)[21]. The ψ angle is also named *polarization azimuth angle*. This technique allows to distinguish among different kinds of seismic waves, estimating the RL and the mentioned angles for each temporal window, as shown in tab.4.1.

Moreover the versus of polarization vector **p** gives much more information when the propagation azimuth is known. In fact while for a P wave the

Type of wave	RL	β	γ	$\psi - \phi$
P	1	α	0°	0°
S	1	–	90°	–
SV	1	90°-α	90°	0°
SH	1	90°	90°	90°
Rayleigh	~ 0.5	0°	90°	0°
Love	1	90°	90°	90°

Table 4.1: Polarization parameters in the case of well-defined seismic signal that contains no noise.

azimuth and the polarization azimuth angle must be very close each other, for a SV wave they must differ by about 180°.

For S waves and all other arrivals, the incidence angle α is generally different from β and it cannot be estimated as described previously because the nature of the secondary arrivals (P, S or surface waves) is unknown. Then for these arrivals, two wave vectors k_p and k_s are calculated: k_p is obtained fixing v_{eff} at v_p (P-wave velocity) and k_s fixing v_{eff} at v_s (S-wave velocity, with $v_s = v_p/1.73$). So it is possible to estimate the two incidence angles, α_p and α_s and the two different angles γ_p and γ_s. If the average $(\gamma_p + \gamma_s)/2$ is greater than 45°, we assume $\gamma = \gamma_p$ and $k = k_p$, while if that average is greater than 45°, we take arbitrarily $\gamma = \gamma_s$ and $k = k_s$.

In the calculus of covariance matrix, the use of many stations improve the stability and the quality of the results because it reduces seismic noise effects and errors due to possible wrong orientation of the horizontal components. Moreover, in order to have better results, a narrow band pass filter is applied to seismic signals before to calculate the covariance matrix. In this way only few requested seismic waves are considered. After the calculus of covariance matrix for every station, the values are stacked to have a unique covariance matrix for each temporal window. This gives a stable estimation of the polarization parameters. Analyzing the earthquake wavefield, a *rms* (root mean square amplitude of the signal) threshold is used so that selected temporal windows contain the most part of the seismic event. Instead to analyze seismic noise, no *rms* threshold is selected.

A program in C language, named *polarsac*, estimates polarization parameters, using only one station with three components. Rose diagrams of polarization azimuth which give an immediate view of the wave motion are an example of this application.
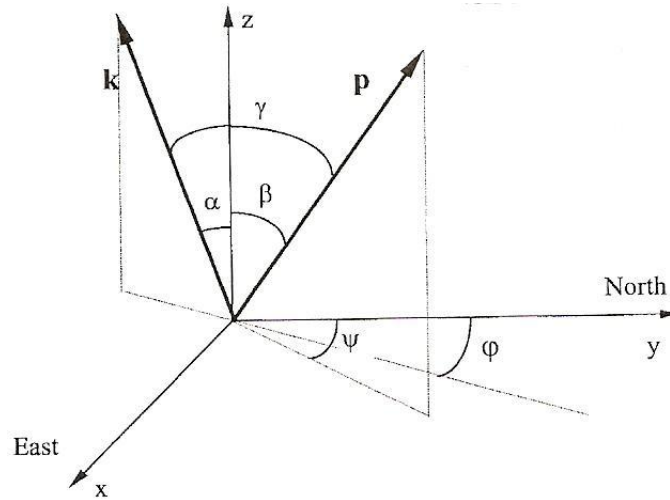
Figure 4.1: Vectors and angles used in the polarization analysis of seismic wavefield.

4.1 Examples of Polarization analysis

The polarization analysis was carried out for the most of selected earthquakes, especially for their coda waves. In fact, as previously observed, direct P wave and sometimes direct S wave are generally identifiable just looking at the seismogram. The uncertainty is on all other arrivals. In order to have a better interpretation of the results, a combined array analysis for different components of ground motion is necessary. Separating vertical and horizontal components, different nature of seismic waves (particulary for Rayleigh and Love waves) is simpler to identify. This can't be true for the coda waves, along which many seismic phases are uncorrelated and superimposed, each with different slowness and backazimuth. Another difficulty in the identification of the seismic waves concerns also small local earthquakes, characterized by a higher frequency contents. Polarization analysis

was applied on the same temporal windows of those used in ZLCC methods. Among array techniques, it doesn't have restrictions on the window length of the analyzed signal. Each seismic event was studied in many bands of frequency. Narrow temporal windows were chosen to estimate polarization parameters to have few variations of wavefield characteristics and to consider the lowest number of waves.

Focusing the attention on the last part of seismogram, we can see within the coda several well-correlated phases especially at UNDERSEIS array, as noted previously. Calculated slowness values are much lower at depth than at surface. This indicates the presence of different kinds of waves in the recording at the two arrays. Rms threshold is the same for both recordings, showing more results at depth where the coda is longer.

In fig.4.2 and in fig.4.3, polarization analysis results of coda waves are shown respectively at Fontari and UNDERSEIS array again for 200709260814 earthquake. Both graphs show the results relative to all stations of an array and no body waves results are observed. Estimated polarization incidence β angle is quite different between the two arrays, being almost constant at Fontari array. Its values of β near 90° indicate strong presence of surface waves. The confirmation also comes from higher rectilinearity values at Fontari array with respect to those of UNDERSEIS recording. Low slowness values and non homogeneous distribution of β angle indicate the presence at UNDERSEIS coda of body waves, mostly of shear waves. While at depth ψ angle shows random distribution, at surface its values are distributed around two bands. As both graphs show only coda waves results, polarization azimuth is mostly relative to superficial waves at Fontari array. In this context, we aren't interested to a fine identification of seismic waves, but only to understand a large scale common property or differences between recordings at the two arrays.

Fig.4.4 and fig.4.5 show polarization azimuth distribution computed for any stations of the two arrays for the same earthquake. The results are relative to coda waves. At Fontari array a common direction among the stations is evident. At UNDERSEIS the distribution is quite random. As well correlated noise could be superimposed to the seismic signal, especially within the coda, polarization azimuth distribution of noise was made too.

Background noise is quite uncorrelated both at Fontari and at UNDERSEIS arrays (fig.4.6 and fig.4.7). The temporal window is about 80 sec. The particular trend of polarization azimuth found for this earthquake at surface will be more evident at Fontari stations in chapter 7, where a statistical analysis will be applied to all data set. In fact, polarization parameters will be used to find common behaviors to all selected earthquakes. We can suppose the presence of strong scatterers which would generate correlated signals and could be superimposed on the uncorrelated signals, characteristic of the most of coda. As noted by *Del Pezzo et al., 1997* [20] the surface scatterers play an important role in the formation of the coda at high frequency: they generate high energy wave packets that arrive at the array with a high value of coherence. These packets are superimposed on a background uncorrelated radiation.

Finally, the importance of polarization analysis is particularly evident when unclear events must be studied, especially when sharp pulses are absent in the recordings (for example, tremor recordings). This analysis was made also for "particular" events of chapter 2, whose nature is unclear.
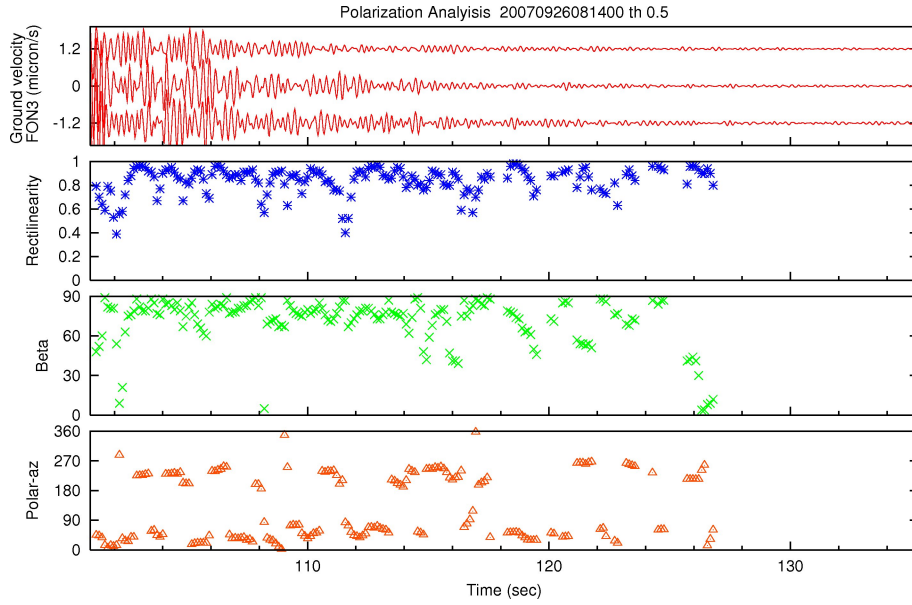
Figure 4.2: 200709260814. Polarization analysis of coda waves at Fontari array. From top: seismograms (red), rectilinearity (blue), beta angle (green), polarization azimuth (orange).
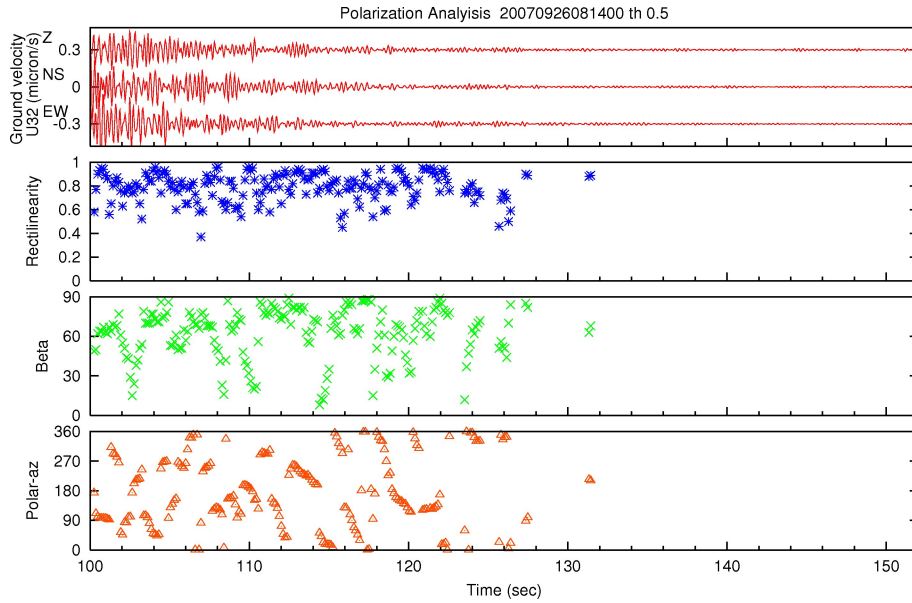
Figure 4.3: 200709260814. Polarization analysis of coda waves at UNDER-SEIS array. From top: seismograms (red), rectilinearity (blue), beta angle (green), polarization azimuth (orange).
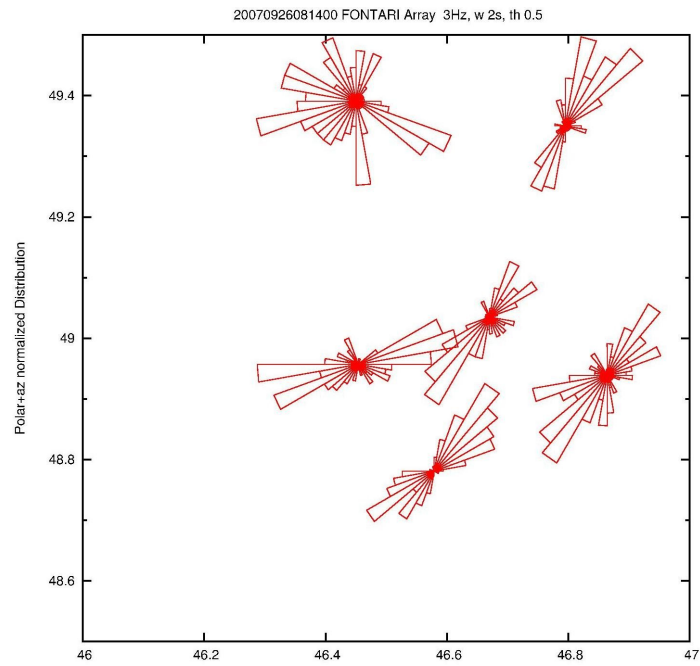
Figure 4.4: 20070926081400. Polarization azimuth of coda waves at Fontari array with rose diagram.
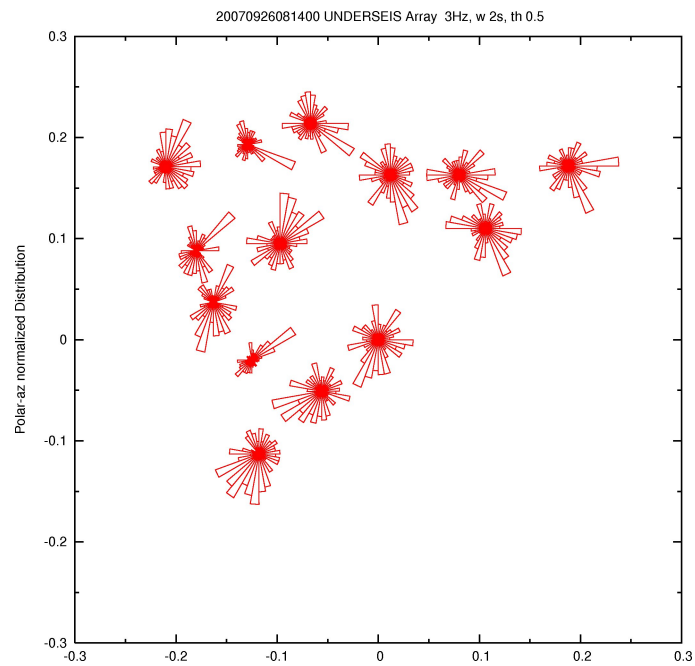
Figure 4.5: 200709260814. Polarization azimuth of coda waves at UNDER-SEIS array with rose diagram.
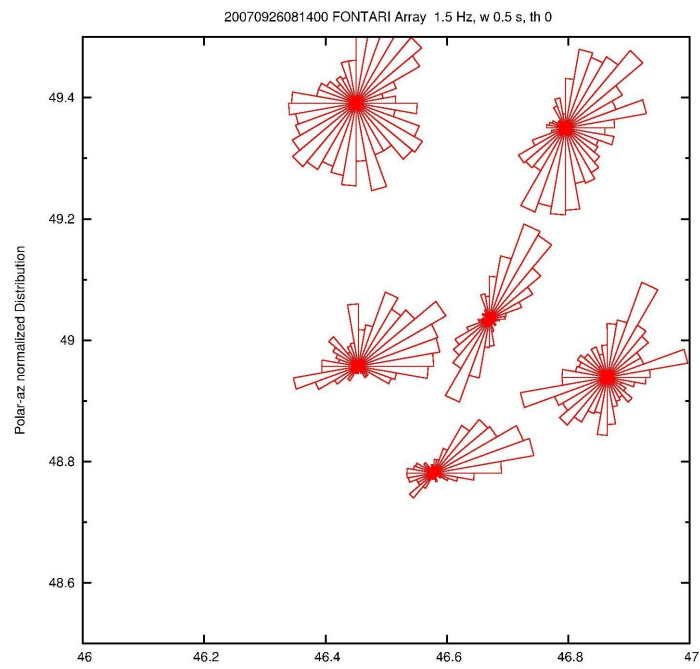
Figure 4.6: 200709260814. Polarization azimuth of noise at Fontari array with rose diagram.
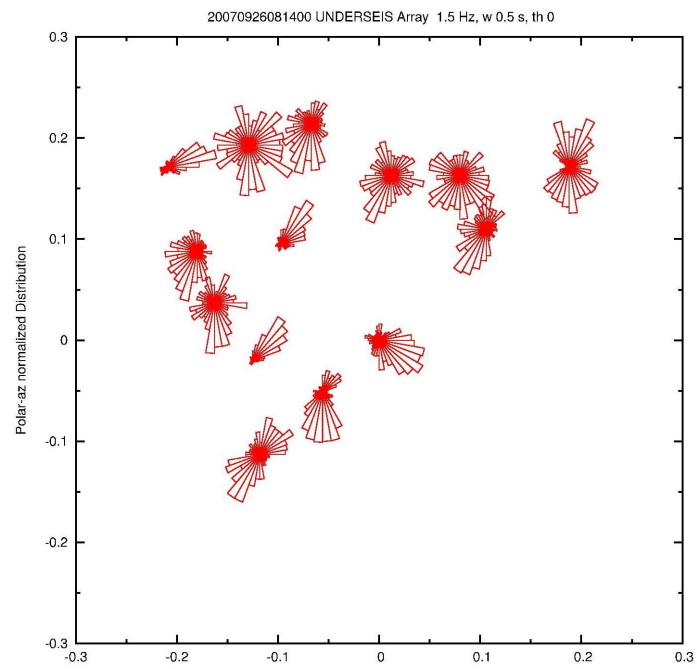
Figure 4.7: 200709260814. Polarization azimuth of noise at UNDERSEIS array with rose diagram.

Chapter 5

Site response study

Effects as attenuation, amplification and scattering of seismic waves in the near-surface rocks are commonly referred to as site effects. During an earthquake they may produce large ground-motion amplification, increasing seismic hazard in the interested area [54]. The site amplification depends strongly on topographic irregularities, the presence of basin and surface geology, assuming different behaviors for hard rock, sedimentary and alluvial filled sites. Site effects contributions can be so large that they can dominate the observed wavefield at surface or near surface stations. As shown by *Abercrombie (1997)* [43], surface topographic irregularities can strongly influence the evaluation of source parameters (such as rupture dimensions and stress drop) and, as noted by *Blakeslee and Malin (1991)* [44], a few hundred meters is not deep enough to minimize the entire site effect because seismograms can be still contaminated by local conditions and surface reflections. The availability of a bedrock site which is not affected by site effects has been a matter of debate in the scientific community [39]. For this reasons, the possibility to use low noise seismograms recorded at sites located on rock give the opportunity to naturally eliminate site effect distortion and to use this site as a reference for the station located in a different geological and morphological environment.

5.1 H/V Ratio

Many studies have been performed to analyze the site effects, based essentially on spectral ratios. The *standard spectral ratio* (SSR) technique compares the site of interest to a bedrock reference site. But unfortunately this method has a limit because of definition of a hard-rock reference site. In many experiments, data from a seismometer installed on hard-rock aren't available and site effects may affect the ground motion even on hard rock. So it is not always easy to find an adeguate reference station. Then we can consider as reference station that where site effects are small relative to soft-soil amplification or we can assume as a reference the average spectrum among the stations. This assumption is right when the mean spectrum is very close to the spectrum recorded at the reference hard-rock site. Often the spectral ratio method was applied on S waves; other times coda waves or whole seismogram is used.

A technique which doesn't depend on the availability of a reference station is the *horizontal to vertical spectral ratio* (HVSR). It uses the spectral ratio of horizontal components on the vertical one recorded at the same site. It is used to investigate soft-soil site effects and topographic site effects [49].

Originally proposed by *Nakamura* (1989) to interpret microtremor measurements, recently this technique has been used for different purposes, like studies of sedimentary basins, to estimate the fundamental frequency of buildings, to characterize the seismic hazard in a small scale and to provide detailed information for seismic microzonation. Theoretical investigation about HVSR are widely discussed [35]. Horizontal-to-vertical spectral ratios technique has been also applied to earthquake records to identify the fundamental frequency of the investigated site [37] and, in some cases, the results were also compared with other techniques based on a reference site [38]. The studies dedicated to the comparison of different site response estimation techniques indicate that HVSR and other techniques are capable to estimate the fundamental resonance frequency of a site but HVSR provide different levels of amplification.

In this work, HV spectral ratios were evaluated on 8 s window of signal starting 0.5 s before P onset of local earthquake signals. The HV were evaluated

for three stations at UNDERSEIS array and at Fontari array respectively and the final values of spectral ratios were obtained by averaging HV on 22 local earthquakes signals. The amplitude of spectral ratio and their stability among different earthquake are fundamental characteristics to obtain some indication about the site effects of the investigated area. The average result for 22 local earthquakes are shown in fig.5.1. In these figure the results for 6 stations (U01, U23 and U32 for UNDERSEIS and FON3, FON4 and FON7 for Fontari array) which are indicative for the other sites, are shown. The HVSR evaluated for UNDERSEIS stations show a clear constant pattern equal to unity for all the investigated frequency range (U01, U23 and U32 H/V trend, right side in fig.5.1). This result, averaged on 22 local earthquakes signals, is a clear indication that the site can be considered a good hard-rock site characterized by no frequency peak of amplification. On the contrary, HV spectral ratios evaluated for Fontari sites show in some case appreciable frequency peaks (FON4 H/V in fig.5.1). Peak frequency of amplification ($H/V > 2$) is identifiable in the frequency range [4-8] Hz for FON4 and the other sites (FON3 and FON7) show a constant H/V pattern more than 1. This result suggests that site effects at Fontari sites cannot be negligible and some further investigations should be done in an area where a large variability of site amplification effect has been observed [36]. The analysis of HVSR for different directions doesn't indicate a clear dependence from the azimuth of propagation.

The results for two local earthquakes are shown in fig.5.2 and in fig.5.3. In these figures spectral ratio for only two stations (U32 for UNDERSEIS and FON3 for Fontari array) were shown. It is clear again that the amplitude of earthquake signals recorded at Fontari is considerable higher than the same event recorded at UNDERSEIS.
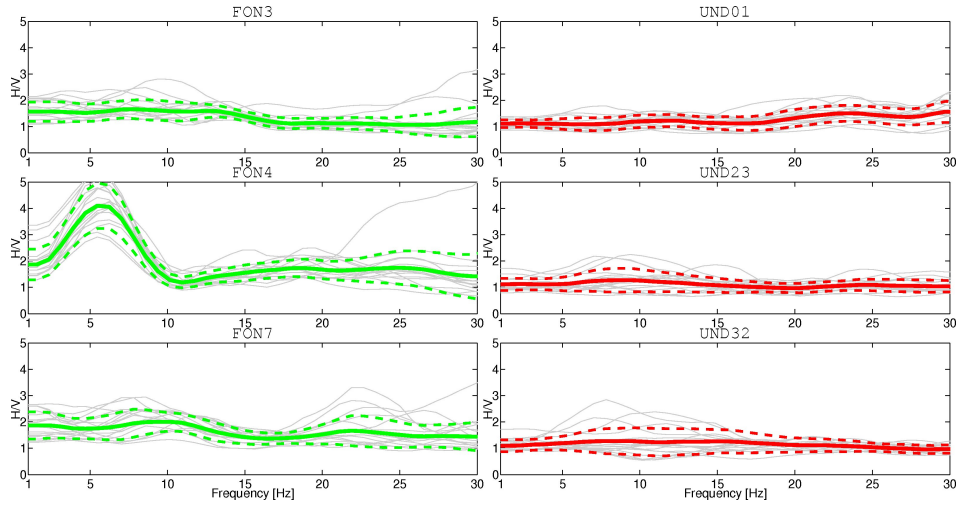
Figure 5.1: Mean Spectral Ratio at both arrays for some stations (with green for Fontari and with red for UNDERSEIS). In the background (gray color) there are the results for each earthquake.
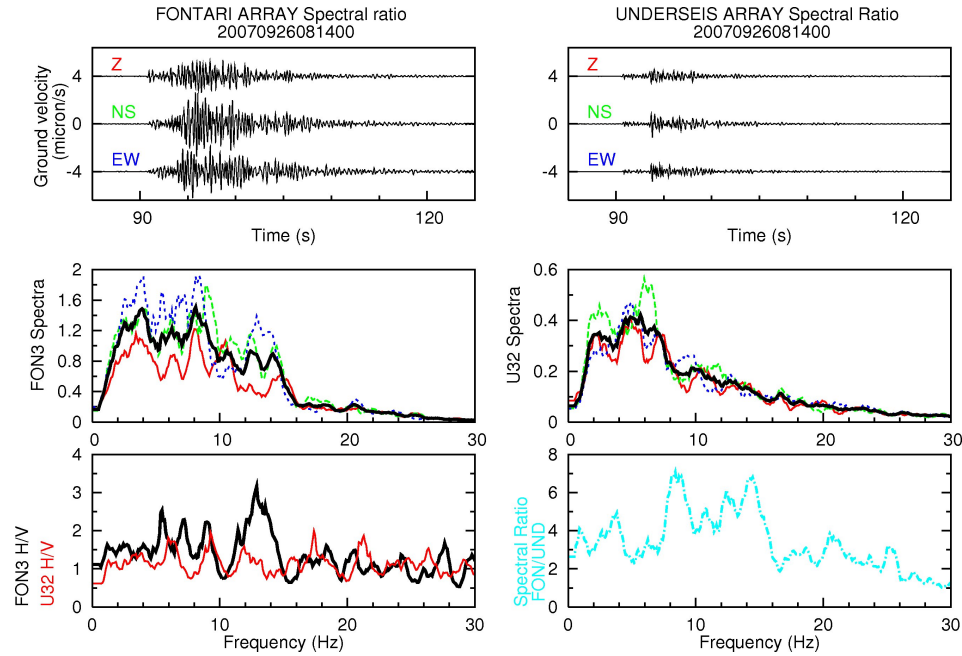
Figure 5.2: 200709260814. Spectral Ratio at both arrays.
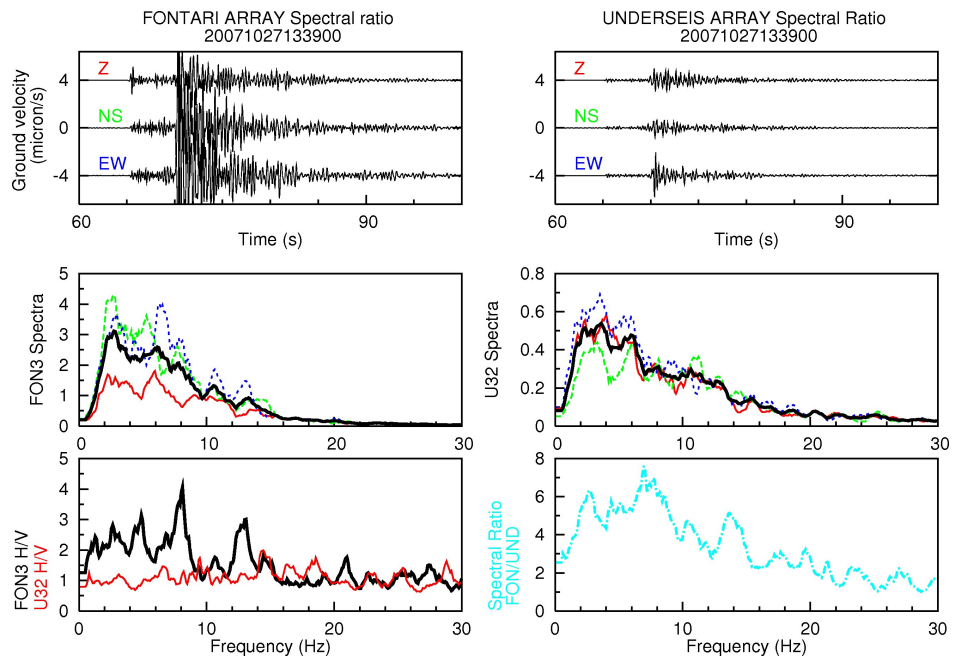
Figure 5.3: 200710271339. Spectral Ratio at both arrays.

Chapter 6

The earthquake of 6 April 2009

The city of L'Aquila is located in the Apennines chain, the most active seismogenic region of Italy. The seismic sequence triggered by the earthquake of April 6, 2009 $M_w6.3$ was well recorded by the array UNDERSEIS, 23 km from the epicenter of the main shock. The main event was located at 9.5 km depth and at distance of about 2 km from L'Aquila town center. In the last years, before 2009, the local seismicity rate was low with small shallow earthquakes. After the main shock, the accumulated strain energy was released during the following months with a large number of aftershocks.

Several studies on 2009 L'Aquila earthquake have been published: *Chiarabba et al., 2009*[40], *Amoruso et al., 2009*[41], *Walters et al., 2009*[42], *Di Luccio et al., 2010*[7], and more. The main shocks (6 April $M_w = 6.3$, 7 April $M_w = 5.6$, 9 April $M_w = 5.4$) and aftershocks are consistent with a predominantly normal-faulting mechanisms striking NW-SE of central Apennines. The events are concentrated in the upper 15 km of the crust. The main shock fault segment extends for about 15-18 km. The central sector of the chain is affected by NE-SW striking extension and uplift. The locations and geometry of faults accomodate this extension, responsible for the formation of intra-mountain basins bounded by NW-SE striking faults. Many studies observe a migration of seismicity along the north of mountain chain. For its tectonics, the region of central Apennines has one of the highest seismic

hazard in Italy. In this chapter, only coherence analysis is discussed on the sequence of April 2009. From the results, some events that seem not to belong to the sequence emerged.

6.1 Coherence analysis

Starting on late 2008 the rate of local earthquakes in the Gran Sasso area increased significantly. A swarm of hundreds of events was recorded during the first months of 2009. Ten of these earthquakes were $M > 3$ and many of them were shallow enough to be felt by people. This swarm was the foreshock of $M_w = 6.3$ earthquake of 6 April 2009.

Also the graphs of UND daily coherence confirm a significant increase of the number of local earthquakes (for an example see fig.6.1). In the past there were periods particularly rich of seismic swarms not followed by a large earthquake. During the sequence of April 2009 in Abruzzo, the increase of coherence is very significant. It remains very high, more than 0.6, for almost one month. Seismic sequence was characterized by tens of thousands of earthquakes recorded with high signal to noise ratio at UNDERSEIS array. As an example, 21 April 2009 is shown in fig.6.2. The seismogram shows the entire day. As numerous earthquakes happened and overlapped, the coherence value could not diminish (see fig.6.3 and fig.6.4). In fig.6.3 Julian day 96 (6 April 2009) shows a sharp increase of coherence that is relative to the main shock.

In fig.2.19 and fig.6.5 the mean coherence respectively six and twelve months after April 2009 is shown. As we can see, the number of local earthquakes in a day is still very high. A detailed coherence and array analysis of the period showed some particularities, as illustrated in the next section.

6.1.1 Coherence at UNDERSEIS array in the period April-May 2009

Seismic signals recorded in the period April-May 2009 were first observed trough their coherence and then analyzed with array and polarization techniques to identify anomalous and/or peculiar characteristics of the local

Coherence 1 February 2009 - 20 February 2009
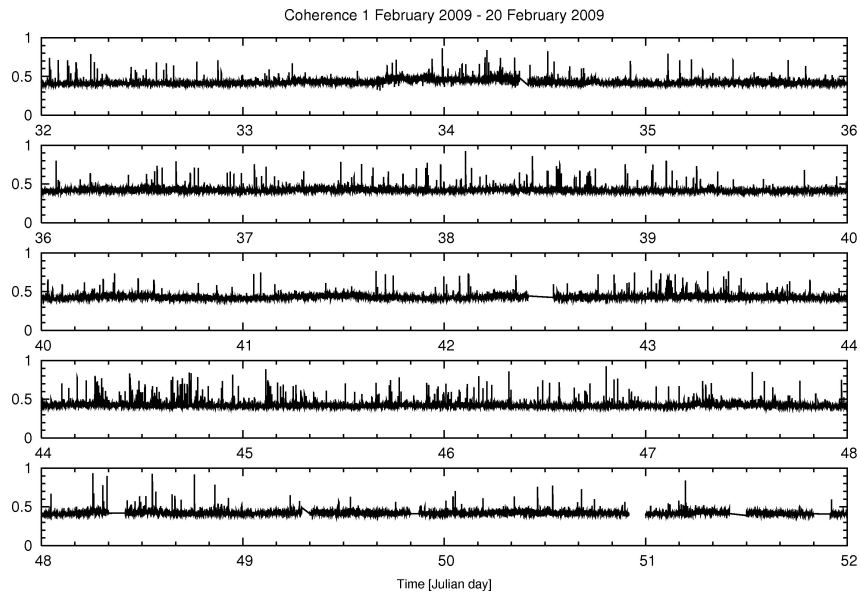
Figure 6.1: 1-20 February 2009, coherence versus time. Before the sequence of 6 April 2009 the graphs of coherence confirm a significant increase of the number of local earthquakes.

20090421, UNDERSEIS ARRAY, Station U32 Z, Mark L4C, lowpass 15 Hz
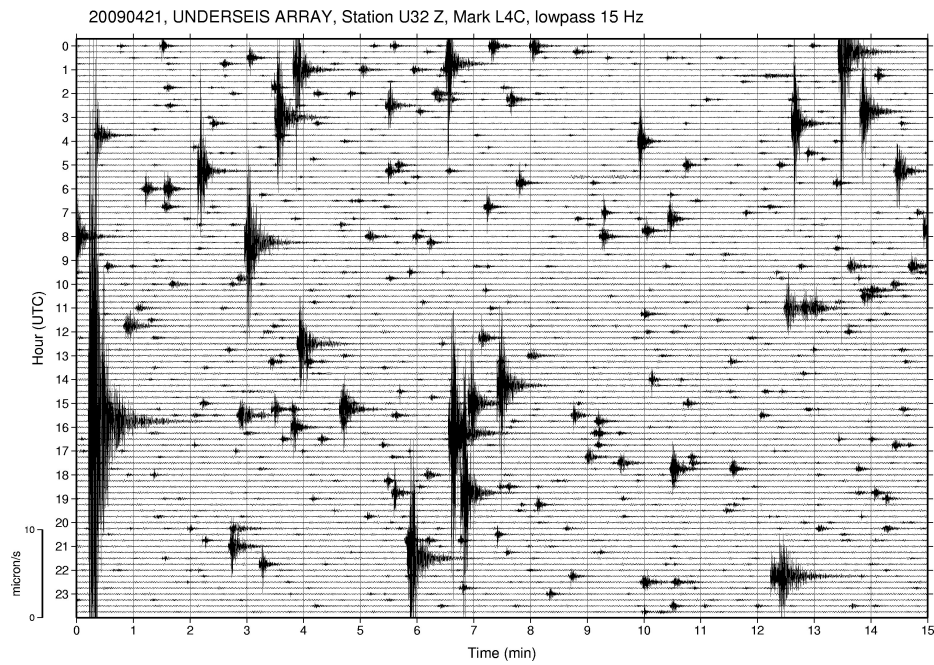
Figure 6.2: 21 April 2009, seismograms relative to entire day at one station of UNDERSEIS array (U32), Vertical component.
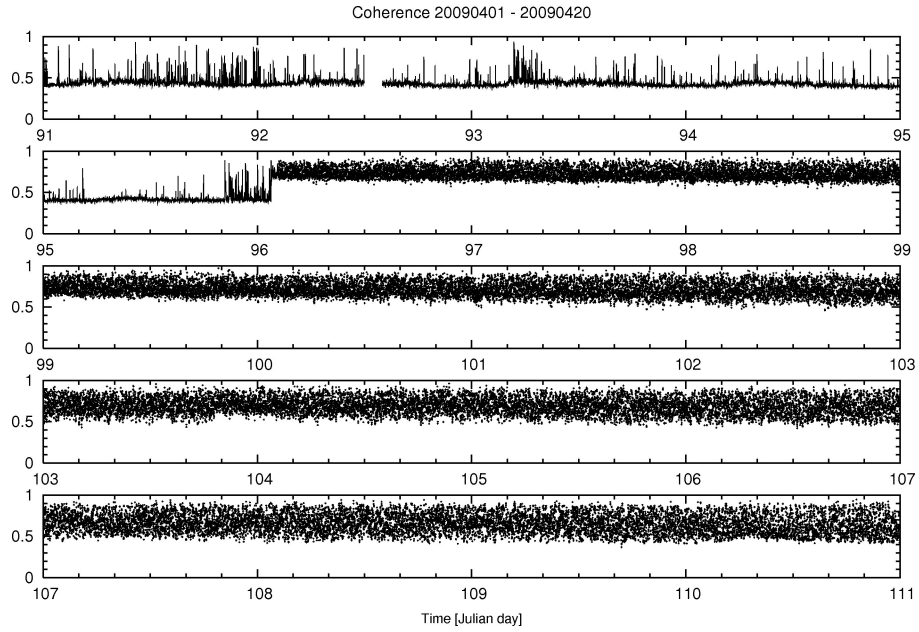
Figure 6.3: 1-20 April 2009, coherence versus time. 96 Julian day (6 April 2009) shows a sharp increase of coherence that is relative to main shock.
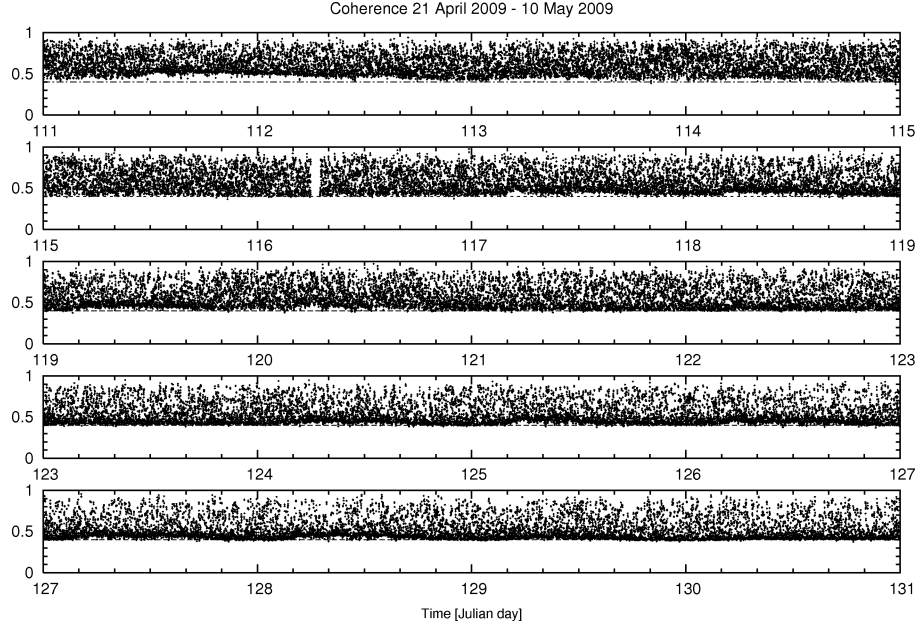
Figure 6.4: 21 April - 10 May 2009, coherence versus time. The increase of background coherence is very significant, remaining high for almost one month.
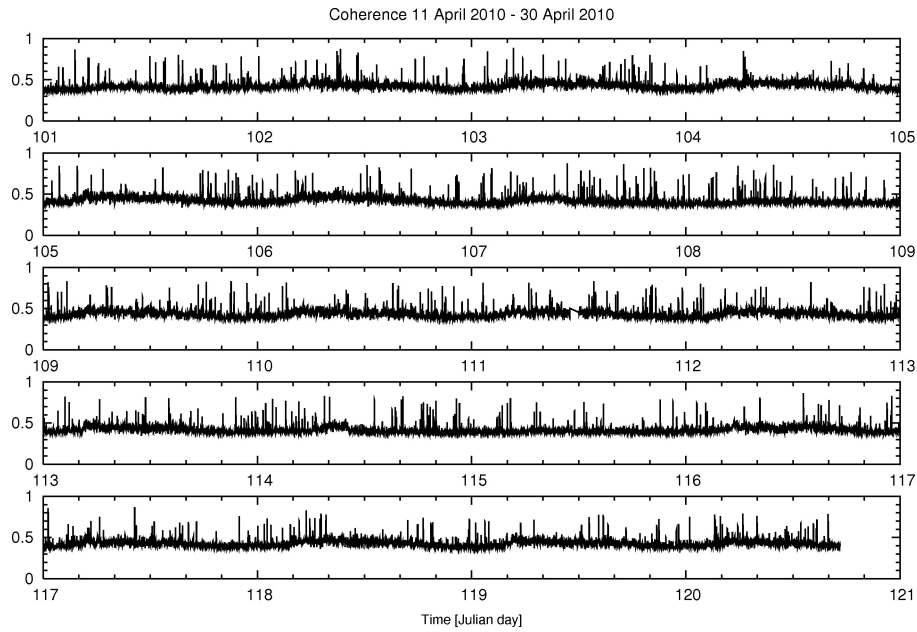
Figure 6.5: 11-30 April 2010, coherence versus time. Mean coherence after twelve months the swarm of 6 April 2009. The number of local earthquakes in a day is still very high.

seismicity during this period. Coherence analysis, performed in many band of frequency, shows an interesting result. For about two days, 21 and 22 April, the minimum value of coherence is higher than the days before and after, also in absence of local microearthquakes. In the same time, the minimum amplitude of the seismic signal is greater than the days before and after. The figure 6.6 shows lower envelope of coherence (red line) and amplitude (blue line) of the seismic signal calculated in two different frequency bands. The increment is more clear in the band 2-6 Hz.

For this period, array analysis shows coherent signals that arrive from completely different directions than those associated with local earthquakes in the sequence triggered by the main shock. The increase is due to the presence (fig.6.7) of signals propagating from the east, north-east respect to UNDERSEIS array (backazimuth between 30 and 90 degrees), contrary to the signals associated with local earthquakes of the sequence, which come from the third quadrant (backazimuth between 180 and 270 degrees). BF and HR methods highlight about 20 phases with backazimuth between 30

and 90 degrees. The anomalous signals detected on 21 and 22 April are characterized by small amplitude, low signal to noise ratio, emergent onset, duration from tens of seconds to some minutes, and no clear phases classified as P and S direct. The location of the source is very difficult since there are no constraints on the distance. Slowness values estimated by the array analysis are between 0.3 and 0.4 s/km, indicating a rather shallow source.

Using the 'anomalous' backazimuth we extracted single events. Some of those are difficult to evidence, as they are along the coda of a local earthquake or covered by a local earthquake. Their mean coherence rises, arriving for a single event to 0.9. In fig.6.8 and in fig.6.9 two examples of these signals are shown. The first is barely visible, characterized by small amplitude and no phases classified as impulsive P and S, with slowness values between 0.3 and 0.5 s/km. The second has a constant backazimuth values for about 20 sec (duration of the entire event) with very high coherence. Coherence and rms are respectively drawn with red and black color in top plot.

The nature of these signals is still unclear. For their characteristics, I hypothesize noise spatially correlated, due to particular meteorological conditions. Some of this seismic signals have similarities with landslides. Further analysis and the possible acquisition of data from National network could help to locate and to characterize the source of these signals.
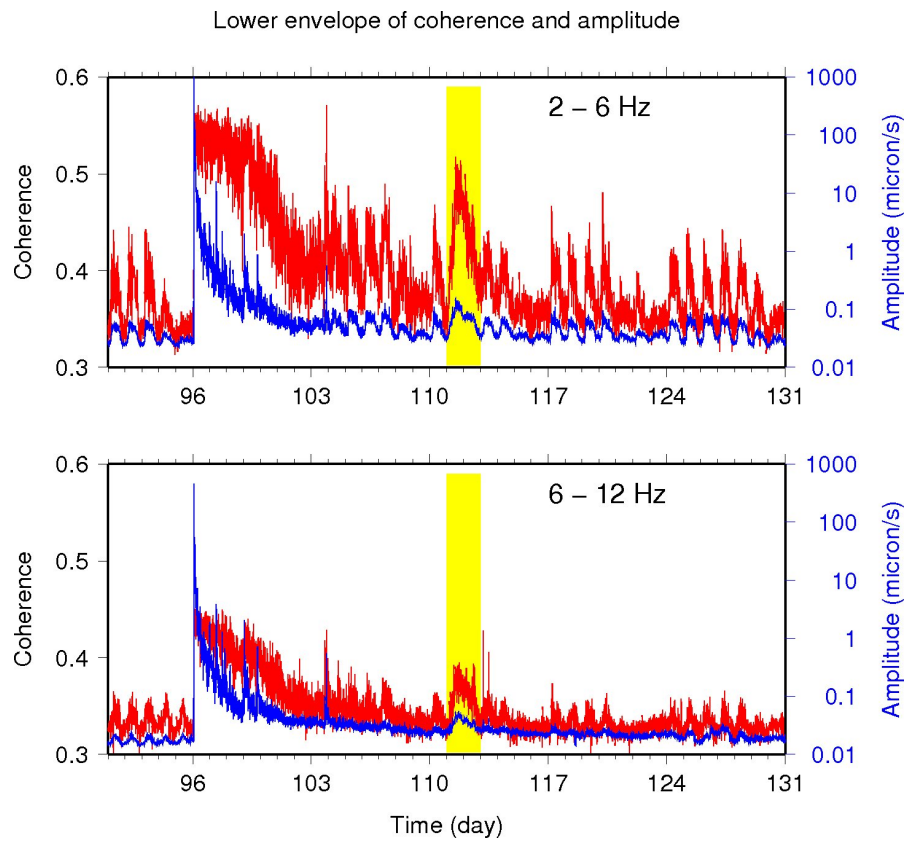
Figure 6.6: Lower envelope of coherence (red line) and amplitude (blue line) of the seismic signal calculated in two different frequency bands. Yellow box highlights the period when both functions show a significant increase compared to the days before and after, without any correlation with the seismic sequence of April-May 2009.
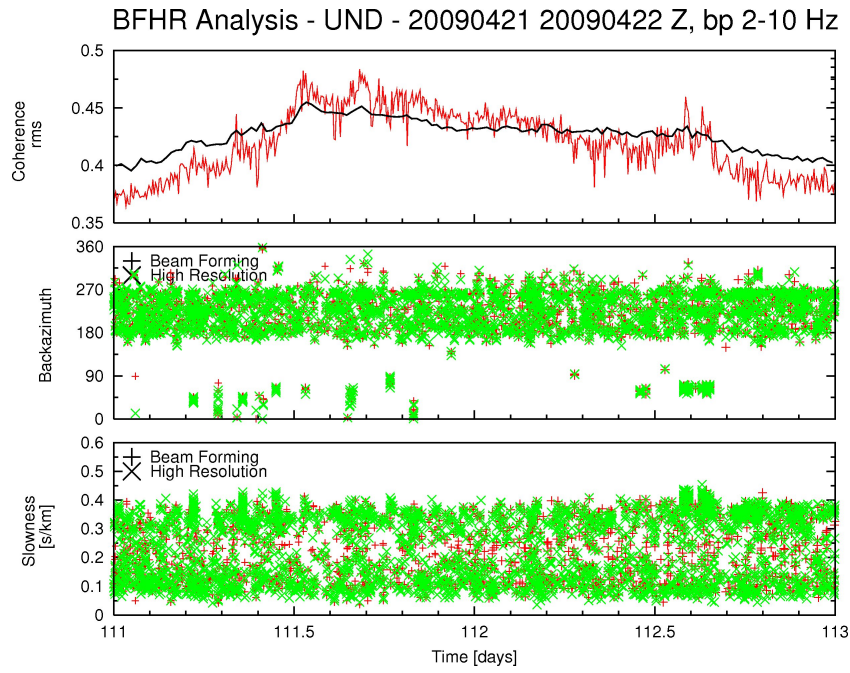
Figure 6.7: 21 and 22 April 2009, array analysis. BF and HR methods highlight about 20 phases with backazimuth between 30 and 90 degrees. Coherence and rms are respectively drawn with red and black color (top plot).
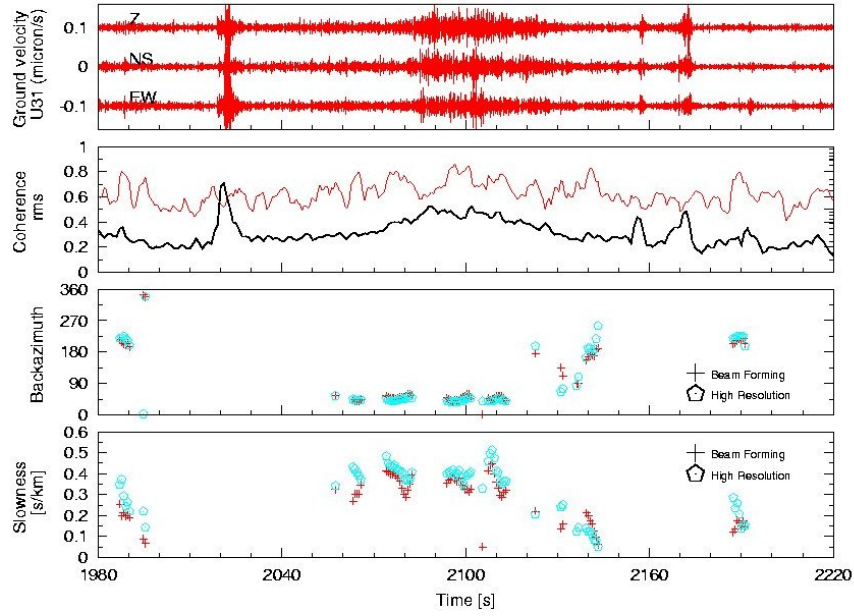
Figure 6.8: 21 April 2009, an example of array analysis on extracted event.
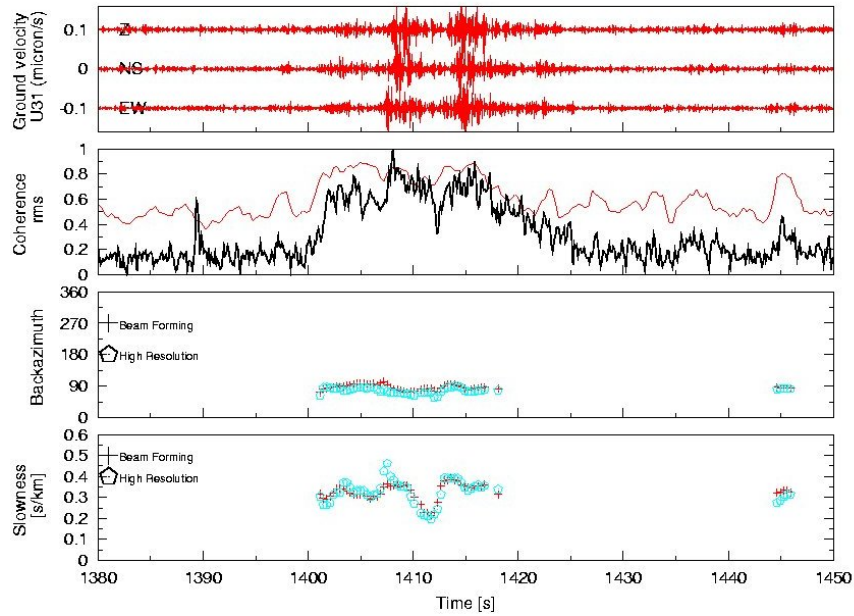
Figure 6.9: 21 April 2009, an example of array analysis on extracted event.

Chapter 7

Statistical analysis of the results obtained with array and polarization techniques

A statistical analysis was applied to the parameters estimated by array and polarization techniques. The distributions of slowness, backazimuth and polarization azimuth were computed at both arrays and compared each other. This was made on the most of analyzed earthquakes and in particular on their coda waves. Moreover, a teleseismic event was studied to compare signals with wavelengths greater than the distance between two arrays. The comparison of the results obtained at surface and at depth shows some significant differences, confirming also the previous observations.

7.1   Distributions of the results

The statistical procedure was performed on two parts of the seismograms: body waves (P, P coda and S waves) and coda waves (all others). The coda beginning was estimated as two times the Ts (shear-wave travel time). For each earthquake, the temporal window used for coda waves analysis go from twice the S-wave travel time to the end of the seismic event, established from the rms. For both accounted parts of seismograms, the results of array and polarization analysis were plotted using an appropiate threshold of coher-

ence for BF and HR methods and correlation for ZLCC method. As noted previously, at depth the coda of earthquake is characterized by coherence and correlation much higher than at surface and by longer duration. These two observations must be considered in the discussion of the end result. The procedure described above, was first applied to single events to make a detailed comparison between the two arrays. For example in fig.7.1 and fig.7.2 there are the histograms of BF and HR methods relative to 200709260814 earthquake, respectively for the two arrays. In each graph the normalized coda wave results, relative to the same earthquake recorded at two arrays, are shown. As expected, backazimuth distributions are almost random at both arrays. At UNDERSEIS array, slowness distribution of coda waves shows values typical of body waves. At Fontari array the polarization azimuth distribution of coda waves shows that most values are around two preferred directions. These observations are common to all analyzed earthquakes, both local and regional.

In the next graphs there are the distributions calculated for all data set. In everyone the green color indicates the outcomes of Beam Forming while the black color that of High Resolution. The outcomes of Zero Lag Cross Correlation are drawn with red color. Every distribution was calculated in many bands of frequency to analyze the differences. Here only two bands are shown, 1-3 Hz and 3-6 Hz. At low frequency, the distributions of coda wave backazimuth for both arrays are quite uniform (see fig.7.3 and fig.7.4). The distributions of slowness values (see fig.7.5 and fig.7.6), at depth confirm that the contribution of surface waves is negligible. The values are very low and rarely exceed 0.5 s/km. On the contrary the presence of surface waves may be predominant in the coda recorded at surface. At Fontari array slowness values are distributed around 1 s/km, indicating the presence of surface waves.

An interesting result is obtained on polarization azimuth distribution of earthquakes recorded at Fontari array. Unlike UNDERSEIS, polarization azimuth at Fontari array shows a preferred direction both for body (see fig.7.7 and fig.7.8) and for coda waves (see fig.7.9 and fig.7.10). This trend is particularly clear for coda waves where a well defined direction, NE-SW, appears. The two angles (45° and 135°), around which most values are

distributed correspond to direction NE-SW. This trend is not observed at UNDERSEIS array.

The results among used array techniques are very similar. All observations obtained with BF and HR methods in frequency domain are confirmed by ZLCC method in time domain. Particularly NE-SW polarization azimuth is clear in any frequency bands also with restriction on coherence, slowness and rectilinearity values.

Polarization azimuth distributions of coda waves (mean among all earthquakes) were computed for any stations of the two arrays (see fig.7.13 and fig.7.14). These results are obtained with polarization analysis. At surface a predominant NE-SW preferred direction is again evident for all stations. I think this result, not seen at depth, is mostly a topographic effect. In fact the main reliefs of Gran Sasso massif are oriented NW-SE. At Fontari array the mean of polarization azimuth is oriented NE-SW, that is perpendicular to the main orientation of Gran Sasso massif. This results will be explained better in next section. The differences among some stations of UNDERSEIS array (see fig.7.14) are mainly produced by local sources of noise. Their distributions are quite uniform. In order to give a complete view of this phenomenon, in fig.7.11 and in fig.7.12 there are the polarization azimuth distributions of body waves at the two arrays. At Fontari array there is still a common trend among the stations.
In fig.7.15 and in fig.7.16, P coda wave distributions of 200709121110 southern Sumatra, Indonesia ($Mw8.4$) telesismic event are shown. The results are relative to polarization azimuth. At low frequency ($< 1Hz$) the preferred NE-SW polarization direction is found at both arrays. This was expected, being the wavelength longer than the distance between the two arrays (about 2 km) and roughly comparable with the Gran Sasso extension.

In general, statistical analysis shows the important aspects of a distribution. Here we have the possibility to compare distributions of the same parameters estimated at two different arrays for the same earthquake, which in theory should be similar each other. The statistical evidence confirms the hypothesis about the importance of the presence of free surface for Fontari recordings. As surface waves are almost absent to UNDERSEIS, seismic wavefield show significant differences on main propagation parameters.
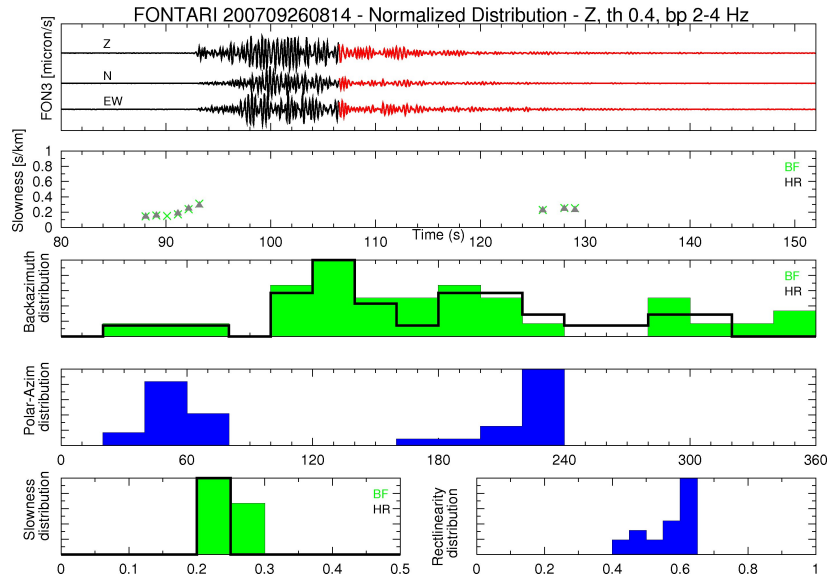
Figure 7.1: 200709260814. BFHR statistical analysis for FON. From top: Seismograms of local earthquake at FON, slowness values, normalized back-azimuth, polarization azimuth, slowness and rectilinearity distributions.
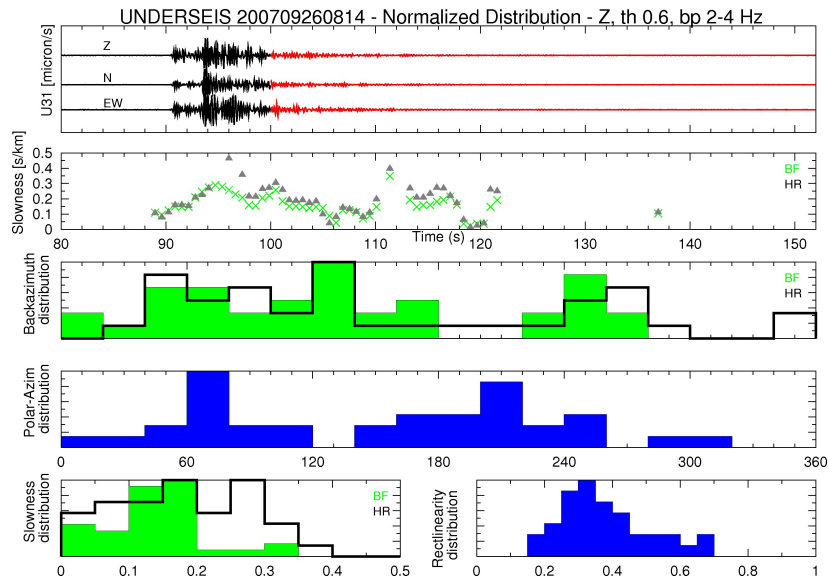
Figure 7.2: 200709260814. BFHR statistical analysis for UND. From top: Seismograms of local earthquake at UND, slowness values, normalized back-azimuth, polarization azimuth, slowness and rectilinearity distributions.
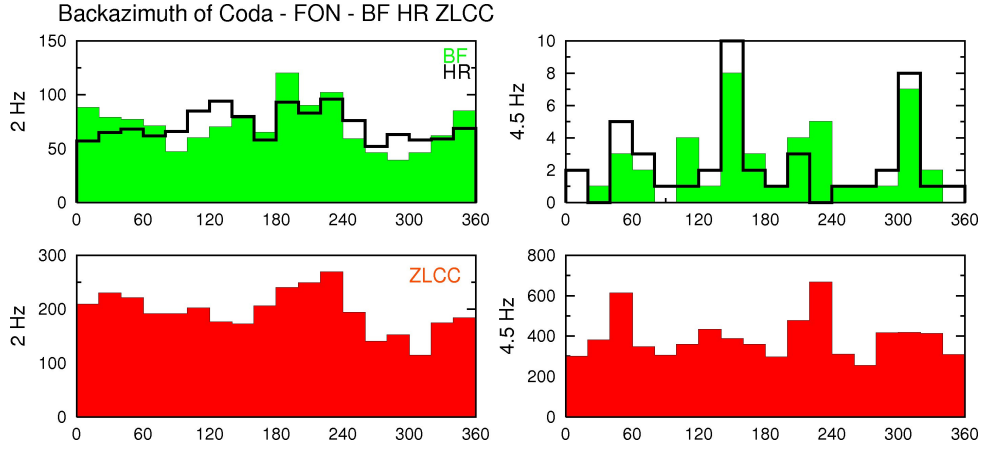
Figure 7.3: Backazimuth distributions of coda waves at Fontari array with BF(green), HR(black) and ZLCC(red) methods at 2 and 4.5 Hz.
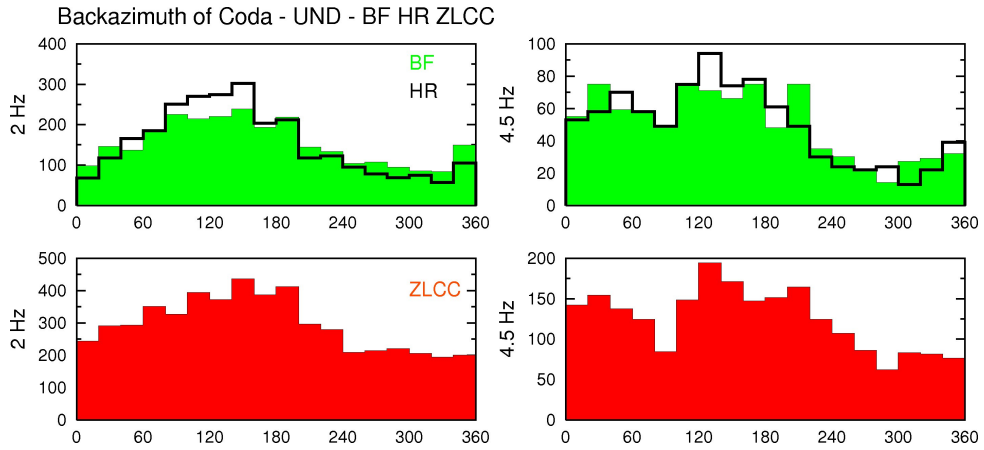
Figure 7.4: Backazimuth distributions of coda waves at UNDERSEIS array with BF(green), HR(black) and ZLCC(red) methods at 2 and 4.5 Hz.
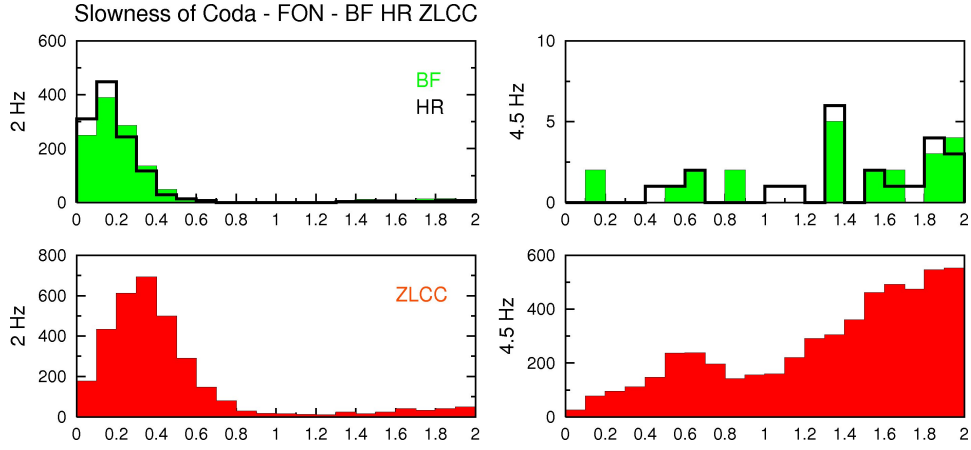
Figure 7.5: Slowness distributions of coda waves at Fontari array with BF(green), HR(black) and ZLCC(red) methods at 2 and 4.5 Hz.
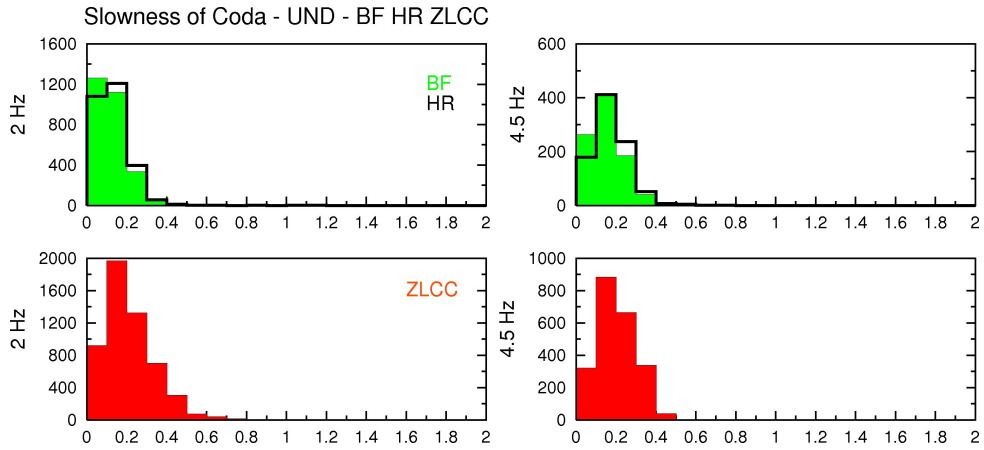
Figure 7.6: Slowness distributions of coda waves at UNDERSEIS array with BF(green), HR(black) and ZLCC(red) methods at 2 and 4.5 Hz.

Polar-Azim of Body Waves - FON - BF HR ZLCC
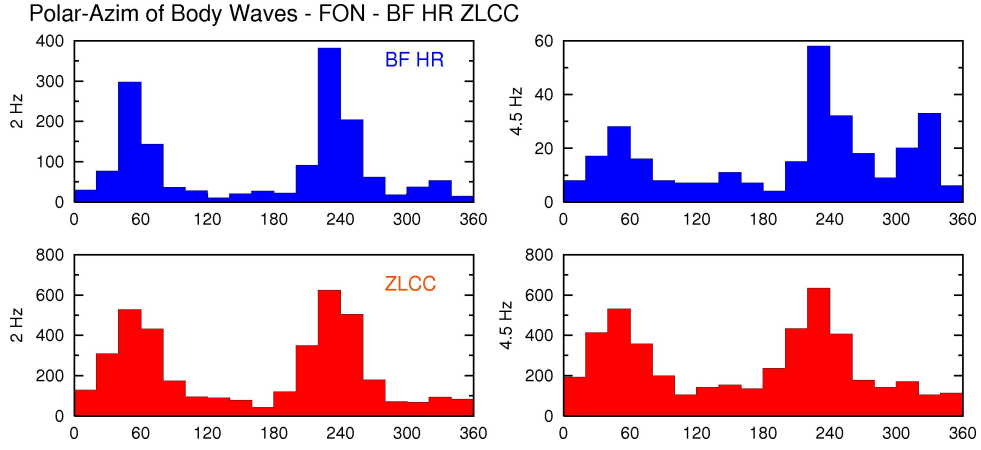
Figure 7.7: Polarization Azimuth distributions of body waves at Fontari array with BF, HR (the results are shown with blu color) and ZLCC methods (red color).

Polar-Azim of Body Waves - UND - BF HR ZLCC
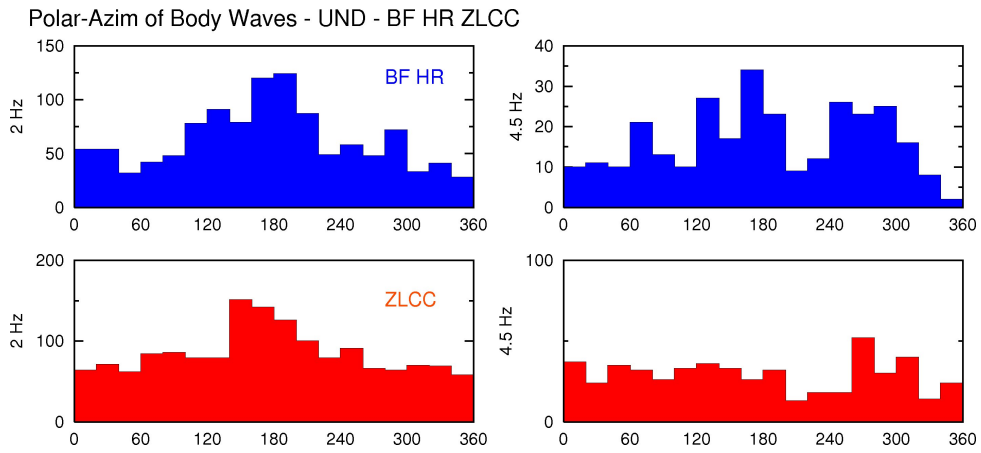
Figure 7.8: Polarization Azimuth distributions of body waves at UNDER-SEIS array with BF, HR (the results are shown with blu color) and ZLCC methods (red color).
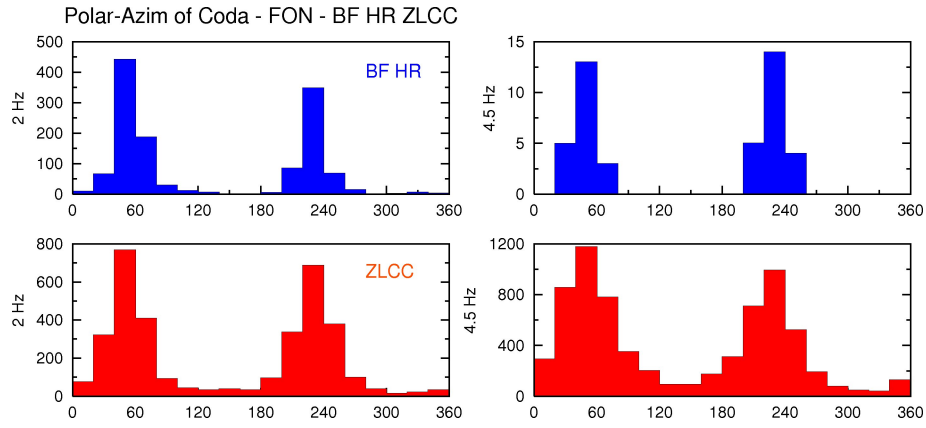
Figure 7.9: Polarization Azimuth distribution of coda waves at Fontari array with BF, HR (the results are shown with blu color) and ZLCC methods (red color).
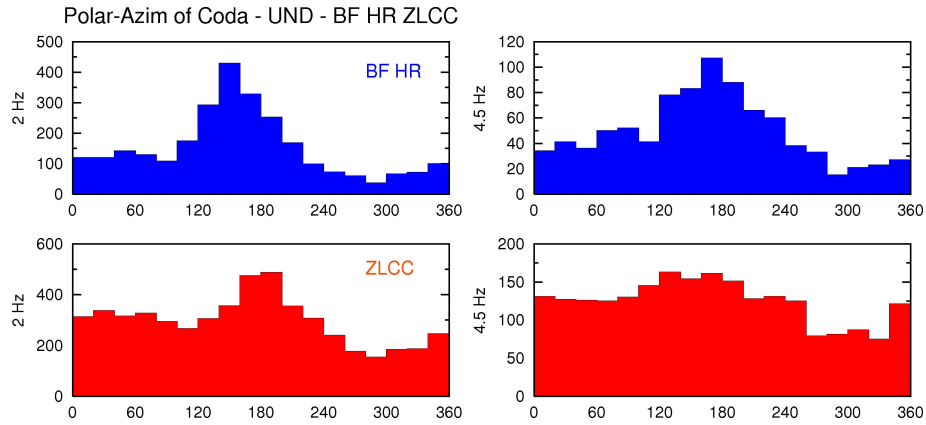
Figure 7.10: Polarization Azimuth distribution of coda waves at UNDER-SEIS array with BF, HR (the results are shown with blu color) and ZLCC methods (red color).
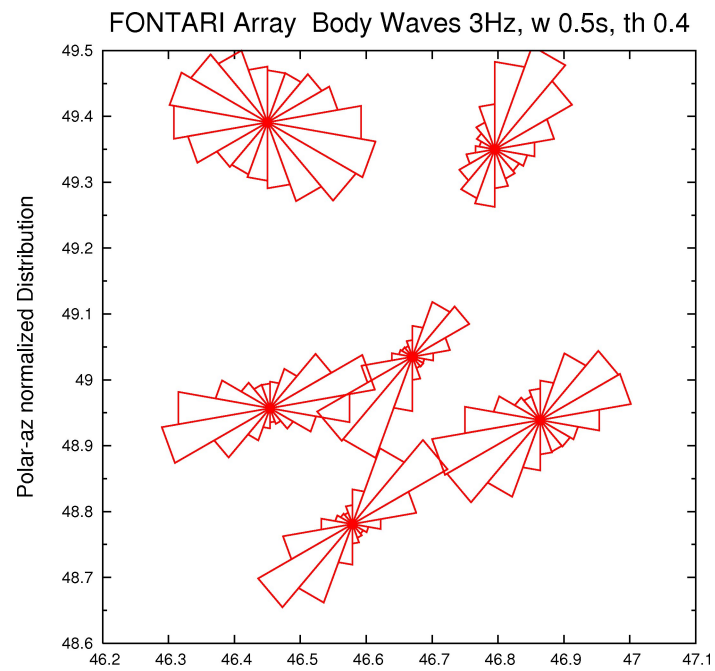
Figure 7.11: Polarization Azimuth distribution with rose diagram of body waves at Fontari array.
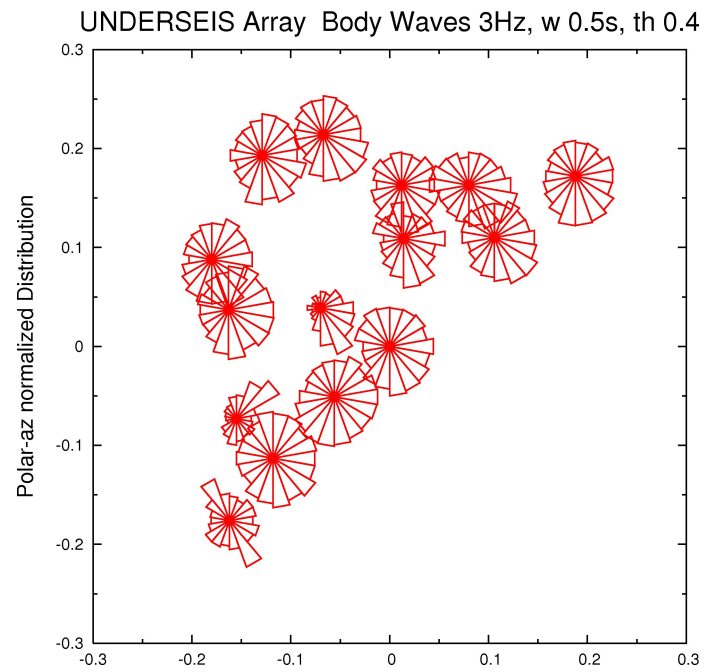
Figure 7.12: Polarization Azimuth distribution with rose diagram of body waves at UNDERSEIS array.
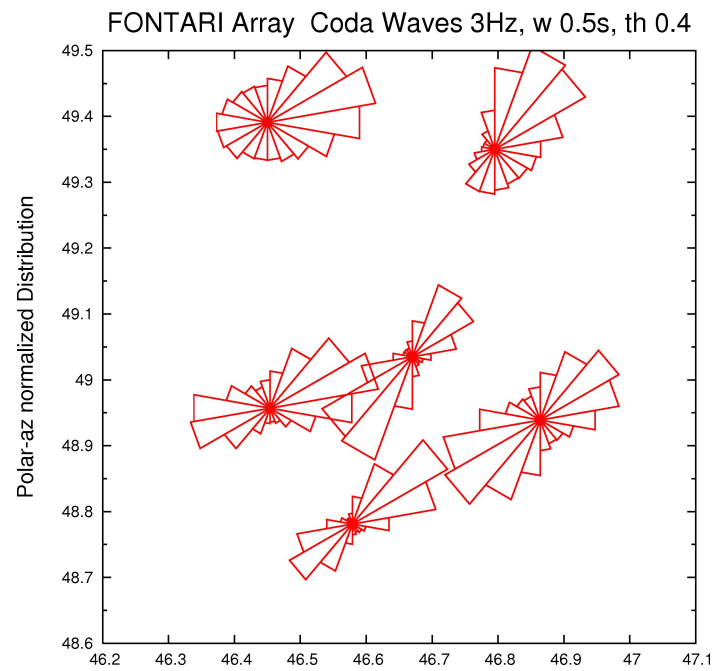
Figure 7.13: Polarization Azimuth distribution with rose diagram of coda waves at Fontari array.
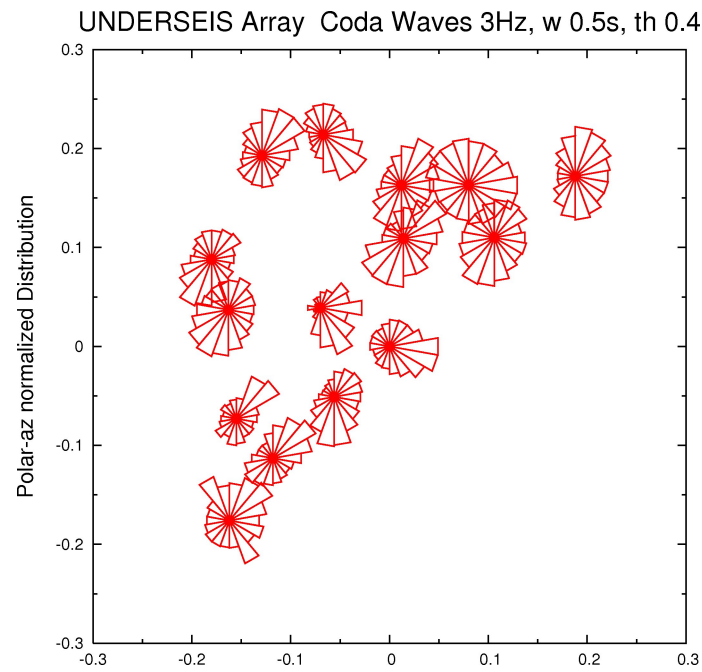
Figure 7.14: Polarization Azimuth distribution with rose diagram of coda waves at UNDERSEIS array.
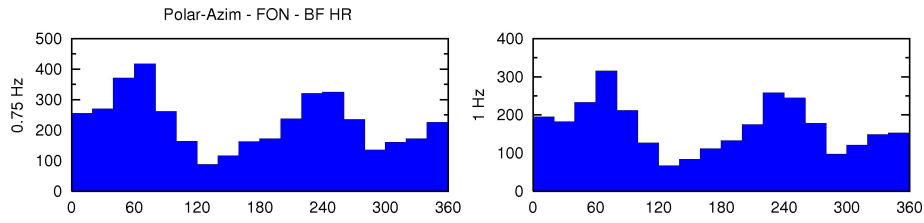
Figure 7.15: P coda wave distributions (Polarization Azimuth) of 200709121110 southern Sumatra, Indonesia (Mw8.4) telesismic event are shown at Fontari array with BF and HR methods.
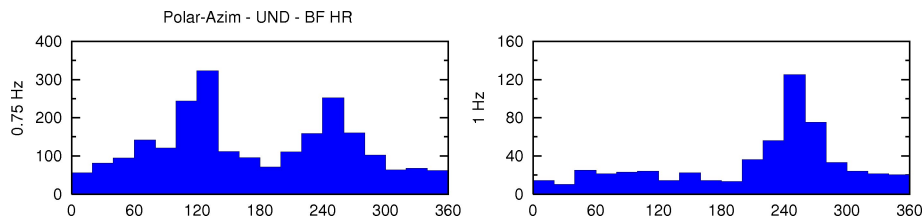
Figure 7.16: P coda wave distributions (Polarization Azimuth) of 200709121110 southern Sumatra, Indonesia (Mw8.4) telesismic event are shown at UNDERSEIS array with BF and HR methods.

7.2 Topographic effects

Many studies found that topographic irregularity can considerably affect the amplitude and frequency contents of ground motion. Generally, the *topographic amplification effect* is the phenomenon where the surface topography modifies the magnitude of ground motion and may increase the damaging effects during an earthquake. Many observations suggest that this effect is not easy to understand depending by many factors. *Geli et al. (1988)* [48] comparing observations and theoretical models, inferred that (1) seismic amplitude are amplified at crests and are de-amplified at valley or bottom of hill, (2) the frequency at which the amplification occurs corresponds to wavelengths comparable with mountain widths and (3) there is a quantitative disagreement between theoretical and observed amplification. All theoretical models, neglect small scale heterogeneities, underestimating observations. Also the observed amplifications are often much larger than theoretical predictions. Many studies observes that maximum amplification

is roughly related to the "sharpness" of the topography and amplification at mountain tops is generally larger on horizontal components and for S waves. To quantify the level and the frequency band of amplification, spectral ratios can be used. Topographic complexity (presence of neighboring ridges, sub-surface layering, smaller scale geological irregularities) can be responsible for large crest-base amplifications and also for directional effects on the polar-ization of seismic waves. Moreover, the response of the topographic profile depends on the incident angle: signals can be amplified or deamplified for different incidence angles. In the observations, the influence of near surface velocity gradients must also be considered. Many other phenomena may be related to topography in quantitative or qualitative way. For example, the occurrence of a landslide at or near ridge crests during an earthquake has also been attributed to topographic effects. Therefore, to interpret the observations in terms of constructive and destructive interference between upcoming, incident waves and the downgoing, surface-reflected waves, many factors related to topography must be considered.

The phenomenon found on polarization azimuth at Fontari array can be interpreted as a topographic effect. The polarization azimuth is oriented NE-SW both for body and coda waves and it is perpendicular to the main orientation of Gran Sasso massif (NW-SE). In fig.7.17 polarization azimuth of coda waves at Fontari array with rose diagram is shown. The result is relative to all stations and all earthquakes of data set. In fig.7.17, where topography of Gran Sasso area is shown in background, many ridges are evident. The geological structure is quite complex. NE-SW direction isn't found in underground recordings, except for teleseismic waves at frequency lower than 1 Hz. The presence of mountain and of 1400 meters of rocks between the two arrays influence the polarization of seismic waves.

The amplification of surface recordings can be explained also in terms of topography. All comparisons show higher amplitude of FON recordings respect to UND and this is not only due to the presence of free surface. In chapter of site effects some observations were made. Finally, azimuth polarization was estimated also for seismic noise (see fig.7.18). The common trend is found at some stations of Fontari.
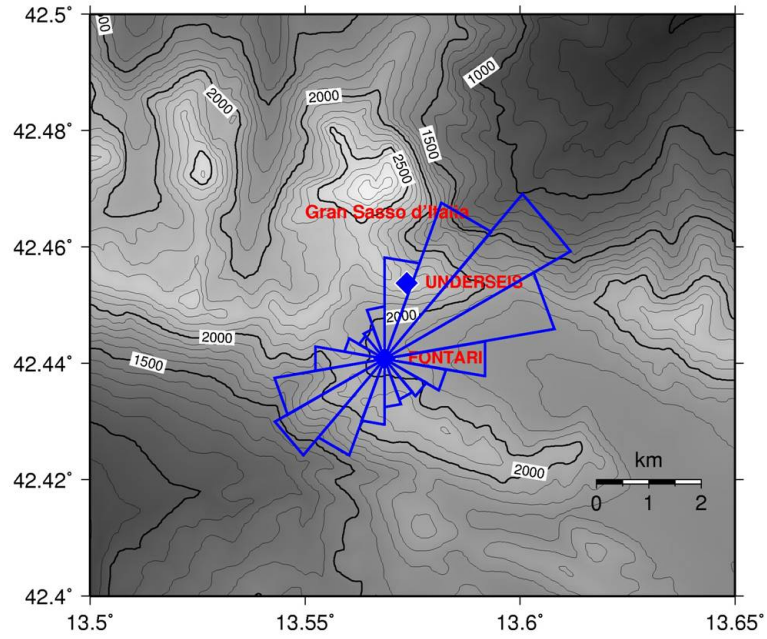
Figure 7.17: Polarization Azimuth distribution of coda waves at Fontari array for all its stations and for all earthquakes of data set.
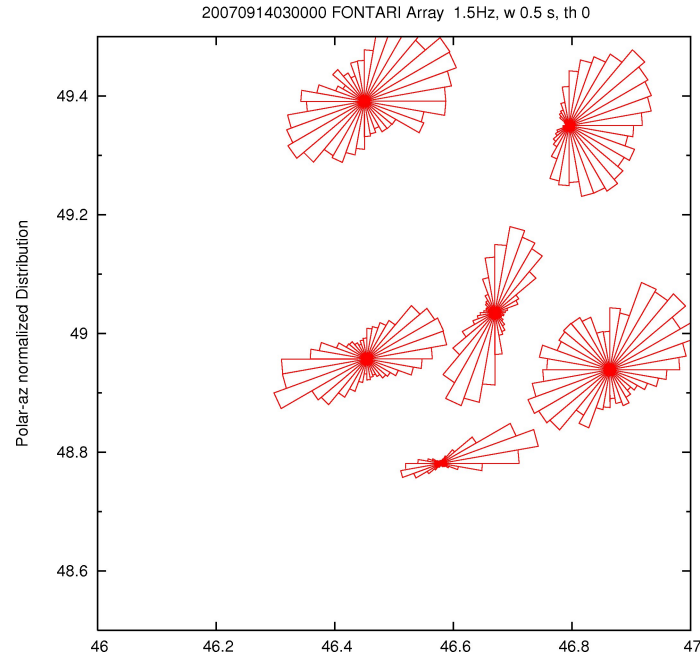
Figure 7.18: Polarization Azimuth distribution of noise at Fontari array on a windows of 600 s.

7.3 Features of local seismicity at Gran Sasso

From many observations and analysis made on data recorded by UNDER-SEIS and Fontari array, the most important features of local seismicity at Gran Sasso concern several aspects, as described below.

Considerable seismic activity and high seismic risk. Mt. Gran Sasso and surrounding area is affected by a considerable seismic activity, associated mainly to distensive NE-SW tectonics with the presence of many active seismic faults along the Gran Sasso massif. As cited previously, large earthquakes affected this area in the past causing severe damage to people and infrastructures. The analysis of continuous data since 2004 never shows periods longer than a few days without the occurrence of local earthquakes. On the contrary, many seismic swarms and a great number of microearthquakes have been detected. Many local earthquakes recorded at UNDERSEIS array have similar characteristics and they can be used to make observations on seismic wavefield in optimal conditions of low seismic noise.

Topographic effects. The topographic effects were found by polarization analysis, especially on FON data. The topography of Gran Sasso massif is complex, with the presence of many ridges and small scale geological irregularities. The topographic complexity is responsible for large crest-base amplification and for directional effects on the polarization of seismic waves, observed particularly at Fontari array.

Occurrence of landslide. Many landslides were recorded during the years, due to many causes. In chapter 3 I described the analysis of a large landslide occurred in 2006. Results indicate that a seismic array is a good instrument to detect and analyze the seismic signals produced by such events.

Site effect. The site effects at surface on Mt. Gran Sasso depend strongly on topographic irregularities and shallow geology. The HV spectral ratio has been computed at surface and at depth for local earthquakes. The results show that the underground laboratory where UNDERSEIS array is located can be considered a good hard-rock site characterized by the absence of significant amplification peaks, while the Fontari area shows a large variability of site amplification effect.

Conclusions

In this work I analyzed a large amount of data recorded from 2003 to 2010 by the underground UNDERSEIS array, and data recorded during six months in 2007 by a surface array installed at Fontari. Particular attention has been given to the analysis of local and regional earthquakes by applying three different techniques to estimate the propagation parameters of the correlated phases in the seismic wavefield, that are slowness and backazimuth. An analysis of the coherence of continuous data has also been done with the aim of detecting coherent signals produced by sources different from earthquakes. This analysis permitted the identification of several interesting events, that were analyzed in detail to understand their nature. The most of them resulted to be produced by artificial sources, while some have been interpreted as landslides. A few events of very low amplitude, emergent onset and duration of hours, shows tremor-like characteristics, but the data available do not allow a reliable classification. Finally, polarization analysis and site effect study have been done at the two arrays and results have been compared each other. The comparison of the results obtained at surface and at depth showed some significant differences. First of all, both seismic noise and earthquake signals have smaller amplitude at depth, where the surface and topographical effects are negligible for frequency greater than 2 Hz. Therefore the SNR is not very different between the two arrays. However, signals recorded at depth are much more similar among the array stations compared with the surface recordings. This is due to the much more uniform site response at depth and the much more variable seismic noise and surface effects at Fontari.

Numerous earthquakes were elaborated with BF, HR and ZLCC meth-

ods. All earthquakes have coherence or correlation higher at UNDERSEIS array. The same seismic event recorded by the two arrays shows some similarity and interesting differences. The wavefield composition is very similar for the earthquake onset, where backazimuth and slowness values calculated by array methods are in good agreement among them and with the expected values. The most relevant differences between surface and deep recordings are found along the earthquake coda. At depth the coda of local earthquakes is characterized by a coherence much higher than at surface. This is explained by the more uniform site response among the deep stations compared with the site effects observed at surface. The contribution of surface waves at depth is negligible for frequency higher than 2 Hz, as expected. In fact the slowness estimated along the coda shows values typical of body waves. On the contrary, the contribution of surface waves may be predominant in the coda recorded at surface. Along the coda there are some well-correlated phases, particularly at depth. The seismic noise in the high frequency range ($> 5Hz$) is considerably different at the two sites, with much smaller amplitude and lower variations with time at depth.

For this reason, the same earthquake has a slightly different duration at the two arrays. Generally the coda at depth is longer although the presence of surface waves is negligible.

The HV spectral ratios evaluated for UNDERSEIS stations show a constant pattern around one for all the investigated frequency ranges. The HV ratios are very similar among the array stations and this result is a clear indication that the site can be considered a good hardrock characterized by absence of particular amplification frequency peak. On the contrary, HV spectral ratios evaluated for Fontari stations show appreciable differences among them.

The importance of array and polarization analysis was particularly evident when unusual events were studied, especially when sharp pulses were absent in the recordings. This analysis was made also for the "particular" events described in chapter 2 and chapter 6, whose nature is still unknown.

On the seismic sequence of April 2009 only the coherence analysis was discussed. From the results, some events that seem not to belong to the sequence emerged. Array analysis shows coherent signals that travel from

completely different directions than those associated with local earthquakes in the sequence triggered by the main shock. The nature of these signals is still unclear, however a spatially correlated noise, possibly related with weather conditions, seems the most reasonable source. Some of this seismic signals have similarities with landslides.

The statistical distributions of slowness, backazimuth and polarization azimuth were computed at both arrays and compared each other. An interesting result is obtained on polarization azimuth distribution of earthquakes recorded at Fontari array. Unlike UNDERSEIS, polarization azimuth at Fontari array shows a preferred direction both for body and for coda waves. This result, not seen at depth, has been interpreted as a topographic effect.

In this study I had the rare opportunity to analyze the signals of the same earthquakes recorded by two arrays in the same area, one at surface and the other at 1.4 km depth. All results of my analysis indicate that deep recordings are very useful and often give more information about the wavefield features (composition, propagation, polarization, etc) if compared with surface recordings. The highly homogeneous site response among the array stations, the hard rock local characteristics, and the absent or negligible surface effects in the signals recorded by UNDERSEIS array are the most important aspects of deep recordings. Unfortunately, the high quality of those signals is compromised at some stations by local sources of noise (produced in the underground laboratory by human activity, engines, vehicles, pumps, air conditioning, and so on) and in some cases by electromagnetic interferences with the seismic equipment. However, the importance of such deep array data is beyond any doubts to improve the knowledge of seismic sources and wave propagation. Therefore, the UNDERSEIS project should be supported to keep it working in the future, to further improve the data quality, and to make those data available to the scientific community on line in real time.

List of Figures

List of Tables

Bibliography

[1] S.Rost, C.Thomas, *Array seismology: Methods and Applications*, Reviews of Geophysics, 40 (2002).

[2] R.Scarpa, R.Muscente, F.Tronca, C.Fischione, P.Rotella, M.Abril, G.Alguacil, W. De Cesare, M.Martini, *UNDERSEIS: The Underground Seismic Array*, Seismological Research Letters, 75 (2004).

[3] A.Amoruso, L.Crescentini, A.Morelli, R.Scarpa, *Slow rupture of an aseismic fault in a seismogenic region of Central Italy*, Geophysical Research Letters, 29 (2002).

[4] G.Saccorotti, B.Di Lieto, C.Fischione, F.Tronca, R.Scarpa, *Performances of the UNDERground SEISmic array for the analysis of seismicity in Central Italy*, Annals of Geophysics, 49 (2006).

[5] P.Galli, F.Galadini, M.Moro, C.Giraudi, *New paleoseismological data from the Gran Sasso d'Italia area (central Apennines)*, Geophysical Research Letters, 29 (2002).

[6] R.Adinolfi Falcone, A.falgiani, B.Parisse, M.Petitta, M.Spizzico, M.Tallini, *Chemical and isotopic multi-tracing for groundwater conceptual model of carbonate aquifer (Gran Sasso INFN underground laboratory - central Italy)*, Journal of Hydrology, 357 (2008).

[7] F.Di Luccio, G.Ventura, R.Di Giovambattista, A.Piscini, F.R.Cinti, *Normal faults and thrusts re-activated by deep fluids: the 6 April 2009 Mw 6.3 L'Aquila earthquake, central Italy*, Journal of Geophysical Research, 115 (2010).

[8] J.Capon, *High Resolution frequency-wave number spectrum analysis*, Proc. IEEE, 57 (1969).

[9] J.Capon, R.J.Greenfield, R.J.Kolker, *Multidimesional Maximum-Likelihood Processing of a Large Aperture Seismic Array*, Proc. IEEE, 55 (1967).

[10] R.Scarpa, A.Amoruso, L.Crescentini, C.Fischione, L.A.Formisano, M.La Rocca, F.Tronca, *Slow earthquakes and low frequency tremor along the Apennines, Italy*, Annals of Geophysics, 51 (2008).

[11] P.G.Catalano, G.P.Cavinato, F.Salvini, M.Tozzi, *Analisi strutturale nei laboratori dell'INFN del Gran Sasso d'Italia*, Mem. Soc. Geol. It., 35 (1986).

[12] M.R.Foster, N.J.Guinzy, *The coefficient of coherence: its estimation and use in geophysical data processing*, Geophysics, 32 (1967).

[13] M.J.Hinich, C.S.Clay, *The Application of the Discrete Fourier Transform in the Estimation of Power Spectra, Coherence and Bispectra of Geophysical Data*, Reviews of Geophysics, 6 (1968).

[14] F.L.Vernon, J.Fletcher, L.Carrol, A.Chave, E.Sembera, *Coherence of Seismic Body Waves From Local Events as Misured by a Small-Aperture Array*, Journal of Geophysical Research, 96 (1991).

[15] J.Park, C.R.Lindberg, F.Vernon III, *Multitaper Spectral Analysis of High-Frequency Seismograms*, Journal of Geophysical Research, 92 (1987).

[16] N.S.Neidell, M.Turhan Taner, *Semblance and other coherency measures for multichannel data*, Geophysics, 36 (1971).

[17] C.A.Langston, P.Bodin, C.Powell, M.Withers, S.Horton, W.Mooney, *Explosion Source Strong Ground Motions in the Mississipi Embayment*, Bulletin of the Seismological Society of America, 96 (2006).

[18] K.D.Saunders, F.C.Hamrick, *A note on Cross Spectrum and Coherence Calculations*, Journal of Geophysical Research, 87 (1982).

[19] W.S.Phillips, K.Aki, *Site amplification of coda waves from local earthquakes in central California*, Bulletin of the Seismological Society of America, 76 (1986).

[20] E.Del Pezzo, M.La Rocca, J.Ibanez, *Observation of High-Frequency Scattered Waves Using Dense Arrays at Teide Volcano*, Bulletin of the Seismological Society of America, 87 (1997).

[21] M.La Rocca, E.Del Pezzo, M.Simini, R.Scarpa, G.De Luca, *Array analysis of Seismograms from Explosive Sources: Evidence for Surface Waves Scattered at the Main Topographical Features*, Bulletin of the Seismological Society of America, 91 (2001).

[22] M.La Rocca, D.Galluzzo, G.Saccorotti, S.Tinti, G.B.Cimini, E.Del Pezzo, *Seismic signals Associated with a Landslides and with a Tsunami at Stromboli Volcano, Italy*, Bulletin of the Seismological Society of America, 94 (2004).

[23] M.La Rocca, W.McCausland, D.Galluzzo, S.Malone, G.Saccorotti, E.Del Pezzo, *Array measurement of deep tremor signals in the Cascadia subduction zone*, Geophysical Research Letters, 32 (2005).

[24] M.La Rocca, D.Galluzzo, S.Malone, W.McCausland, G.Saccorotti, E.Del Pezzo, *Testing Small-Aperture Array Analysis on Well-Located Earthquakes, and Application to the Location of Deep Tremor*, Bulletin of the Seismological Society of America, 98 (2008).

[25] M.La Rocca, D.Galluzzo, S.Malone, W.McCausland, E.Del Pezzo, *Array analysis and precise source location of deep tremor in Cascadia*, Journal of Geophysical Research, 115 (2010).

[26] J.F.Montalbetti, E.R.Kanasewich, *Enhancement of Teleseismic Body Phases with a Polarization Filter*, Geophys. J. astr., 21 (1970).

[27] A.Jurkevics, *Polarization analysis of three-component array data*, Bulletin of the Seismological Society of America, 78 (1988).

[28] K.Bataille J.M.Chiu, *Polarization Analysis of High-Frequency, Three-Component Seismic Data*, Bulletin of the Seismological Society of America, 81 (1991).

[29] J.Park, F.Vernon III, C.R.Lindberg, *Frequency Dependent Polarization Analysis of High-Frequency Seismograms*, Journal of Geophysical Research, 92 (1987).

[30] G.De Luca, R.Scarpa, L.Filippi, A.Gorini, S.Marcucci, P.Marsan, G.Milana, E.Zambonelli, *A detailed analysis of two seismic sequences in Abruzzo, Central Apennines, Italy*, Journal of Seismology, 4 (2000).

[31] G.De Luca, E.Del Pezzo, F.Di Luccio, L.Margheriti, G.Milana, R.Scarpa, *Site response study in Abruzzo (Central Italy): underground array versus surface stations*, Journal of Seismology, 2 (1998).

[32] R.Maresca, D.Galluzzo, E.Del Pezzo, *H/V Spectral Ratios and Array Techniques Applied to Ambient Noise Recorded in the Colfiorito Basin, Central Italy*, Bulletin of the Seismological Society of America, 96 (2006).

[33] K.Konno, T.Ohmachi, *Ground-Motion Characteristics Estimated from Spectral Ratio between Horizontal and Vertical Components of Microtremor*, Bulletin of the Seismological Society of America, 88 (1998).

[34] T.Braun, J.Schweitzer, *Spatial Noise-Field Characteristics of a Three-Component Small Aperture Test Array in Central Italy*, Bulletin of the Seismological Society of America, 98 (2008).

[35] D.Albarello, E.Lunedei, *Alternative interpretations of horizontal to vertical spectral ratios of ambient vibrations: new insigths from theoretical modeling*, Bull. Earth. Eng. 8:519-534 (2010).

[36] D.Bindi, F.Pacor, L.Luzi, M.Massa, G.Ameri, *The Mw6.3, 2009 L'Aquila earthquake: source, path and site effects from spectral analysis o strong motion data*, Geophysical Journal International 179 (2009).

[37] J.Lermo, F.J.Chavez-Garcia, *Site Effect evaluation using spectral ratios with only one station*, Bulletin of the Seismological Society of America, 83 (1993).

[38] S.Parolai, D.Bindi, M.Baumbach, H.Grosser, C.Milkereit, S.Karakisa, S.Zunbul, *Comparison of different site response estimation techniques using aftershocks of the 1999 Izmit earthquake* Bulletin of the Seismological Society of America, 94 (2004).

[39] H.J.Steidl, G.A.Tumarkin, R.J.Archuleta, *What Is a Reference Site?*, Bulletin of the Seismological Society of America, 86 (1996).

[40] C.Chiarabba et al., *The 2009 L'Aquila (central Italy) M_w 6.3 earthquake: Main shock and aftershocks*, Geophysical Research Letters, 36 (2009).

[41] A.Amoruso, L.Crescentini, *Slow diffusive fault slip propagation following the 6 April 2009 L'Aquila earthquake, Italy*, Geophysical Research Letters, 36 (2009).

[42] R.J.Walters et al., *The 2009 L'Aquila earthquake (central Italy): A source mechanism and implications for seismic hazard*, Geophysical Research Letters, 36 (2009).

[43] R.E.Abercrombie, *Near-Surface Attemuation and Site Effects from Comparison of Surface and Deep Borehole Recording*, Bulletin of the Seismological Society of America, 87 (1997).

[44] S.Blakeslee, P.Malin, *High Frequency site effects at two Parkfield downhole and surface stations*, Bulletin of the Seismological Society of America, 81 (1991).

[45] F.J.Chavez-Garcia, L.R.Sanchez, D.Hatzfed, *Topographic Site Effects and HVSR. A comparison Between Observation and Theory*, Bulletin of the Seismological Society of America, 86 (1996).

[46] G.Cultrera, A.Rovelli, G.Mele, R.Azzara, A.Caserta, F.Marra, *Azimuth-dependent amplification of weak and strong ground motions*

within a fault zone (Nocera Umbra, central Italy), Journal of Geophysical Research, 108 (2003).

[47] M.Pischiutta, G.Cultrera, A.Caserta, L.Luzi, A.Rovelli, *Topographic effects on the hill of Nocera Umbra, central Italy*, Geophysical Journal International, 182 (2010).

[48] L.Geli, P.Y.Bard, B.Jullien, *The effect of topography on earthquake ground motion: a review and new results*, Bulletin of the Seismological Society of America, 78 (1988).

[49] P.Y.Bard, B.E.Tucker, *Underground and ridge site effects: a comparison of observation and theory*, Bulletin of the Seismological Society of America, 75 (1985).

[50] K.Obara, *Nonvolcanic Deep Tremor Associated with Subduction in Southwest Japan*, Science, 296 (2002).

[51] J.L.Rubinstein, J.E.Vidale, J.Gomberg, P.Bodin, K.C.Creager, S.D.Malone, *Non-volcanic tremor driven by large transient shear stresses*, Nature, 448 (2007).

[52] Aki, Richards, *Quantitative Seismology*, Second Edition, W. H. Freeman, New York, (1980).

[53] Bath, *Spectral Analysis in Geophysics*, ELSEVIER SCIENTIFIC PUBLISHING COMPANY, (1974).

[54] Kramer, *Geotechnical Earthquake Engineering*, (1996).

[55] Lay, Wallace, *Modern Global Seismology*, Academic Press, (1995).

[56] Scherbaum, *OF POLES AND ZEROS, Fundamentals of Digital Seismology*, 2nd Edition, Kluwer Academic Publishers, (2001).